Biomolecule-Induced Ordering Transitions at the Liquid Crystal-Aqueous Interface

A Thesis Submitted for the Degree of

DOCTOR OF PHILOSOPHY

by

Dibyendu Das

Department of Chemical Sciences

Indian Institute of Science Education and Research (IISER) Mohali

Sector 81, Knowledge city, S. A. S. Nagar, Mohali, 140306.

Punjab, India.

March 2018

DEDICATED TO

MY BELOVED PARENTS

DECLARATION

The entire work presented in this thesis entitled as "*Biomolecule-Induced Ordering Transitions at the Liquid Crystal-Aqueous Interface"* has been performed by me under the supervision of **Dr. Santanu Kumar Pal** in the Department of Chemical Sciences, Indian Institute of Science Education and Research (IISER) Mohali, Mohali.

The work has not been published as a part or full for a degree or diploma or fellowship to any other university or institute.

Whenever contributions of others are involved, every effort is made to indicate this clearly with due acknowledgements of collaborative work and discussions. This thesis is a bona fide record of original work done by me and all sources listed within have been detailed in the bibliography.

Dibyendu Das

Date

Place

In my capacity as the supervisor of the candidate's thesis work, I certify that the above statements by the candidate are true to the best of my knowledge.

Date **Dr. Santanu Kumar Pal**

Place **Associate Professor**

Department of Chemical Sciences

Indian Institute of Science Education and Research (IISER) Mohali

Acknowledgements

At the end of doctoral research, I take the privilege to express my gratitude to those persons who supported and motivated me constantly during my research work.

I express my gratitude to my PhD supervisor ***Dr. Santanu Kumar Pal*** for giving me the opportunity to work in this exciting field of liquid crystal. His constant support and motivation helped me enormously during my research work. Without his guidance it would not have been possible to complete this work.

I would like to acknowledge our former director ***Prof. N. Sathyamurthy*** and present director ***Prof. Debi Prasad Sarkar*** for providing proper infrastructure and environment to carry out my research without any problem.

I would like to thank our former HOD, Department of Chemical Sciences, ***Prof. K. S. Viswanathan*** and present HOD ***Dr. S. Arulananda Babu*** for various helpful discussions.

I am also thankful to all faculty members of department of chemical sciences for teaching various scientific topics and giving valuable suggestions.

I would like to thank ***Dr. Sabyasachi Rakshit*** and ***Dr. Sugumar Venkataramani***, members of doctoral committee, for yearly assessment of my research work and fruitful discussions.

I am thankful to ***Dr. Samrat Mukhopadhyay*** lab for helping me to use CD instrument.

I want to acknowledge IISER Mohali for the instrumental facilities, infrastructure and fellowship.

I want to thank the lab assistants, Mangat, Bahadur, Satwinder, all the staff members of administrative, library, computer facility for helping me in various ways.

I want to acknowledge the former PhD students of our lab ***Dr. Sumyra Sidiq*** *and* ***Dr. Shilpa Setia*** for helping in my research work and providing valuable suggestions.

I want to thank the post docs in our lab ***Dr. Golam Mohiuddin***, ***Dr. Rajib Nandi***, ***Dr. Santosh K. Gupta and Dr. Manisha Devi*** for helping me in various ways.

I am thankful to my PhD Colleagues: ***Joydip, Indu bala, Indu Verma***, ***Harpreet***, ***Monika, Supreet, Vidhika, Ipsita, Varsha, Shruti, Mustafa, Yogi*** for their cooperation and for making nice friendly atmosphere to work.

I would like to thank MS students in our lab ***Nitya, Lisha, Neelima, Vaishnavi, Swathy, Manmohan, Aneeshma, Ayush*** and summer students in our lab ***Irin, Angel, Swaraj, Shiny, Diksha, Subhhodip***.

I want to acknowledge my friends ***Joydip, Prithwis, Sanjeeb, Bishnu, Pritam, Ankan, Ishan, Arjun, Debjit, Suchand, Debojyoti*** for their cooperation and joyful companionship.

I am thankful to my PhD batchmates ***Hema, Kanupriya, Monika, Ginny, Biswajit, Sandeep***, ***Abhijeet.***

I would like to acknowledge my childhood friends ***Ayan, Debprakash, Rakesh, Subhankar, Debapriya, Aparna, Simi, Tanmay*** for their love and support.

I deeply acknowledge my ***parents*** and ***family members*** for their never ending love, support and motivation.

Contents

Chapter 1

Introduction of liquid crystal & its application in biosensing

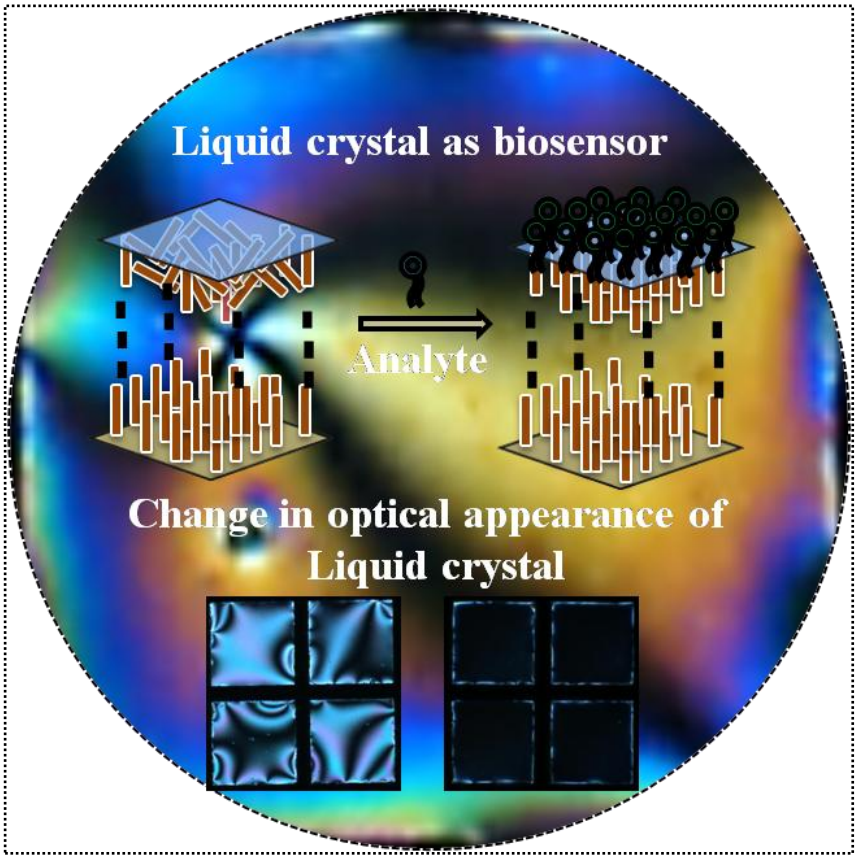

In recent decade thermotropic liquid crystal has drawn widespread interest in the field of biosensor for the recognition of several biomolecular interactions at the interface. Any biomolecular interactions at the interface of LC and water can be easily reported through ordering transition of LC and hence provide a level free platform that mimics biological phenomenon without requirement of any complex instrumentation.

1.1 Overview

Molecular interactions in synchronized pattern are key factors to the evolution of life. The interplay between several biomolecules for example proteins, nucleic acids, lipids, carbohydrates directs each and every cellular process in living system.[1] Every biomolecule has its own distinct chemical features and definite functions. But, its influence on the mechanism of life can be understood only when it interacts with other biomolecule in living system. These biomolecular interactions are diverse in nature in terms of its thermodynamics as well as kinetic stability.[2] Therefore, to fulfill the necessity of exploring various cellular mechanisms in living system, the primary criterion is to understand these biomolecular interactions at molecular level.[3] Moreover any particular cellular response or mechanism is governed by interactions of certain biomolecules in a highly selective and specific pathway.[4]

Among various kind of biomolecular interactions protein-protein,[5-8] proteins-lipid[9-12] interactions play pivotal role in major cellular functions and hence draw upmost interest to put insight on these interactions. Apart from these interactions, there are several other interactions such as, protein- carbohydrate,[13,14] protein-nucleotide,[15,16] lipid-nucleotide,[17.18] and protein-phosphate,[19,20] which are also quite important in regulating several cellular mechanisms. Therefore, thorough study of these interactions holds immense importance in understanding the process of life. In addition to that, exploring these interactions are equal important from therapeutic point of view.[21,22] Any kind of malfunction or disturbance in the interaction of these biomolecules results in abnormality in cellular process and leads to sickness, disease etc.[23,24] Hence, with progress of science, substantial efforts have been deployed to develop several analytical approaches to put insights into these biomolecular interactions.

Among several available methods, biosensors are the promising assays to study these biological phenomena in precise way. Biosensors are analytical assays which involves biologically derived sensing platform connected with a physico-chemical transducer to detect as well as quantify existence and amount of certain target species by converting certain biological interactions into highly amplified and easily processible physical signals.[25,26] Biosensors hold two major characteristics, first, sensitivity towards the targeted

species i.e. how far this system could be responsive towards lower concentration of targeted species. Second, selectivity of the system, i.e. how precise the system could detect one particular targeted species in an environment where other analytes are also present.

Liquid crystal (LC) is certain type of properties of matter, which is observed in diverse biological system.[27,28] For example DNA, cell membrane found to be exist in LC state.[29,30] But application of commercial liquid crystalline material in characterizing several biomolecular interactions is a new venture in the field of biosensing.[31-42] Recently, LC based sensors have drawn widespread interest in biosensing due to some unique characteristics of LC. First, long range ordering of LC found to be sensitive to report any interfacial biomolecular phenomenon which is further communicated upto few hundred micrometers in bulk phase of LC. This unique feature enables LC to amplify any interfacial biomolecular interaction to many folds. Second, inherent elasticity of LC also play major role in response time of LC towards several biomolecular interactions. Liquid like mobility and low interface anchoring energy enable LC to be responsive towards any interfacial disturbance by external stimuli within milliseconds. This allows LC as potential candidate for fast and real time detection. Third, LC possess optical anisotropy i.e. exhibits birefringence. Therefore, LC appears in different optical texture and color depending on its long range orientation, which in turn dependent on presence of external stimuli at LC interface. Thus LC based sensor offers simple visible detection technique without requirement of any complex instrumentation. The high sensitivity of orientational ordering of LC on nanoscale topography or chemically functionalized surface provides amplification and transduction of biological binding events into optical read-out, which is easily visible by naked eye. The application of LC material as a biosensor is based on interaction of several biomolecules with LC molecules at the interface. As a whole, the optical anisotropy and elasticity are the two main features of LC, which enable LC as a potential tool for recognition of biomolecular interactions. Nevertheless, there are requirements of further development of LC based sensing technique and expansion of this method towards the study of diverse biomolecular interactions which are yet to be explored. The approaches towards the fulfillment of these requirements are the motives behind this thesis.

The thesis describes the application of thermotropic LC in recognition of several biomolecular interactions at the interface. This kind of LC is immiscible with aqueous solution and form an interface between LC and water. Any biomolecular interactions at the interface of LC and water can be easily reported through ordering transition of LC. In this thesis our goal is to develop the approaches to fabricate LC as suitable candidate to study interfacial biomolecular interactions and also to extend this method to recognize several biomolecular interactions which are yet to be explored.

1.2 Introduction of LC

LCs are known as intermediate state of matter exhibiting physical properties like order and fluidity in between solid and liquid (Figure 1.1). They are found to possess certain solid like properties (for example, birefringence, magnetic properties, conductivity etc.) as well as liquid like properties (for example mobility, droplet formation etc.).[43-46] In confined surface LC molecules tend to align to certain direction and the average orientation of LC molecules is known as LC director. There are certain shapes observed in LC molecules like rod shape or disc shape, and these shapes are anisometric in nature.[47,48] But the molecules, which are in isometric shape, also have found to exhibit LC properties by self-assembling in anisometric fashion. In addition to that LC possesses optical anisotropy i.e. shows colorful texture when observed through crossed polars. In presence of electric, magnetic field or with variation of temperature LC molecules found to alter their optical appearances. Based on this, LC materials have been used extensively in display industries, for example, in manufacturing television screens, watches, calculators etc. Besides, in recent decades, LC materials also have been employed in different areas of science and technologies other than displays. In this regard, LC has shown promising applications in developing methods in the area of biological and chemical sensing.[49-51]

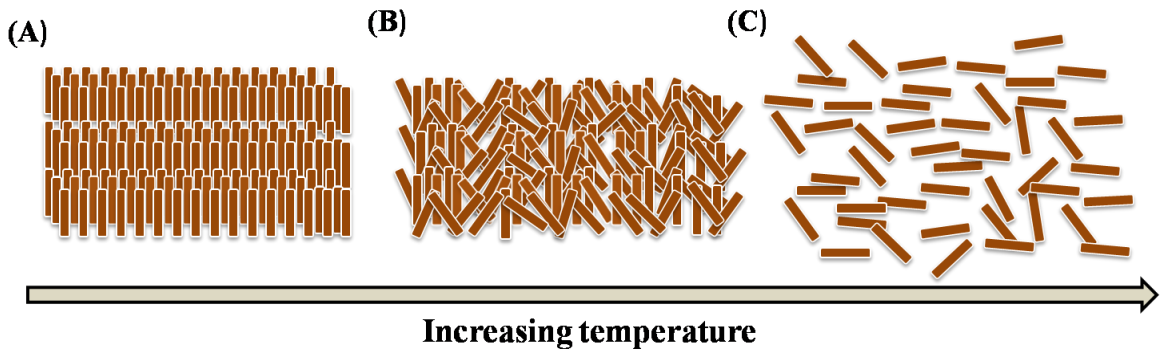

Figure 1.1 Schematic representation of (A) crystal, (B) liquid crystal, (C) liquid state of matter.

1.3 Historical background of LC

The discovery of liquid crystal took place in late nineteenth century. Before that scientists considered that matter exists in three phases solid, liquid and gas. In 1888, an Austrian botanist Friedrich Reinitzer found that cholesterol benzoate (Figure 1.2) shows two different melting points. At 145.5° it converts from solid to a milky turbid phase and then at 178.5° that milky phase turns into clear liquid state.[52] To gain detailed information regarding this observation, he met the German scientist Otto Lehman. Lehman observed the compound under polarized optical microscope carefully and explained the milky phase as different state of matter other than solid, liquid and gas. He also found that this particular phase exhibits both solid and liquid like properties. There, he termed the phase as "liquid crystal".[53] After that scientist Georges Freidel extended the thorough study of the LC phase. In 1922 he classified this particular phase into three categories nematic, smectic and cholesteric. He also termed the molecules form this phase as "mesogen". He described that mesogens combinely form the LC phase, which he preferred to term as meso phase.[54]

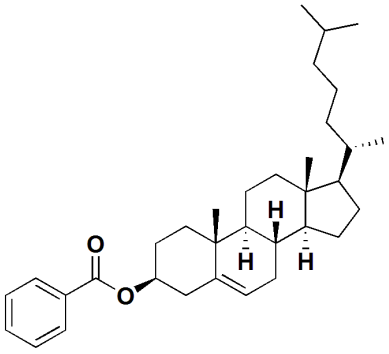

Figure 1.2 Chemical structure of cholesterol benzoate.

In late twentieth century, during 1960-1970, the materials which exhibit LC properties have found to be widely applicable in display industries.[55] There was a steep growth in the research of LC in the development of electronic accessories. Later on the existence of LC phase in biological system was also discovered. DNAs, some protein phospholipid membranes in mammalian cell were found to be exist in LC phase.[56,57] This discovery encouraged scientists further to establish a connection between LC material and the development of biological science. They have successfully employed this type of materials in the building up of artificial muscle fiber,[58] in the fabrication of tunable lasers,[59] optical data storage[60] etc. In recent decades Abbott *et al*. further extended the applicability of LC in the area of biosensing and chemical sensing. They used LC as promising tool in the recognition of biomolecular interactions as well as toxins detection at the aqueous-LC interface.[61,62] In continuation of this development, at present, a large number of scientists in worldwide are involved in utilizing LC in fabrication of biosensors to unveil several unexplored bimolecular interactions. Therefore, we expect in coming days LC will appear as potential medium in exploration of new scientific findings as well as in the development of biosensing.

1.4 Nematic LC

The ongoing interest in using LC in the area of bio-sensing is mainly centered on thermotropic liquid crystal which exhibits nematic phase. This particular type of LC shows mesophase with variation of temperature. They appear in different anisometric shapes like rod like or calamatic, disc like or discotic etc.[63-64] In the nematic phase LC molecules possess certain long range orientational order but they don't have any positional order. The average direction of LC molecules in this phase is denoted by vector n(r) which is called nematic director. This particular phase shows uniaxial behavior because in this phase mesogens can rotate using long axes and therefore there is no possibility of any preferred arrangement along two ends of the mesogens. So, the director vector doesn't have any significant sign *i.e.* n=-n. When viewed under crossed polars, nematic phase appears as thread like texture (Figure 1.3. A). The term nematic has been given for this reason. In Greek language nematic means thread.[65]

The widely used commercial nematic LC for sensing purpose are 4-cyano-4'-n-pentylbiphenyl (5CB), E7 etc.[66-68] 5CB shows room temperature LC property in the temperature range from 18° C to 35° C. E7 is a mixture of different types of alkoxycyanobiphenyls such that, 51 wt.% of 5CB, 16 wt.% of 4-cyano-4'-n-oxyoctylbiphenyl (8OCB), 8 wt.% of 4-cyano-4'-n-penty-p-terphenyl (5CT), 25 wt.% of 4-cyano-4'-n-heptyl-biphenyl (7CB) (Figure 1.3. B, C). E7 also exhibits LC properties in the wide temperature range from -10 °C to 60°C. In this thesis the entire work has been performed using nematic room temperature LC.

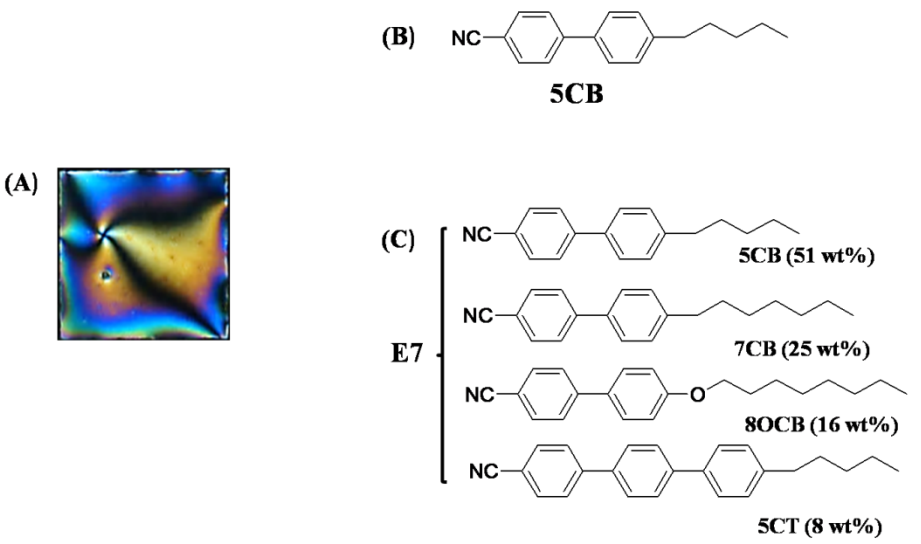

Figure 1.3 (A) Polarized optical microscope view of nematic LC. (B) and (C) represent chemical structure of 5CB and E7 respectively.

It is also important to discuss on the physical significance of the ordering of nematic LC. The average orientation of mesogens is indicated by the parameter S. This parameter represents a Legendre polynomial which gives the insights into the orientational ordering of LC.[69,70] In this equation θ represents the angle formed between the nematic director and local mesogen orientation. The optical property like birefringence of LC material is dependent on the value of S. For LC S value comes in range between 0.3 and 0.8. For isotropic or liquid compound, where molecules are completely disarranged, S value is 0. In crystalline material where all molecules are positionally ordered, S value is 1.

$$S = < P_2(\cos\theta) > = < \frac{3\cos^2\theta - 1}{2} > \qquad (1.1)$$

1.5 Functions and properties of nematic LC at the interface

The wide applications of nematic LC in the area of bio-sensing are entirely dependent of interfacial behavior of LC. Therefore it is very important to discuss on interfacial properties of nematic LC.

1.5.1 Orientation-dependent surface energetics of nematic LC

As already discussed earlier, LC molecules, when confined in surface, orient themselves to certain direction to minimize surface free energy. The average direction of mesogen is denoted by nematic director. The orientation at which mesogens possess minimum free energy is denoted by nematic director termed as "easy axis" (Figure 1.4). Any external disturbance at the surface causes the deviation of nematic director from the easy axis. The amount of energy required for this deviation is known as surface anchoring energy. This anchoring energy set the scale of energetics that dependent on the orientation of mesogens. The following equation describes the relation.

$$\boldsymbol{S = S_0 + \frac{1}{2} W_a \, Sin^2(\theta_s - \theta_e)} \text{.....(1.2)}$$

W_a is anchoring energy, S is interfacial free energy, S_0 is interfacial free energy that independent on the orientation of mesogen, θ_s is orientation surface director and θ_e is orientation of easy axis.

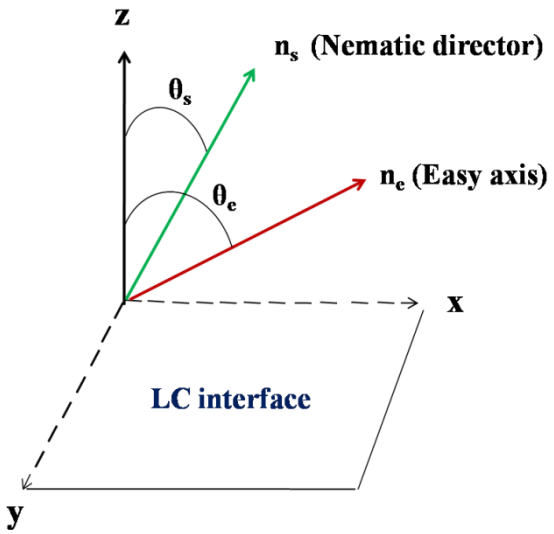

Figure 1.4 Orientation of LC at the interface.

For nematic LC, the value of S falls in the range between 10^{-3} to 1 mJ/m^2. Due to this small range of value, any little disturbance by external stimuli at the interface could lead towards change in the orientation of LC. This phenomenon is the key factor behind the application of nematic LC in bio-sensing.[71] For isotropic compounds, S value is very high nearly 72 mJ/m^2. Therefore, very high magnitude of force is required to alter any orientation of surface molecules.

1.5.2 Elastic property of nematic LC

When confined in a surface, mesogens in LC near the surface can communicate within the bulk phase of mesogen upto a distance of 1-100 mm. This is called cooperative interaction of the LC. If the orientation of mesogen at the interface is disturbed by external stimuli that will be communicated into the bulk phase this upto 1-100 mm. This long range orientational ordering of mesogens imposes elasticity in LC phase. When orientation of LC in a confined surface is defined, the elastic property in LC leads to distortion of nematic director.[72] Three major deformations observed in nematic LC, splay, bend and twist as shown in following Figure 1.5.

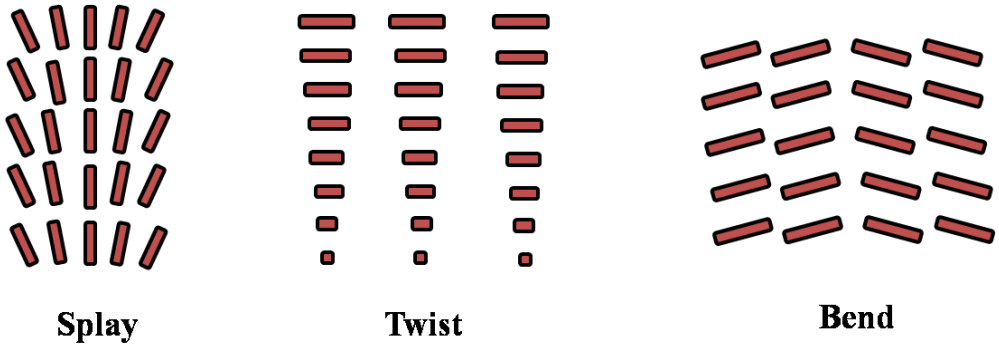

Figure 1.5 Cartoon diagrams of three deformations of nematic LC splay, twist and bend.

To put insight into the energetic for the deviation of LC orientation from its uniform alignment, we need to understand equilibrium profile of nematic LC director. For this we need to follow a continuum approximation. With help of Frank and Oseen equation, we can explain the possible curvatures of nematic director with respect to three types of deformations, splay, twist and blend. These three deformations are associated with three

elastic constants, K_{11}, K_{12} and K_{13} respectively. These elastic constants are temperature dependent. For nematic LC the elastic constants values are in order of 10^{-11} N

The elastic free energy density is related to the strain of nematic LC, which has been expressed using following equation.

$$\boldsymbol{F_d = \frac{1}{2}K_{11}\ (\nabla.\underline{n})^2 + \frac{1}{2}K_{22}\ (\underline{n}.\nabla\times\underline{n})^2 + \frac{1}{2}K_{33}\ (\underline{n}.\nabla\times\underline{n}\times(\nabla\times\underline{n}))^2 \ldots\ldots\ldots\ldots (1.3)}$$

So, the total free energy of LC confined any surface is combination of the free elastic energy stored in the LC and surface anchoring energy of LC. Overall, total free energy of LC regulates interfacial behavior of LC.

1.5.3 Optical anisotropy of LC

LC material exhibits birefringence property. Birefringence arises when refraction index of polarized light, passes through LC medium, in one direction is different from two other directions. Both uniaxial and biaxial LC shows birefringence. When the refractive index is perpendicular to the nematic director, it is known as ordinary index (n_o) and parallel refractive index to the nematic director is known as extraordinary index (n_e). Therefore birefringence property any LC material is defined as $\Delta n = n_e - n_o$. If any LC material has $n_e > n_o$ the material is termed as positive uniaxial material. In vice versa, When $n_o > n_e$ the material is termed as negative uniaxial material. The order parameter of LC is directly related to the difference of square of these to refractive indices *i.e.* $n_e^2 - n_o^2$.

Due to this optical anistropic property of LC, when light passes through LC medium, the velocity of light differ from each other along perpendicular and parallel directions with respect to nematic director. Therefore we observe LC material showing colored texture under crossed polar. Overall the birefringence property is the key factor for the application of LC in biosensing.

1.5.4. Directional behavior of mesongens during surface anchoring LC

During surface anchoring of liquid crystal, mesogens align themselves in certain angle with respect to nematic director. This orientation of mesogen is described using two different angles namely, polar angle (θ) and azimuthal angle (ϕ). Polar angle is the angle between

nematic director and the normal with respect to surface. Azimuthal angle is the angle between nematic director and in plane azimuthal axis. Orientation of mesogens can be three types with respect to Polar angle. When $\theta = 90°$, the anchoring is defined as homeotropic anchoring. When $\theta = 0°$, the meogens adopt planar anchoring and when θ value is in between 0° and 90°, the anchoring of LC is called tilted anchoring. Similarly, depending on azimuthal angle, LC can adopt two different orientations, first, uniform anchoring with average azimuthal orientation and second, degenerate anchoring with equally probable azimuthal orientations.

1.6 Practical approach of utilizing LC interface in biosensing

In past few years LC has been introduced as potential medium in the area of bio-sensing. As already discussed above some special properties of LC like elasticity, surface anchoring and birefringence enable LC to be responsive towards recognition of several biomolecular interactions which, in turn, can be amplified to simple visual observation. Presence of any external stimuli or modification of surface topography results in change in orientational ordering of nematic LC. As LC is birefringent in nature, such orientational transition of LC appears as different colour when viewed under crossed polars. Thus LC has become a simple tool to study biomolecular interactions without help of any complex instrumentation. The entire work described in this thesis involves the application of the interface formed between nematic LC (5CB) and aqueous solution containing biomolecules. The use of aqueous solution provides similar physiological environment and low elasticity of nematic LC make the interface more distortable.

Past studies have reported several approaches to fabricate the interface formed between LC and aqueous phase. The widely used method involves the assembly of optical wells, glass surface, TEM grid and micro pillar. In this method, first the glass surface is chemically functionalized to allow firm establishment of nematic LC over it. In particular, the glass slides are coated with some hydrophobic compounds such as, *N*,*N*–dimethyl-*N*-octadecyl-3 aminopropyltrimethoxysilyl chloride (DMOAP), octadecyltrichlorosilane (OTS) etc. such hydrophobic coating on glass slides orients LC in homeotropic fashion over it. In other method, gold deposited glass slides are coated with self assembled monolayers of alkanethiols. LC aligns in planar or tilted fashion on this kind of coated surface.[73] The role

of TEM grid is to confine LC on the chemically modified glass surface. Using any micro syringe or capillary tube all the small squares can be filled with LC. In next step, This LC filled gold grid supported on glass slides is immersed into water. At this condition, LC adopts planar orientation at the aqueous-LC interface but at the glass surface LC remains hydrophobic due to strong hydrophobic interaction between mesogens and coating agent.

When viewed this assembly under crossed polar, LC appeared in bright colorful texture, due to its planar alignment at the interface. When certain biomolecules are introduced into aqueous solution, the optical appearance of LC changes from bright to dark, indicating homeotropic alignment of LC at the interface (Figure 1.6). Here this type of switch of optical appearance of LC bright to dark depends on the chemical structures of adsorbed biomolecules at the interface. It has been observed that amphiphiles like surfactants, phospholipids induce homeotropic alignment of LC at the aqueous-LC interface.[74] The homeotropic alignment of LC arises due to strong hydrophobic interaction between long alkyl chains of LC and long fatty acid moiety of lipids or surfactants. Overall the long range ordering of mesogens and elasticity enable LC an easily tunable medium for the recognition of biomolecular interaction at the interface. In literature it has been well documented that chemically functionalized aqueous-LC interface can be employed as model system to replicate certain biological phenomena at the interface. Therefore application LC medium as biosensor offers a facile approach where the interface can be easily tunable through manipulation of biomolecular environment exposed at interface and long range orientational ordering of LC. Past studies have shown the lipid or surfactant decorated aqueous-LC interface could be useful in recognition of several kind of proteins, even different physical state of same protein also possible to differentiate. Many membrane phospholipid-peptide interactions has been successfully characterized at the aqueous-LC interface, which further helps in understanding different toxin activity on mammalian cell membrane. In addition to that different substrate specific enzymetic reactions for example trypsin activity, catalase activity have been successfully studied at the aqueous-LC interface. More recently sensing of DNA hybridization, aptamer based heavy metal ion detection, antigen-antibody detection, tumor cell marking etc. have been widely studied at the aqueous-LC interface. In comparison to conventional biosensing approaches for example nuclear magnetic resonance (NMR),[75] fourier-transform infrared (FTIR)

spectroscopy,[76] electron spin resonance (ESR),[77] surface plasmon resonance (SPR),[78] calcein release assay,[79] fluorescence study[80] etc, LC based interfacial shows superiority in terms of simplicity, robustness, cost- effectiveness and non requirement of complex instrumentations.

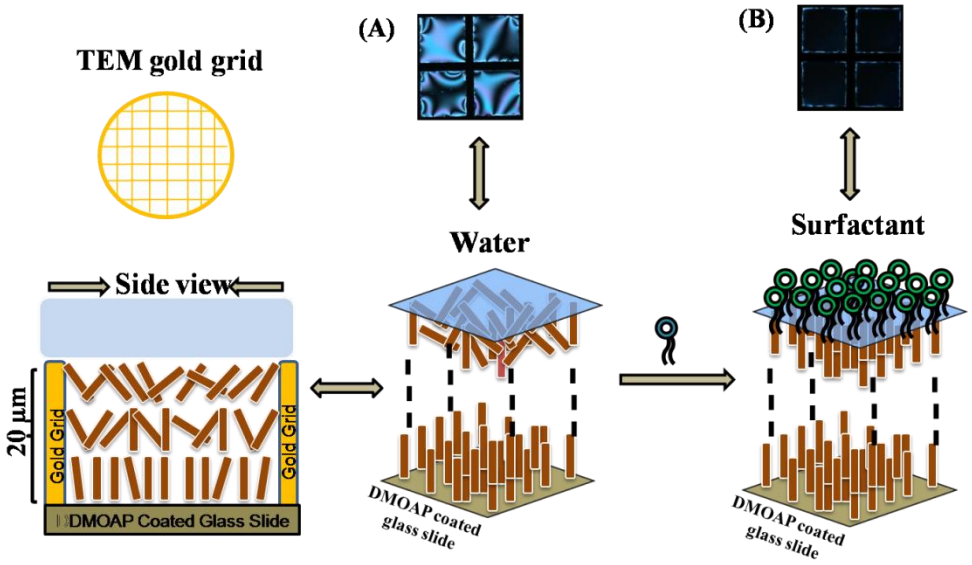

Figure 1.6 Cartoon representation of aqueous-LC interface. Polarizied optical microscope images and corresponding schematic diagrams of anchoring of LC of A) in water, B) in presence of surfactant.

1.7 Important biomolecules mentioned in different chapters in this thesis

1.7.1 Lipopolysachchaide or bacterial endotoxin

Lipopolysachcharide (LPS) also known as bacterial endotoxin is outermost cell membrane component of gram negative bacteria. The primary function of endotoxin is to provide a protective barrier on bacterial cell membrane which could be impermeable towards any foreign substances.[81] When bacteria attacks animals, endotoxin releases from bacterial cell memebrane and impedes into animal cell membrane and interacts with several serum components. The toxicity imposed by endotoxin in animals depends on its interaction with blood serum components. The toxic effect of LPS was first discovered by German physician Richard Pfeiffer. LPS is composed of central lipid moiety (Lipid A) and outer O-antigen moiety. Among these Lipid A is most conserved part of LPS, responsible for

inducing toxicity in animal host. Lipid A moiety is made of long polysaccharide units branched with long lipid chains of variable lengths. The unit of polysaccharide moieties and length of lateral lipid chains varies with strains and species of gram negative bacterial. LPS takes active role towards inflammatory response when bacteria attack animal host.[82]

Another fatal activity of LPS on animal host is inducing sepsis. In blood serum, LPS get phagocystosed by macrophages. The macrophages generate several sepsis mediators like Interleukin-1, interleukin-2, tumor necrosis factor α (TNF α), reactive oxygen species etc. These mediators cause several septic syndromes like, septic shock, high fever, multiple organ failure etc. When LPS induced septic mediators release in large amount in certain environment, The septic shock becomes lethal to the host animals.[83] Overall, the entitre activites of endotoxin in animal host depend on its interaction with blood serum proteins. Some proteins enhance its activity (for example hemoglobin, serum albumin) and some proteins function in opposite way (e.g. lysozyme, lactoferrin). Therefore, there should be some precise, sensitive methods to careful recognition of bacterial endotoxin with serum proteins.

1.7.2 Phospholipids

Phospholipids are main building blocks of animal cell membrane. They form protective lipid bilayers in cell membrane. This bilayers help in passage essential neutrients across the cell membrane, regulates osmotic pressure.[84] On the other hand bilayers prevents cell from the attack of foreign toxic substances. Most of the Phospholipids are composed of phosphate group containing di or tri glyceride head group and long fatty acid chains of varying length depending on types of phospholipids. The head group of phospholipid is hydrophilic in nature and the long tail shows hydrophobic property. The first isolated phospholipid from animal cell membrane was phosphocholine. French chemist Theodore Nicolas Gobley successfully extracted phosphocoline from egg yolk. During formation of lipid bilayers long chains in phospholipids aggregate with each other due to hydrophobic interaction. In cell membrane phospholipids are found to adhere to several components like proteins, sterols glycolipids etc.[85]

In cell membrane phosphlipids layers acts as semi permeable membrane. It allows only selective molecules to enter into cell and thus maintain cell integrity. Phospholipid can be broken down in the cell and energy released is helpful for operating several cellular functions. Phospholipids broke into smaller molecules which also take part in separate cellular functions. Phospholipids also found in different joint areas of body like elbow, knee where Phospholipids help in lubricating muscle fibers. Phospholipids act as precursor in prostaglandin signal pathways.[86] Enzyme lipase use phospholipids to synthesis prostaglandin. Apart from its protective role in biological cell membrane, phospholipids, *in vitro* are widely used in preparation of liposomes, ethosomes etc. They are also used in preparation of several drugs in purpose of increasing bio-compatibility of those drugs and decreasing toxicity. Phospholipids are also used in preparation of synthetic membranes. In food industry phospholipids are widely used as emulsifier and food additive. Common sources of phospholipids are eggs, milk, soybean, sunflower seeds etc.

There are lacks of simple techniques to characterize phospholipids. They are often characterized using dual polarization interferometry, in which order and disruption of lipid bilayers is measured. Apart from this they are often characterized on basis of measuring the abundance of total available phosphorus in phospholipids and total mass of phospholipids based on molecular weight of fatty acids. ^{31}P-NMR, HPLC-ELSD are few available techniques to characterize phospholipids.

The following phospholipids (Figure 1.7) have been addressed in different study reported in this thesis.

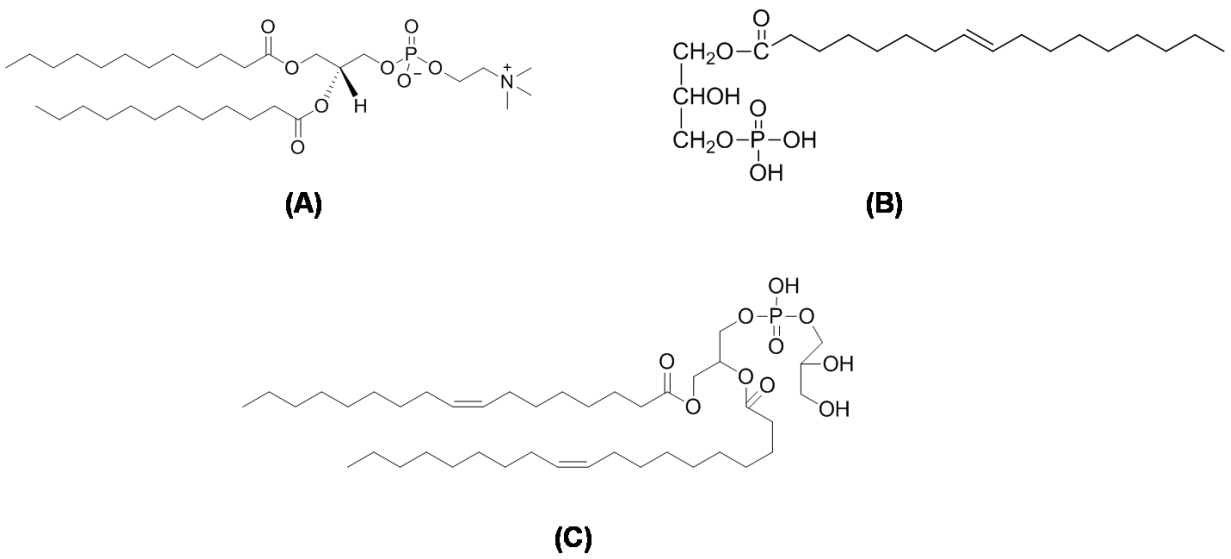

Figure 1.7 Chemical structures of (A) 1,2-Didodecanoyl-Sn-glycerol-3-phosphocholine (**DLPC**), (B) lysophosphatidic acid (**LPA**) and (C) 1,2-dioleoyl-Sn-glycero-3 phospho-rac-(1-glycerol) (**DOPG**)

1.7.3 Hemoglobin

Hemoglobin (Hb) is major oxygen carrier protein found in red blood cell of all types of vertebrates. Hb is iron containing metallo-protein which carries oxygen from respiratory organs (lungs, gills) to the entire parts of body where oxygen is utilized as fuel to process aerobic respiration to produce energy.[87] This phenomenon is known as metabolism.

Hemoglobin is a combined form of four units of globular proteins. Each unit contains Prosthetic heme group deeply shielded with protein chains. All four proteins units exist in alpha helical conformation. The heme group consists of central Fe ion coordinated to porphyrin ring. The heme moiety play important role in binding oxygen in reversible fashion. The sixth vacant coordination of Fe is available for binding oxygen. When oxygen binds to the heme group, oxyhemoglobin is formed. Then this oxyhemoglobin travels through blood stream and release oxygen at different cell terminals, where oxygen is consumed to generated energy. The oxygen binding capacity of Hb is 1.3 mL oxygen per gram. Thus it increases oxygen carrying capacity of blood at about 20 folds.[88]

Hemoglobin deficiency can cause anemia. In this case, blood oxygen carrying capacity of hemoglobin decreases to a significant extent. The common sources of deficiency of Hb are kidney failure, sickle cell disease, nutrition deficiency; bone marrow abnormality etc. sometimes due to mutation in globular proteins in Hb, oxygen carrying capacity of Hb gets altered. This is known as hemoglobinopathies, which is responsible for thalassemia. Iron deficiency in Hb causes iron deficiency anemia. In vice versa, if Hb levels in blood cells gets elevated, the size of red blood cell increases. This is known as polycythemia. Polycythemia causes pulmonary dysfunction, congenital heart disease etc. The reasons behind abnormal increase of Hb level in blood are excessive smoking, dehydration, lungs disease, growth of certain tumors etc.

Normal level of Hb in men is from 13.5 to 18 g/dL, in women 12 to 15.3 g/dL and in children 11 to 16 g/dL. Conventional methods to measure Hb levels in blood samples are CO-oximetry and hematology analyzer. Apart from this the concentration of oxyhemoglobin and deoxyhemoglobin can be monitored with help of Infrared spectroscopy.[89] More recently, magnetic resonance imaging technique has been used to measure the amount of Hb present in red blood cells.

1.7.4 Serum albumin

Serum albumin (SA) is a globular protein found in vertebrate blood serum. SA acts as a carrier of several biomolecules in different parts of body. SA is produced in liver. This is the most abundant carrier protein present in blood serum.[90] SA is a glycosataed globular protein having molecular mass 66 kDa. In physiological pH, SA is negatively charged. SA exists in α helical conformation in blood serum. This conformation is very essential to provide protein a thermodynamically stable shape and also to regulate blood pressure. Normal level of SA in blood serum is 3.5-5 mg/dL.

The main function of SA is to carry several biomolecules for example, proteins, fatty acids, sterols, and hormones to different parts of body. SA also helps in maintaining volume of extracullar fluid and thus controls oncotic pressure.[91] SA proteins of human and bovine are also used in various commercial purposes for example, as cell culture media, laboratory reagent, immunodiagnostic reagent etc. SA solution is also used for replacement of loss

fluid and to control blood fluid volume for trauma, surgery patient. The presence of SA in urine is considered as marker of kidney failure. SA is characterized from change in absorption spectra on its interaction with fluorescent bromocresol green.[92] Low level of SA in blood serum is known as hypoalbuminemia which is caused by malnutrition, kidney failure, liver dysfunction etc. Excess level of SA in blood serum is known as hyperalbuminemia which is caused due to dehydration and high protein intake.

1.7.5 Lysozyme

Lysozyme (LZM) is an immuno protein, found in secretions of wide range of animals. LZM exhibits antibacterial and anti microbial properties and therefore builds a strong immune system in animal body.[93] LZM is most abundant in saliva, tears, breast milk, mucus etc. Egg white is good commercial source of LZM. LZM is thermally stable proteins with high melting point 72° C. The isoelectric point of LZM is very high 11.3. Therefore, in physiological pH LZM holds positive charge. In 1922, the famous microbiologist Alexander Fleming first isolated LZM from egg white.[94] He first observed antibacterial property of LZM.

LZM is antibacterial in nature. It functions in enzymatic fashion. It binds with peptidoglycan, which is major building block of bacterial cell membrane. LZM hydrolyzes and breaks glyocosidic bond formed between n-acetyl muramic acid (NAM) and N-acetyl glucosamine (NAG). Thus it destroys cell membrane intergrity of bacteria and causes lysis of cell.[95] Apart from this commercially produced LZM is used in catalysis and biomedical application. The activity of LZM is highest in the pH range from 6 to 7.

1.7.6 Lactoferrin

Lactoferrin (Lf) is a globular glyco protein of transferrin family. It exhibits antibacterial, antimicrobial property. Lf is widely found in different kind of animal secretions like, milk, mucous, saliva etc. Human milk contains highest amount of Lf (700 mg/L). Lf exists in mostly tetrameric form under physiological pH.[96] In blood serum Lf exists in both monomer and tetramer in of 1:4. With increasing concentration of Lf, tetrameric form starts to predominate. Lf exists in α helical conformation in physiological pH. With help of X ray diffraction study it has been observed that Lf consists of two lobes namely, N-

terminal domain and C- terminal domain. Each domain contains one iron atom in center and long carbohydrate chain at the terminal. Lf also binds with other metal ions like copper, zinc in reversible fashion. Lf has the highest iron binding affinity compared to other transferring proteins. In acidic pH Lf shows highest activity to sequester iron. Therefore, in case of inflammation, muscle strain, when lactic acid accumulates in muscle tissue, iron transfers to Lf from tranferrin.

Lf shows antibacterial properties and helps in building immune system in body. Lf binds with LPS of gram negative bacteria.[97] Strong interaction between Lf and LPS damages cell wall integrity of bacteria, resulting in lysis of cell. Lf also shows anti viral activities. Lf suppresses replication of virus inside mammalian cell. Lf also binds with virus and destroys its activity. In some cases Lf binds with same lipoprotein where virus prefers to interact and thus repels virus to settle on mammalian cell membrane. Lf also has been found to exhibit some antifungal activities. It inhibits the growth of diploid fungi responsible for skin disease. Apart from these, Lf also helps in bone formation, binds with double stranded DNA, takes part in hydrolyzing RNA and thus stops reverse transcription of RNA genome responsible for breast cancer. Lf also has been used in clinical purpose. In dry eye syndrome where Lf level in tear decreases, Lf solution is incorporated in body to bring back tear volume to normal range.[98] Commercially produced Lf is widely used in yogurts, baby foods, chewing gums etc.

1.7.7 Peptidoglycan

Peptidoglycan (PG) is outer cell membrane component of bacteria. It forms mesh like three dimentional structure and helps in providing stability in bacterial cell membrane.[99] PG is polysachchride compound where each alternative monosaccharide unit is linked with a tetrapeptide. Each unit of PG is consists of two amino sugars, *N*-acetyl muramic acid (NAM) and *N*-acetyl glucosamine (NAG). NAM and NAG are connected with β-(1,4) glycosidic bond. Each NAM is connected with a small tetra peptide chain (Figure 1.8). The types of amino acids present in peptide chain vary with genre of bacteria. Crosslinking between peptide chains of different PG molecules form a large three dimensional rigid network which provides stability to bacterial cell membrane. The PG layer is thicker in Gram positive bacteria about 80 nm compared to that of Gram negative bacteria (about 7

nm). Thus determination of amount of PG can lead to characterization of strain of bacteria.[100]

Some antibacterial proteins like Lf, LZM have found to bind with PG and resulting in hydrolyzing glycosidic bonds between NAG and NAM. Some antibacterial drug like penicillin also have been found to damage three dimensional structure of PG and thus causes lyses of bacterial cell.[101]

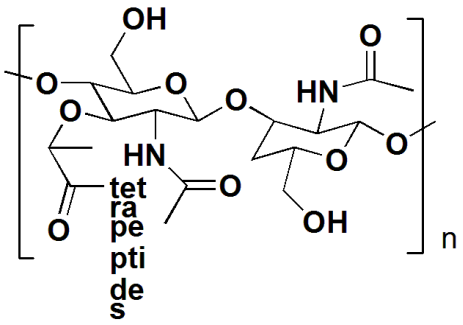

Figure 1.8 Chemical structure of peptidoglycan

1.7.8 Lipoteichoic acid

Lipoteichoic acid (LTA) is the outer cell membrane component of Gram positive bacteria.[102] LTA form thick layer upto 80 nm over the layer of PG. LTA is a polymer consists of ribitol phosphate and polysaccharides connected with phosphodiester moiety (Figure 1.9). LTA binds with a lipid chain on cytoplasmic membrane of Gram positive bacteria. It forms crosslinkage with terminal peptides of PG and helps in formation of three dimensional rigid structures.

The major function of LTA is to form stable and rigid layer on outer cell membrane of Gram positive bacteria and protect bacterial cell from attack of antibiotics. LTA also participate in cell growth mechanism in bacterial cell.[103] LTA functions as a receptor molecule on cell membrane and allows the passage of sodium, calcium ions across the cell membrane. When bacteria attack animal cell, LTA binds with animal cell membrane. LTA also binds with Toll like receptor 2, CD14 and thus helps in generate inflammation by up regulating release of interleukin-10.[104]

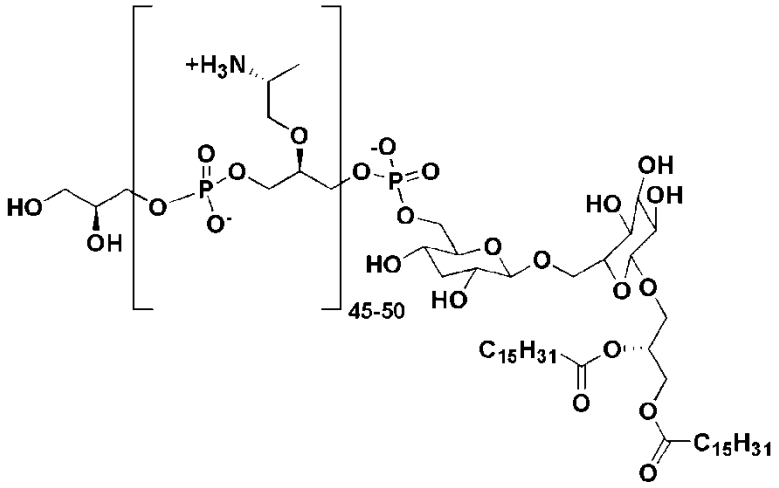

Figure 1.9 Chemical structure of lipteichoic acid.

1.7.9 Melittin

Melittin (Mt) is the main component of honey bee (*Apis mellifera*) venom or apitoxin. It consists of more than 60% weight of bee venom. Mt is a small polypeptide containing only 26 amino acids.[105] The entire structure of Mt can be divided into two parts N-terminal and C-terminal. C- terminal part consists of basic amino acids and therefore hydrophilic in nature. N-terminal part is composed of amino acids having alkyl side groups and therefore hydrophobic in nature. In aqueous solution melittin exists as tetramer. Under physiological pH Mt adopts α helical conformation. The complete sequence of Mt is NH_2-Gly-Ile-Gly-Ala-Val-Leu-Lys-Val-Leu-Thr-Thr-Gly-Leu-Pro-Ala-Leu-Ile-Ser-Trp-Ile-Lys-Arg-Lys-Arg-Gln-Gln-$CONH_2$. In neutral pH Mt shows cationic property bearing +6 charges.

Mt activates pain receptor in mammalian cell and increases pain sensation. When honey bee stings on animal skin, Mt releases with bee venom and interacts with phospholipids bilayers of skin. First Positively charged C-terminal domain of Mt interacts with lipid biyers through electrostatic interaction with negative charged phosphate of lipids. Then hydrophobic N- terminal domain starts interacting with long alkyl chains of phospholipids and thus enters into the self-assembly of phospholipids of bilayers.[106] This action of Mt results in disintegration of bilayer structure and collapse of membrane. Once membrane is collapsed, venom can easily spread into the blood serum and starts inflammation. Besides the pore formation on membrane Mt also binds with blood vessels and destroys red blood

cells. Mt activates nociceptor and helps in releasing Pro-inflmmatory cytokines which is mainly responsible for increasing pain sensation. In cell membrane Mt shows strong affinity towards Ca^{2+} and results in increasing ion permeability across the cell membrane. Mt blocks Na^{+}/K^{+} transport ion pump and results in morphological and functional change in cell membrane. Mt also inhibits functions of different Ca^{2+} proteins (calmodulin, myosin) by sequestering Ca^{2+} ions from those proteins.[107] Very few biological assays, namely isothermal titration calorimetry, fluorescence quenching, calcein release assay, circular dichroism are available to recognize the mode of action of mellitin on phospholipid membrane. Therefore reliable and precise methods are required to study such interactions.

Recently, Mt also has been used for clinical purpose. Mt is targeted to bind with tumor cell membrane so that it can cause lyses of tumor cell.

1.8 Instrumental techniques used in different studies mentioned in the thesis

1.8.1 Polarizing optical microscope

Polarizing optical microscope (POM) is the principle technique to characterize the orientation of LC.[108] In POM, LC appears in different colors and textures which are the indicators of different orientational ordering of LC. In this microscope sample is placed on sample plate kept between two polarizers. Both polarizers are placed perpendicular to each other. Polarizer that placed bottom of the POM can linearly polarizes a light coming from halogen bulb, the light source. When linearly polarized light is transmitted through LC, the plane of polarizantion of light could be altered depending on the orientation of LC.[109,110] The reason behind this is the LC shows birefringence and has two different indices of refraction. If the mesogens are in tilted or planar orientation at the interface, the plane of transmitted polarized light changes and the light passes through analyzer. Therefore, we observe colored and bright texture through objectives. But when LC adopts homeotropic alignment *i.e.* in perpendicular with respect to surface as well as interface, the transmitted light gets completely blocked by analyzer. Therefore we observe dark optical view under crossed polars. Overall this is working principle of POM in characterizing the orientation of LC.

1.8.2 Polarization modulation infrared reflection absorption spectroscopy

Polarization modulation infrared reflection absorption spectroscopy (PM-IRRAS) is a modern version of infrared spectroscopy to characterize the presence of any surface bound organic molecules. This technique is very appropriate for studying organic thin films, monolayers, self assembly etc.[111,112] The primary criterion of studying thin organic film coated surface based on this technique is the bottom part of the surface has to be reflecting in nature (made of metal or coated with metal). In this technique linearly polarized IR light get modulated into s polarized and p polarized light beam by photoelastic modulator (PEM). The absorbtion of polarized IR light by the molecules of thin film depends on the dielectric property of metal. When polarized light falls on thin film, the dipole moment of coated molecules and light beam interacts with metal electron. According dipole selection rule, the perpendicular component of dipole moment will be excited whereas parallel component of the surface will be screened by metal electron. Now between s and p polarized lights, s polarized light gets eliminated due to destructive interference and p polarized light gets absorbed by the thin films coated on metal surface. At grazing incident angle the absorbence of p polarized light increased many fold and we can detect presence of molecules in thin film from the infrared reflectance spectrum.[113]

1.8.3 Vibrational circular dichroism

Vibrational circular dichroism (VCD) is a spectroscopic method where circularly polarized IR light is passed through the sample and the difference between attenuation of right and left polarized light is captured in detector.[114] The circularly polarized IR passed through the sample is dependent on molecular orientation of compounds. Therefore this technique provides valuable information about three dimensional structures of proteins, peptides etc.[115-117]

The interaction of right and left polarized light with chiral molecule is different in case of each enantiomer. Therefore, there will be difference in absorbance of left polarized light (A_L) and right polarized light (A_R) in optically active compounds. The absorbance difference $\Delta A = A_L - A_R \neq 0$ for chiral molecules. But in case of achiral molecule or recemic mixture $\Delta A = A_L - A_R = 0$. VCD spectra are recorded in form of transmission with intensity

ranging from 10^{-4} to 10^{-5}. A Michelson-Morley interferometer is used to irradiate sample with light having long range of wavelengths coming from the pattern of periodical constructive and destructive interference. The periodical pattern of interference arise due to back and forth movement of a mirror placed inside interferometer. Slow movement speed of mirror and longer range of movement results in better resolution of spectrum and high signal to noise ratio. To measure the difference between the absorbance of A_L and A_R, modulation of polarization state is required in periodical fashion. For this purpose photoelastic modulator (PEM) is used in VCD. PEM is made of ZnSe crystal which shows change in birefringence with variation of stress applied on it. With periodical variation of stress on PEM, linearly polarized light modulates into circular polarization. Highly sensitive and fast detector is required to get high resolution VCD spectra. In general, MCT detector cooled in liquid nitrogen is used for VCD. Using this type of detector we can record spectra in broad range from 800 cm^{-1} to 4000 cm^{-1}

The sample was held inside a demountable cell with BaF_2 windows and a 100 μm spacer. Spectra were measured in D_2O solvent. For all measurements, the intensity calibration factor was obtained using a multiple-wave retardation plate combined with the second wire grid polarizer, whereby the system tuning was exactly the same as for the sample measurement. The spectra were corrected by subtracting the absorption (or VCD) of the corresponding solvent

1.8.4 Langmuir Blodgett technique

LB technique provides a method to organize molecular assembly in a uniform fashion. In this technique organic molecules form monolayer on water and then this monolayer is transferred on solid surface. In this technique we can have control any film or coating at molecular level and able to maintain desired thickness of the layer. The Monolayer of molecules forms on water known as LB film and the assembly on which the experiment is done is known as LB trough. Now a day's LB technique has wide applications in optics, electronics, lithography, biosensing etc.[118,1119]

The invention of this technique is credited to an American scientist Benjamin Franklin. He observed the behavior of an oil drop on pond water and the idea of floating monolayer in

thin film struck in his mind. Later on Irving Langmuir and his assistant Katherine blodegett built up this technique. Langmuir was awarded noble prize for this in 1932. Langmuir later modified and developed several new methods of transferring monolayer on solid surface. The attractive features of LB techniques are intrinsic control over molecular organization on thin films as well as thickness of the film deposited on solid support. We can get thin coating of desired material of different functionalities and therefore able to engineer the surface at molecular level. For the formation of LB film, the chosen molecule must be water insoluble and soluble in some volatile solvents like chloroform, methanol etc. In general, amphiphilic compounds are ideal for formation of LB films.[120] This types of compounds are consist of two parts polar head group (for example, OH, COOH functionalities) and non polar or hydrophobic tail (for example long alkyl chains). When amphiphlic molecules are introduced at air water interface, they tend to organize by pointing non polar tail towards air and polar head towards water. The entire techniques consist of three important assemblies, namely, trough, pressure balance and barrier. LB trough contains the subphase on which dilute solution of desired molecules are added. Volatile solvent evaporate quickly and the chosen molecules spreads over the surface of subphase. In this case wilhelmey plate, a small piece of filter paper intercepting air-water interface hanging from a rod attached to microbalance, is used to determine surface pressure (π) during the formation of monolayer. To control the surface pressure and organize molecules in a monolayer the barriers from both sides are compressed with a constant compression rate. Surface pressure and trough area are recorded simultaneously using Nima software. Based on the volume of the solution added, molecular weight of the compound and concentration of solution, the average area per molecule was calculated. From Surface pressure (p)–area per molecule (A_m) isotherm, we can accurately control and monitor the formation of Monolayer.[121] From this isotherm we can observe monolayer forms at a certain surface pressure. On further increasing surface pressure causes collapse of the monolayer.

1.9 Outline of thesis

The results depicted in the thesis represent thermotropic liquid crystal as robust innovative sensing tool for imaging molecular level biological interactions occur at the aqueous-LC

interface. Due to long range ordering in the LC phase, chemical or biomolecular phenomenon occurring at the aqueous-LC interface can be precisely reported by rapid ordering rearrangements of interfacial mesogens. Keeping this promising responsiveness of LC towards biological interactions in mind, we address further development in the fabrication of LC interface to transduce and amplify several biomolecular events in specific and sensitive way. Therefore, here, we aim to provide the basis of new approaches to the design of interface comprise of stimuli-responsive soft materials for the detection of several biomolecular interaction.

Second chapter reports the fabrication of LC based stimuli-responsive interface for imaging of LPS–protein binding events through interfacial ordering transition of LC. We demonstrated that the optical response of the LC changes from dark to bright after exposure of aqueous solutions of different proteins such as hemoglobin (Hb), bovine serum albumin (BSA), and lysozyme (LZM) onto LPS-laden aqueous–LC interface. The consequence of interactions of different proteins with LPS is also found to differ from one to another in terms of ordering transition of interfacial LC. Furthermore measurements of optical retardance value of LC during LPS-protein binding events at the interface provides a quantitative insight into protein–LPS binding affinity. Interestingly, we found that the retardation values were in accord with the binding constants values between LPS and different proteins; a higher binding constant resulted in a greater tilt angle of LC (LPS-Hb>LPS-BSA>LPS-LZM) Overall the entire result provide a noble analytical approach to report LPS-protein binding event in a quantitative way.

Third chapter advances simple, robust experimental design for imaging the interaction of LPS with peptidoglycan (PG) and lipoteichoic acid (LTA). We observe optical appearance of nematic 4-cyano-4’-pentylbiphenyl (5CB) LC undergoes from dark to bright on exposure of an aqueous solution of PG and LTA on LPS–laden aqueous–LC interfaces implying strong interaction between PG and LTA with interfacially laden LPS. We also have found these interactions of PG and LTA with LPS are highly specific compared to other lipids. Aditionally, we also put insights into the characterization of the LPS laden aqueous-LC interface using Langmuir–Blodgett technique and PM-IRRAS measurement. Furthermore we have also these binding events by measuring the optical retardance of the

LC at aqueous–LC interface. We affirmed that binding affinity of LTA towards LPS is higher compared to PG. Overall the entire result provide a promising approach to quantify the specific binding of PG and LTA on LPS at the aqueous-LC interface.

Fourth chapter reports an approach to build up a LC based biosensonsors to study the interaction between Lf and LPS. Self assembly of LPS at aqueous-LC interface orients interfacial nematic 4-cyano-4'- pentylbiphenyl (5CB) LC in a homeotropic fashion (exhibiting dark optical image). Whereas, on the exposure of Lf on LPS–laden aqueous-LC interface optical image of LCs changed from dark to bright implying an ordering transition of interfacial LC from homeotropic to tilted/planar state. The ordering transition reveals the strong interfacial binding between Lf and LPS. Using epifluorescence microscopy, we further confirmed the interfacial LPS-Lf binding event by imaging the presence of FITC tagged Lf at the LPS laden aqueous-LC interface. In our experiment, we also found that LPS-Lf binding phenomenon is highly specific over other membrane lipids as well as other milk proteins. Furthermore, we have quantitatively correlated the anchoring transition of 5CB with this interfacial binding event by measuring tilt angle of LCs. Finally, we have looked into the conformational behavior of Lf in solution as well as in presence of LPS using Ciruclar Dichroism (CD) spectroscopy and further confirmed with Vibrational Circular Dichroism (VCD) spectroscopy. As a whole the results mentioned in this chapter establish a new approach to investigate the interaction between LPS and Lf based on ordering transitions of LCS at aqueous-LC interface.

Fifth chapter describes the fabrication of a LC based interface for quantitative imaging of melittin–phospholipid interaction through orientational rearrangement of interfacial 5CB. LC undergoes from dark to bright appearance on exposure of melittin at 1,2-didodecanoyl-*sn*-glycero-3-phosphocholine (DLPC) laden aqueous-LC interface. This observation implies strong interaction of DLPC with melittin at those interfaces. We further explored that reveal that Ca^{2+} plays significant role to accelerate dynamic response of the LC during this binding events. The influence of Ca^{2+} towards kinetics of this binding event is highly specific compared to other alkaline earth metal ions. Adittionally these interactions have been quantified by measuring gray scale light intensity and optical retardance of the LC. Finally, we have put insights into conformational behavior of the melittin in solution as

well as in presence of DLPC vesicles using circulardichroism (CD). We further affirmed our observation using vibrational circular dichroism (VCD) spectroscopy. Overall, the whole experiments demonstrate a promising approach in fabrication of a robust LC based analytical tool to explore and quantify the binding event of melittin with phospholipid membrane at aqueous-LC interface.

Sixth chapter describes overall conclusive interpretation of the entire work mentioned in the thesis.

1.10 References

(1) Orgel, L. E. *Crit. Rev. Biochem. Mol. Biol.* **2004**, *39*, 99–123.

(2) Blum, H. F. *Time's Arrow and Evolution*. Princeton, N. J: Princeton University Press; **1968.**

(3) Urban, J. L.; Kumar, V.; Kono, D. H.; Gomez, C.; Horvath, S. J.; Clayton, J.; Ando, D. G.; Sercarz, E. E.; Hood; L. *Cell* **1988**; *54*, 577–592.

(4) Cupedo, T.; Mebius, R. E. *J. Immunol.*, **2005**, *174*, 21-25.

(5) Albert, R.; Jeong, H.; Barabási, A.-L. *Nature* **2000**, 406, 378-382.

(6) Wagner, A. *Nat. Genet.* **2000**, *24*, 355-361.

(7) Eisenberg, D.; Marcotte, E. M.; Xenarios, I.; Yeates, T. O. *Nature* **2000**, *405*, 823-826.

(8) Hartwell, L. H.; Hopfield, J. J.; Leibler, S.; Murray, A. W. *Nature* **1999**, *402*, 47-52.

(9) Raghuraman, H.; Chattopadhyay, A. *Biosci. Rep.* **2007**, *27*, 189-223.

(10) Frecer, V.; Ho, B.; Ding, J. L. *Antimicrob. Agents Chemother.* **2004**, *48*, 3349-4457.

(11) Lee, M. T.; Chen, F. Y.; Huang, H. W. *Biochemistry* **2004**, *43*, 3590-3599.

(12) Falanga, A.; Cantisani, M.; Pedone, C.; Galderio, S. *Protein Pept. Lett.* **2009**, *16*, 751-759.

(13) Goldsten, I. J.; Hollerman, C. E.; Smith, E. E. *Biochemistry*, **1965**, *4*, 876–883.

(14) Sumner, J. B.; Howell, S. F. *J. Bacterial.* **1936**, *32*, 227-237**.**

(15) Showalter, S. A.; Hall, K. B. *J. Mol. Biol*. **2004**, *335*, 465–480.

(16) Williamson, J. R. *Nat. Struct. Biol.* **2000**. *7*, 834–837.

(17) Tuerk, C.; Gold, L. *Science* **1990**, *3*, 505–510.

(18) Majerfeld, I.; Yarus, M. *Nat. Struct. Biol.* **1994**, *1*, 287–292.

(19) Traxler, P.; Furet, P. *Pharmacol. Ther.* **1999**, *82*, 195–206.

(20) Kinoshita, K.; Sadanami, K.; Kidera, A.; Go, N. *Protein Eng.* **1999**, *12*, 11–14.

(21) Engel, L. S. *Emerg. Med.* **2009**, *41*, 18-27.

(22) Burr, G. O.**;** Burr, M. M. *J. Biol. Chem.* **1929**, *82*, *345-367.*

(23) Vis, H. L. *Postgrad. Med. J.* **1969**, *45*, 107-115.

(24) Li, C.; Tao, Y.; Yang, Y.; Xiang, Y.; Li, G**.** *Anal. Chem*. **2017**, *89*, 5003–5007.

(25) Huang, Y.; Li, H.; Wang, L.; Mao, X.; Li, G. *ACS Appl. Mater. Interfaces* **2016**, *8*, 28202–28207.

(26) Wang, J. H.-C.; Lin, J.-S. *Biomech. Model. Mechanobiol.* **2007**, *6*, 361–371.

(27) Hirst, L. S.; Charras, G. *Nature* **2017**, *544*, 164-165.

(28) Dogic, Z.; Fraden, S. *Langmuir* **2000**, *16*, 7820-7824.

(29) Vollrath, F.; Knight, D. P. *Nature* **2001**, *410*, 541-548**.**

(30) Tan, L. N.; Orler, V. J.; Abbott, N. L. *Langmuir* **2012**, *28*, 6364-6376.

(31) Sidiq, S.; Das, D.; Pal, S. K. *RSC Adv.* **2014**, *4*, 18889-18893.

(32) Agarwal, A.; Sidiq, S.; Setia, S.; Bukusoglu, E.; de Pablo, J. J.; Pal, S. K.; Abbott, N. L. *Small* **2013**, *9*, 2785-2792.

(33) Popov, P.; Honaker, L. W.; Kooijman, E. E.; Mann, E. K.; Jákli, A. I. *Sens. Biosensing Res.* **2016**, *8*, 31-35.

(34) Das, D.; Sidiq, S.; Pal, S. K. *ChemPhysChem* **2015**, *16*, 753–760.

(35) Munir, S.; Park, S. Y. *Sens. Actuator B-Chem.* **2016,** *233*, 559-565.

(36) Bi, X.; Hartono, D.; Yang, K.-L. *Adv. Funct. Mater.* **2009**, *19*, 3760–3765.

(37) Das, D.; Sidiq, S.; Pal, S. K., *RSC Adv.* **2015**, *5*, 66476–66486.

(38) Hartono, D.; Bi, X.; Yang, K. L.; Yung, L. Y. L. *Adv. Funct. Mater*. **2008**, *18*, 2938-2945.

(39) Sidiq, S.; Verma, I.; Pal, S. K. *Langmuir* **2015**, *31*, 4741–4751.

(40) Verma, I.; Sidiq, S.; Pal, S. K. *Liq. Cryst*. **2016**, *43*, 1126-1134.

(41) Brake, J. M.; Daschner, M. K.; Luk, Y.-Y.; Abbott, N. L. *Science* **2003**, *302*, 2094–2097.

(42) Wei, Y.; Yang, K. L. *J. Mater. Sci.* **2015**, *50*, 4741-4748.

(43) Chen; C. H.; Yang, K. L. *Anal. Biochem.* **2012**, *421*, 321-323.

(44) Tan, H.; Li, X.; Liao, S.; Yu; R.; Wu, Z. *Biosens. Bioelectron.* **2014**, *62*, 84–89.

(45) Imrie, C. T.; Luckhurst; G. R. *in Handbook of liquid crystals, Vol-2B, Wiley-VCH*, Germany, **1998**.

(46) Vorlander, D. *Kristallinisch-flussige Substanzen*. , Enke-Verlag, Stuttgart, **1908**.

(47) Kato, T. *Science **2002**, 295*, 2414.

(48) Demus, D.; Richter, L. *Textures of liquid crystals*, 2nd Ed. **1978.**

(49) Yu; L. J.; Saupe, A. *Phys. Rev. Lett*. **1980**, *45*, 1000-1004.

(50) Lehn, J. M. *Supramolecular Chemistry: Concepts and Perspectives, Wiley-VCH*, New York, **1995.**

(51) Li, D.; Wieckowska, A.; Willner, I. *Angew. Chem., Int. Ed*. **2008**, *120*, 3991−3995.

(52) Hu, Q. Z.; Jang, C. H. *Talanta* **2012**, *99*, 1−4.

(53) Bi, X.; Yang, K. L. *Sens. Actuators, B* **2008**, *134*, 432−437.

(54) Reinitzer, F**.** *Monatsh. Chem***. 1888,** *9*, 421-424**.**

(55) **L**ehmann, O. *Flussige Kristalle*, Engelmann, Leipzig, **1904.**

(56) Friedel, G. *Ann. Phys*. **1922**, *18*, 273-274.

(57) Kawamoto, H. *Proc. IEEE* **2002**, *90*, 460-500.

(58) Strzelecka, T. E.; Davidson, M. W.; Rill, R. L. *Nature* **1988,** *331*, 457–460.

(59) Chapman, D. *Ann. N. Y. Acad. Sci*. **1966**, *137*, 745-754.

(60) Li, M.-H; Keller, P.; Yang, J.; Albuoy, P.-A. *Adv. Mater.* **2004**, *16*, 1922-1925.

(61) Finkelmann, H.; Kim, S. T.; Munoz, A.; Palffy-Muhoray, P. Taheri, B. *Adv. Mater*. **2001**, *13*, 1069-1072.

(62) Jerome, B. *Rep. Prog.Phys*. **1991**, *54*, 391-451.

(63) Bai, Y.; Abbott, N. L. *J. Am. Chem. Soc.* **2012,** *134*, 548-558.

(64) Yang, K. L.; Cadwell, K.; Abbott, N. L. *Sens. Actuators, B* **2005**, *104*, 50−56.

(65) Chandrasekhar; S.; Sadashiva; B. K.; Suresh, K. A. *Pramana* **1977**, *9*, 471-480.

(66) Chandrasekhar, S. *Liquid Crystals*, Cambridge University Press, 2nd Ed. **1992.**

(67) De Gennes, P. G.; Prost, J. *The physics of liquid crystals, Oxford University Press*, **1994.**

(68) Lai, S. L.; Huang, S.; Bi, X.; Yang, K. L. *Langmuir* **2009**, *25*, 311−316.

(69) Kim, S. R.; Shah, R. R.; Abbott, N. L. *Anal. Chem*. **2000**, *72*, 4646−4653.

(70) Gupta, V. K.; Skaife, J. J.; Dubrovsky, T. B.; Abbott, N. L. *Science* **1998**, *279*, 2077−2080.

(71) Lockwood, N. A.; Gupta, J. K.; Abbott, N. L. *Surf. Sci. Rep.* **2008**, *63*, 255-293

(72) Yeung, F. S.; Ho, J. Y; Li, Y. W.; Xie, F. C.; Tsui, O. K.; Sheng, P.; Kwok, H. S. *Appl. Phys. Lett*. **2006**, *88*, 051910 –3.

(73) Lagerwall, S. T.; Rudquist, P.; Giesselmann, F. *Mol. Cryst. Liq. Cryst.* **2009**, *510*, 1282-1291.

(74) Finkelmann, H.; Kim, S. T.; Munoz, A.; Palffy-Muhoray, P.; Taheri, B. *Adv. Mater*. **2001**, *13*, 1069-1072.

(75) Espinoza, L. A. T.; Schumann, K. R.; Luk, Y.-Y.; Israel, B. A.; Abbott. N. L. *Langmuir* **2004**, *20*, 2375-2385.

(76) Skaife, J. J.; Abbott, N. L. *Langmuir* **2001**, *17*, 5595-5604.

(77) Hall, K.; Lee, T. H.; Aguilar, M. I. J. *Mol. Recognit.* **2011**, *24*, 108-118.

(78) Rex, S.; Bian, J.; Silvius, J. R.; Lafleur, M. *Biochim. Biophys. Acta* **2002**, *1558*, 211-221.

(79) Georghiou, S.; Thompson, S. M.; Mukhopadhyay, A. K. *Biophys. J.* **1982**, *37*, 159-161.

(80) Kleinschimdt, J. H.; Mahaney, J. E.; Thomas, D. D.; Marsh, D. *Biophys. J.* **1997**, *72*, 767-778.

(81) Brauner, J. W.; Mendelsohn, R.; Prendergast, F. G. *Biochemistry* **1987**, *26*, 8151-8158.

(82) Brown, L. R.; Brawn, W.; Kumar, A.; Wuthrich, K. *Biophys. J.* **1982**, *37*, 319-328.

(83) Machnicki, M.; Zimecki, M.; Zagulski, T. *Int. J. Exp. Path*. **1993**, *74*, 433-439.

(84) Opal, S. M.; Scannon, P. J.; Vincent, J. L.; White, M.; Carroll, S. F.; Palardy, J. E.; Parejo, N. A.; Pribble, J. P.; Lemke, H. *J. Infect. Dis*. **1999**, *180*, 1584-1589.

(85) Galanos, C.; Freudenberg, M. A. *Mediators Inflamm.***1993**, *2*, S11-S16.

(86) Lasic, D. D. *Biochem. J.* **1988**, *256*, 1–11

(87) Hanczyc, M. M.; Szostak, J. W. *Curr. Opin. Chem. Biol*. **2004**, *8*, 660–664.

(88) Jahn, A.; Vreeland, W. N.; Gaitan, M.; Locascio, L. E. *J. Am. Chem. Soc.* **2004**, *126*, 2674–2675.

(89) Levy, P.S.; Quigley, R. L.; Gould, S. A.; *J. Trauma*. **1996**, *41*, 416–423.

(90) Jurgens, G.; Muller, M.; Koch, M. H. J.; Brandenburg, K. *Eur. J. Biochem*. **2001**, *268*, 4233-4242.

(91) Smith, G.; Weidel, S. E.; Fleck, A: *Nutrition* **1994**, *10*, 335–341.

(92) Kirsch, R.; Frith, L.; Black, E.; Hoffenberg, R. *Nature* **1968,** *217*, 578–579.

(93) Takayama, K.; Din, Z. Z.; Mukerjee, P.; Cooke, P. H.; Kirkland, T. N. *J. Biol. Chem.* **1990**, *265*, 14023-14029.

(94) Lesins, V.; Ruckenstein, E. *Colloid Polym. Sci.* **1988**, *266*, 1187**.**

(95) Noinville, V.; Vidal-Madjar, C.; Sebille, B. *J. Phys. Chem.* **1995**, *99*, 1516-1520.

(96) Ohno, N.; Morrison, D. C. *J. Biol. Chem.* **1989**, *264*, 4434-4441.

(97) Bortner, C. A.; Miller, R. D.; Arnold, R. R. *Infect. Immun*., **1986**, *51*, 373-377.

(98) Gioannini, T. L.; Zhang, D.; Teghanemt, A.; Weiss, J. P. *J. Biol. Chem.* **2002**, *277*, 47818-47825.

(99) Kruzel, M. L.; Harari, Y.; Mailman, D.; Actor, J. K.; Zimecki, M. *Clin. Exp. Immunol.* **2002**, *130*, 25-31.

(100) Parant, M.; Parant, F.; Vinit, M. A.; Jupin, C.; Noso, Y.; Shedid, L. *J. Leukoc. Biol.***1990**, *47*, 164-169.

(101) Wang, J. E.; Jorgensen, P. F.; Ellingsen, E. A.; Almiof, M.; Theimermann, C.; Foster, S. J., Aasen, A. O.; Solberg, R. *Shock* **2001**, *16*, 178-182.

(102) Wary, G. M.; Foster, S. J.; Hinds, C. J.; Theimermann, C. *Shock* **2001**, *15*, 135-142.

(103) Neuhaus, F.; Baddiley, J. A. *Microbiol. Mol. Biol. Rev*. **2003**, *67*, 686–723.

(104) Sugawara, S.; Arakaki, R.; Rikiishi, H., Takada, H. *Infect. Immun.* **1999**, *67*, 1623-1632.

(105) Nisengard, R. J.; Newman, M. G. Ed. *Oral microbiology and immunology*, The W. B. Saunders Co., Philadelphia, Pa., **1994**, *2*nd ed., pp- 360-384.

(106) Shai, Y. *Biochim. Biophys. Acta*, **1999**, *1462*, 55-70.

(107) Sengupta, D.; Leontiadou, H.; Mark, A. E.; Marrink, S. J. *Biochim. Biophys. Acta* **2008**, *1778*, 2308-2317.

(108) Irudayam, S. J.; Berkowitz, M. L. *Biochim. Biophys. Acta* **2012**, *1818*, 2975-2981.

(109) Rosevear, F. B. *J. Soc. Cosmet. Chem.* **1968**, *19*, 581-594.

(110) Miller, C. A.; Ghosh, O.; Benton, W. J. *Colloid Surf.* **1986**, *19*, 197-223.

(111) Hartshore, N. H. *The Microscopy of Liquid Crystals*; Microscope Publications Ltd.: London, **1974**; p 49.

(112) Buffeteau, T.; Desbat, B.; Turlet, J. M. *Appl. Spectrosc*. **1991**, *45*, 380-385.

(113) Zamlynny, V.; Zawisza, I.; Lipkowski, J. *Langmuir* **2003**, *19*, 132-136.

(114) Bin, X.; Zawisza, I.; Goddard, J. D.; Lipkowski, J. *Langmuir* **2005**, *21*, 330-336.

(115) Keiderling, T. A., *Curr. Opin. Chem. Biol.* **2002**, *6*, 682-688.

(116) Giugliarelli, A.; Sassi, P.; Paolantoni, M.; Morresi, A.; Dukor, R.; Nafie, L. *J. Phys. Chem. B* **2013**, *117*, 2645−2652.

(117) Ma, S.; Freedman, T. B.; Dukor R. K.; Nafie, L. A. *Appl. Spectrosc*. **2010**, *64*, 615−626.

(118) Keiderling, T. A.; Silva, R. A.; Yoder, G.; Dukor, R. K. *Bioorg. Med. Chem.* **1999**, *7*, 133−141.

(119) Cheng, D.; Sridharamurthy, S. S.; Hunter, J. T. Park, J.-S.; Abbott, N. L.; Jiang, H. *J. Microelectromech. Syst.* **2009**, *18*, 973–981.

(120) Kim, F.; Kwan, S.; Arkana, J.; Yang, P. *J. Am. Chem. Soc*. **2001**, *123*, 4386-4392.

(121) Kwan, S.; Kim, F.; Arkana, J.; Yang, P. *Chem. Commun*. **2001**, *5*, 447-448.

Chapter 2

A simple quantitative method to study protein lipopolysaccharide interactions using liquid crystals

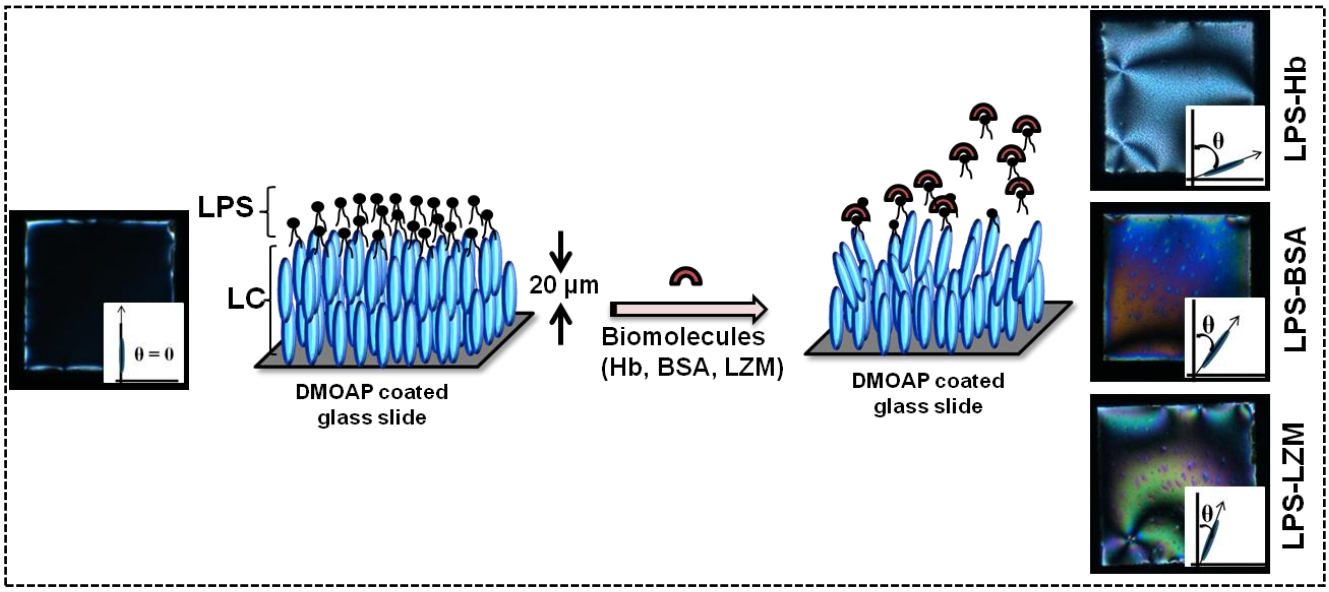

The interaction of proteins with endotoxin has divergent effects on lipopolysaccharide (LPS)-induced responses, which serve as a basis for many clinical and therapeutic applications. It is, therefore, important to understand these interactions from both theoretical and practical points of view. This chapter advances the design of liquid crystal (LC)-based stimuli-responsive soft materials for quantitative measurements of LPS–protein binding events through interfacial ordering transition. Micrometer- thick films of LC undergo easily visualized ordering transitions in response to proteins at LPS laden aqueous-LC interface.

2.1 Introduction

Lipopolysaccharides (LPS) commonly known as bacterial endotoxin, a component of the outer cell membrane of gram negative bacteria, is a principal mediator for many of the patho-physiological effects associated with gram negative bacterial infections.[1] LPS are composed of a hydrophilic polysaccharide unit that is covalently linked to a hydrophobic lipid moiety (known as lipid A), which is the most conserved part of endotoxin and is responsible for biological toxicity. Serious endotoxin infection can cause septic shock leading to severe hypertension, cardiovascular collapse, tissue injury, multiple organ failure and even death.[2-4] These severe biological activities caused by LPS are not direct effects of the LPS molecule but are induced by its interaction with LPS-sensitive cells that are mediated by proteins in the body fluid and on the cell surface. The interactions of LPS with various proteins resulted different effects on endotoxicity, varying from reduction to enhancement.[5-8] As large as the different proteins interacting with endotoxin, as broad are the consequences of these interactions. An understanding of these processes should, however, be important in the light of modification of the LPS-induced responses.[9] Therefore, a thorough and systematic study on LPS–biomolecule interactionsare of great theoretical and practical significance.

In recent years substantial effort has been invested in analyzing the interactions between several biomolecules and endotoxin.[10-19] These interactions were investigated mainly using two biological assays, for example tumor necrosis factor (TNF) –α induction in human mononuclear cells[10,20] and the *Limulus* amoebocyte lysate (LAL) assay.[16,19] Moreover, these interactions are often evaluated by a variety of physical techniques like Fourier transform IR spectroscopy (FT-IR), X-ray diffraction (XRD),[10]*etc*. Although numerous tools are available for the recognition of biomolecular interactions, they are often limited in their sensitivity, high cost, and difficult to modify for various uses. Recently, optical sensing method based on the principle of surface plasmon resonance has been used to study this interaction of LPS with different biomolecules.[21] This technique involves immobilization of biomolecules on CM5 sensor chip (a carboxymethyldextran hydrogel coupled to a gold-coated glass surface) using the amino coupling method and subsequent injection of LPS over the immobilized surfaces. In this study, kinetic parameters of such

interactions have been determined which elucidate different binding affinity of LPS towards different types of proteins. Although, this technique provides valuable information to study biomolecular interactions in real time, the expensive instrumentation and need to choose a method for probe immobilization limits its widespread use. In this chapter, we report a simple but useful advance in the design of an experimental system that enables a quick, quantitative and label free detection of LPS–biomolecular interactions.

The approach that we report in this chapter revolves around surface-driven ordering transitions in LC at aqueous-LC interfaces. Recently, LC-aqueous interfaces in a planar geometry have evolved as a promising system to study biomolecular interactions in biological membranes.[22-28] Due to the long range communication among the LC phase, events taking place at the LC-water interface can be precisely reported by the rearrangement (so called ordering transition) of the bulk of the LC. The sensitivity of the ordering transition of LC to the nanoscale topography and chemical functionality of surfaces enable the transduction and amplification of range of interactions into optical signals that are directly visible by naked eye. So far, fluid biometric membrane systems supported on LC have been used to investigate specific and non-specific lipid protein binding events,[27-31] DNA hybridizations,[32] enzymatic reactions,[26] pathogenic detections,[33-34] and so on. Abbott and his coworkers reported that phospholipase A_2 (PLA_2) triggers a change in the optical response of LC supported within a lipid-laden aqueous-LC interface. This is due to that PLA_2 catalytically hydrolyses the lipid laden interface and induces an orientational ordering transition of the LC.[22] Yang *et al*. reported the activities of phospholipase like toxins (e.g., β-bungarotoxin) towards lipid monolayer at aqueous–LC interface.[25] Liu *et al.* demonstrated the interaction between chitosan, a biopolymer, and lipid membrane at aqueous-LC interface.[35] Recently Jang *et al*. reported the non-specific molecular interactions between antimicrobial peptides and lipid membranes using LC.[36] To date, no work has been done to examine and quantify the interaction between LPS and biomolecules using aqueous-LC planar geometry. There are a number of biomolecules, namely, bovine serum albumin (BSA), lysozyme (LZM) and hemoglobin (Hb) which show diverse interactions with endotoxins. These three proteins of different categories not only possessing the different charge at physiological pH but also have diverse effect on endotoxicity on interaction with LPS.[10,11,16] Past reports demonstrated that these proteins

have different affinity towards LPS which leads to different kinetic parameters measured by surface plasmon resonance biosensor.[21] In the study reported in this chapter, first, we sought to demonstrate a simple technique that can report protein-lipid interactions using surface-driven ordering transitions in LC. Second, we sought to determine if it was possible to quantify these interactions by measuring the tilt angle (associated with the ordering of LC phase) at aqueous-LC interface. In short, our study advances a simple analytical technique based on LC for quantitative and multiplexed measurements of LPS-biomolecular interactions.

2.2 Objective

A number of previous studies reported that the self-assembly of LPS molecules at aqueous-LC interfaces could trigger ordering transitions in LC; thus leading to homeotropic anchoring of LC.[27, 34] These ordering transitions arise from coupling between the aliphatic chains of the adsorbed LPS and the mesogens of the LC. Motivated by this, we hypothesized that the addition of proteins at these interfaces could manipulate the interfacial phase state of the LPS monolayer owing to strong coupling that could occur between LPS and protein molecules, and thus, may have led to changes in the ordering of LC. A key finding reported herein is that protein–LPS interactions switch the orientational ordering of LC, and thus, demonstrate the promise of aqueous-LC interface for reporting interfacial phenomena. We also find evidence that the protein–LPS interactions which lead to changes in the ordering of LC correlate with the affinity constant of that particular protein. Overall, the results of this study provide the basis of new technologically relevant approaches to the design of interfacially stimuli-responsive soft materials.

2.3 Results and discussion

2.3.1 LPS mediated ordering transition of liquid crystal at aqueous-LC interface

To study the interactions between bacterial endotoxin (LPS) and different proteins, we first studied the optical response of LC coupled to the negatively charged LPS at aqueous-LC interface. Figure 2.1 A shows the optical micrographs (crossed polarizers) of nematic 5CB confined within a gold grid supported on DMOAP-coated glass slides in contact with an aqueous solution of Tris buffer (pH 7.4). The optical appearance of the LC became bright,

which was consistent with an orientational ordering transition as a result of contact with water. Figure 2.1 B shows the optical appearance of the same film of 5CB when a 0.1 mg/mL aqueous solution of LPS vesicles in Tris buffer (pH 7.4) was introduced. A change in the optical response of LC from bright to dark was observed immediately after the addition of LPS (Figure 2.1 B). The dark optical appearance of the LC, which was independent of rotation between crossed polarizers, was consistent with the LC film having a homeotropic orientation. This result is in agreement with prior reports of homeotropic anchoring of 5CB at LPS-decorated interfaces.[22, 27] To obtain a stable, self-assemble LPS at fluid interfaces, an aqueous solution of LPS was incubated in the optical cell for 2 h. Prior to exposure to a variety of proteins, the LPS-laden aqueous-LC interface was washed with Tris buffer at pH 7.4 three times to remove free LPS from the bulk solution.

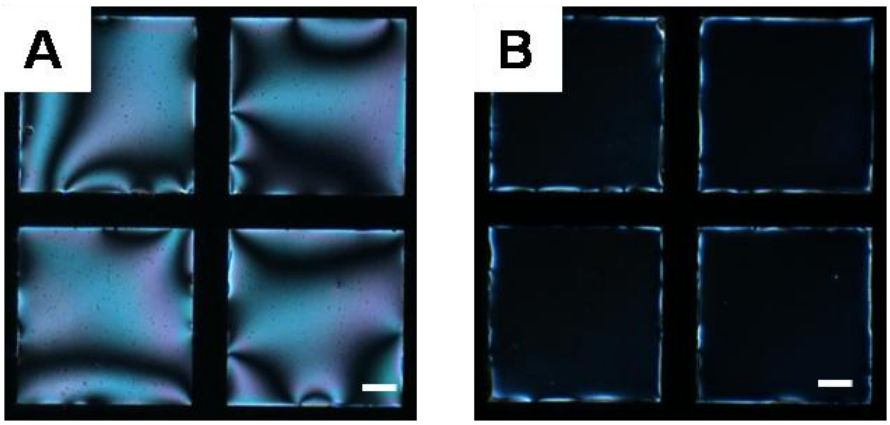

Figure 2.1 Optical micrographs (crossed polars) of 5CB hosted in TEM gold grid supported on DMOAP coated glass slides in contact with A) aqueous solution of Tris buffer of pH 7.4 (10 mM) and B) LPS vesicles of 0.1 mg/mL for 2 h to form a stable self-assembly at aqueous-LC interface. Scale bar = 40 μm.

2.3.2 Interaction of different proteins (Hb, BSA and LZM) with LPS at aqueous-LC interface

We selected three proteins for the study reported herein: 1) Hb, which is the four-subunit, globular, oxygen-carrying protein, binds endotoxins with high affinity, resulting synergistic toxicity, and a noticeable intensification of the biological activity of LPS.[10] 2) BSA, which is the most abundant carrier protein in blood, accelerates the binding of LPS to

the membrane receptors of neutrophils by direct interactions with the LPS.[11] 3) LZM, which is a major cationic protein in polymorphonuclear leukocyte granules, contributes to the lysis of bacterial cell membrane and acts as a nonspecific organism defense.[16] Next, we sought to determine the influence of these proteins (described above) on the orientational ordering of 5CB within LPS-laden aqueous–LC interfaces. In a typical experiment, first, we exposed an aqueous solution of 10 μM Hb in Tris buffer (pH 7.4) to the LPS-laden aqueous-LC interface. An immediate change in the optical appearance of the LC from dark to bright was observed within 15 s of the addition of Hb (Figure 2.2 A, B). This indicates that the LC underwent an orientational ordering transition from homeotropic to a planar/ tilted state upon the introduction of Hb. The planar/tilted orientation of the LC, when combined with prior reports of biomolecular interactions in LC, is suggestive of a physical phenomenon, whereby Hb absorbs and organizes itself at the LPS aqueous–LC interface. This observation could be due to strong hydrophobic interactions between neutral Hb and negatively charged LPS molecules,[10] which play an important role in the rearrangement of the LPS monolayer, and thus, result in a transition in the orientation of LC from dark to bright. Notably, 5CB remains in the homeotropic orientation for days after contact with the LPS-laden aqueous phase. Thus, the ordering transition observed in Figure 2.2 A, B is caused by the presence of Hb; this is strongly coupled with the organization of the assemblies of the LPS molecules at these interfaces. Our next goal was to investigate whether the interaction of negatively charged BSA with negatively charged LPS membrane at the aqueous–LC interface underwent a similar ordering transition to that of LPS–Hb described above. Thus, 10 μM BSA in Tris buffer (pH 7.4) was added to the aqueous–LC interface decorated with LPS. We observed a rapid change in the optical appearance of the LC from dark to bright (Figure 2.2 C, D). The change in the orientation of the LC from homeotropic to planar indicates that the LPS interaction with serum proteins is driven by hydrophobic interactions and can be studied at the aqueous-LC interface. Likewise, in response to the LZM protein, which formed nonspecific interactions with LPS, a similar change was observed in the optical appearance of the LC from dark to bright after immersion of the LPS-laden 5CB interface into a 10 μM aqueous solution of LZM in Tris buffer at pH 7.4 (Figure 2.2 E, F). These measurements revealed that the LPS-laden aqueous–LC interface could provide the basis for a general, facile method to tune and

possibly quantify the response of different proteins. It is noteworthy, however, that in all cases the dynamic ordering transitions towards a planar ordering in different pH conditions other than physiological pH were the same (over a period of seconds), which indicated that the ordering of the LC was independent of electrostatic interactions. This also suggests that specific and nonspecific interactions of different types of protein with endotoxins, leading to changes in the orientation and optical appearance of LC, can be attributed to changes in the ordering of LPS molecules at the interface through hydrophobic interactions.

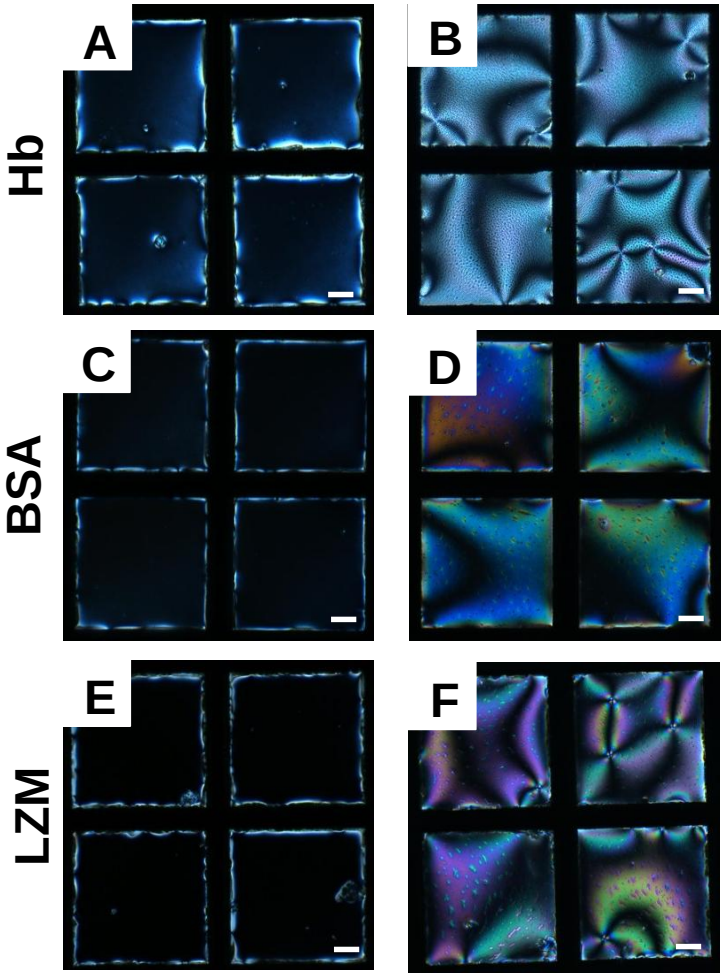

Figure 2.2 A), C), E) Optical images (crossed polarizers) of 5CB hosted in gold grids supported on DMOAP coated glass slides and placed into contact with an aqueous solution of Tris buffer, followed by the introduction of LPS, and incubation for 2 h. Slides after contacting the LPS-laden interface with 10 μM aqueous solutions of Hb (B), BSA (D), and LZM (F). Scale bar=40 μm.

2.3.3 Control experiments

To provide further insight into the proposition that the orientational transition of 5CB was due to the interaction of LPS molecules with Hb, BSA, and LZM, we performed two additional control experiments. First, we observed that there was no optical response when the aqueous–LC interface (without the LPS-laden monolayer) prepared on DMOAP-coated glass slides was in contact with proteins. Figure 2.3 shows the optical micrographs of nematic 5CB confined within a gold grid upon immersion in aqueous Tris buffer (Figure 2.3 A, C, and E) followed by contact with 20 μM solutions of Hb, BSA, and LZM (Figure 2.3 B, D, and F). The optical appearance of the LC did not change (LC remains bright), even after 12 h of incubation in contact with proteins. This result suggests that in the absence of LPS, the orientation of 5CB is not perturbed by the addition of these proteins at the aqueous–LC interface.

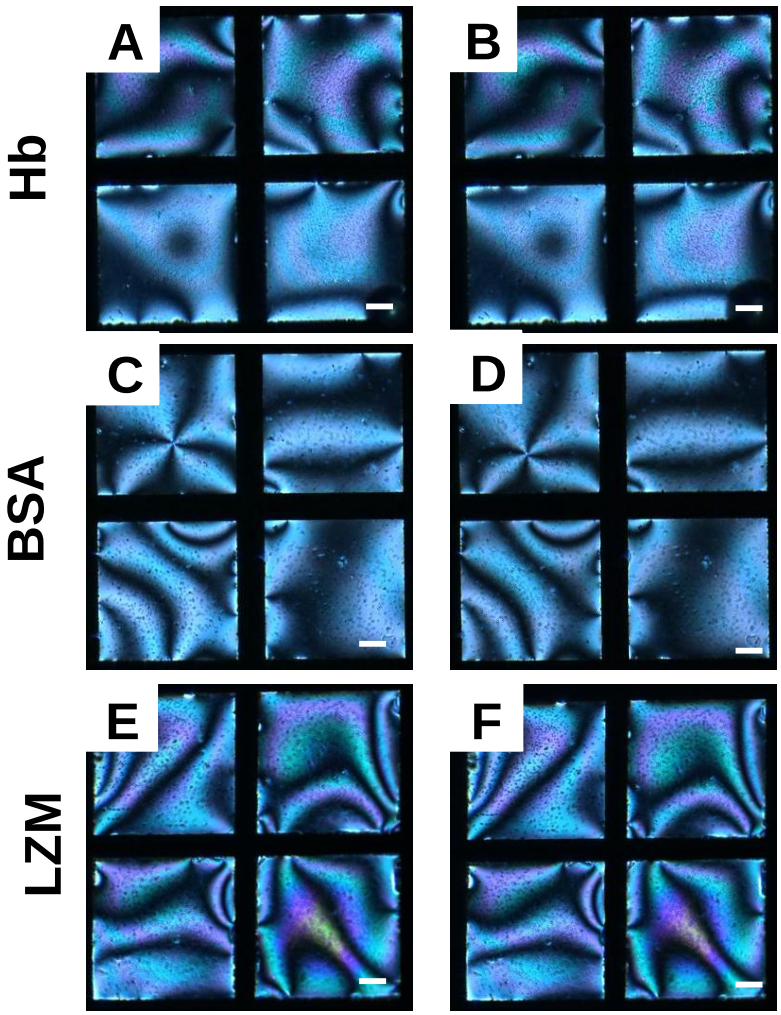

Figure 2.3 Optical images (crossed polars) of 5CB contained in gold grids supported on DMOAP-treated glass slides and placed into contact with A, C, E) aqueous solutions of phosphate buffer (pH 7.4) and B, D, F) in contact with an aqueous solution of 20 μM of Hb, BSA and LZM, respectively. Scale bar = 40 μm.

Second, we observed no change in the optical appearance in the presence of proteins when other lipids (instead of LPS) were introduced to form a monolayer at the aqueous–LC interface. We chose zwitterionic 1,2-didodecanoyl-sn-glycerol-3-phosphocholine (DLPC) and negatively charged lysophosphatidic acid (LPA) and 1,2-dioleoyl-sn-glycero-3-phospho-rac-(1-glycerol) sodium salt (DOPG), which are known to form monolayers at the aqueous–LC interface and align the nematic 5CB molecules in a homeotropic orientation. This study was motivated by two broad goals. First, we sought to find out whether these proteins could interact with other lipids in addition to LPS, as described above. Second, we sought to understand whether electrostatic interactions between charged lipids and proteins (at pH 7.4, Hb is neutral, BSA is negatively charged, and LZM is positively charged) disrupted the organization of the lipid membrane and induced an ordering transition at the interface.

Figure 2.4 shows the optical images (crossed polarizers) of 5CB films at the aqueous–LC interface decorated with DLPC, LPA, and DOPG before and after the addition of 10 μM aqueous solutions of proteins (Hb, BSA, and LZM). The LC remained dark during 1 h of observance, which suggested a homeotropic alignment of LC. In summary, these results provide evidence that binding of these proteins is highly specific towards LPS and the interactions between them are accompanied not by electrostatic but hydrophobic interactions.

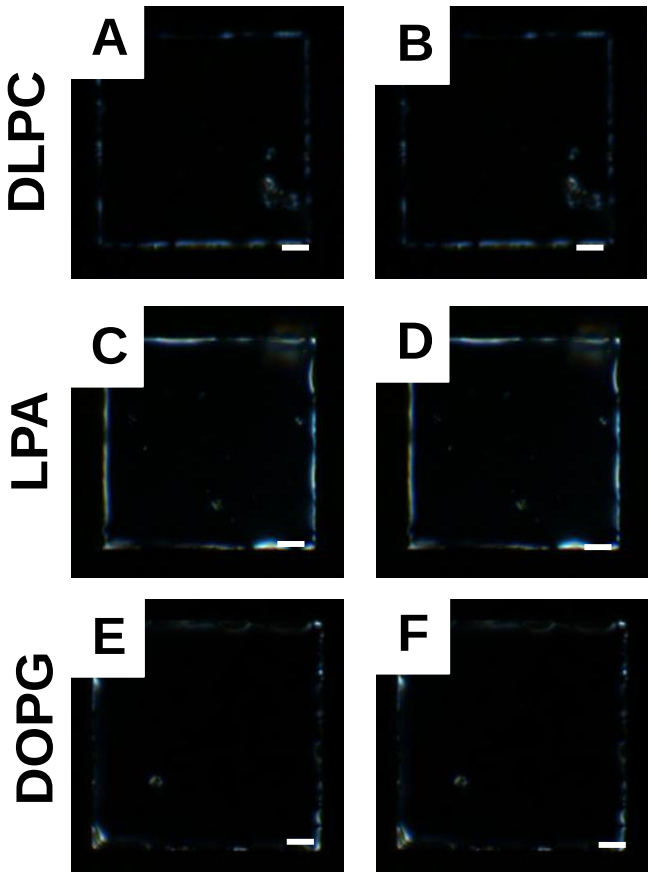

Figure 2.4 Optical images (crossed polars) of 5CB contained in gold grids supported on DMOAP-treated glass slides and placed into contact with aqueous interface laden with A) DLPC C) LPA and E) DOPG. B), D), F) represents the optical response of the 5CB film decorated with DLPC, LPA and DOPG monolayers after addition of protein (Hb, BSA and LZM) solutions, respectively. Scale bar = 40 μm.

In addition to these control experiments, we further looked into the interfacial binding activity of proteins onto self assembled LPS through exploiting epifluorescence measurements with FITC tagged BSA as a fluorescence probe. From this experiment, first, we thought to observe fluorescence density of FITC-BSA on the 5CB containing grid surface decorated with LPS which could stronghold our LC based detection of protein-LPS interaction. Second, depending on the interfacial fluorescence density we could also explain the integrity of assembling protein over self-assembled interfacial LPS during this LPS-protein binding event at interface. In epifluorescence experiment, we coupled 500 nM of BSA mixed with 0.3 mol% FITC–BSA onto LPS laden aqueous-LC interface and kept

for 2 hrs period of incubation. We also run a parallel control experiment where we kept incubation of BSA free LPS laden aqueous-LC interface for 2 hrs period. Figure 2.5 shows the epifluorescence micrographs and the respective polarized optical micrographs of LPS decorated aqueous-LC interface in absence and presence of BSA (mixed with FITC-BSA) respectively. In absence of BSA, interfacial LC Laden with LPS remained in homeotropic orientation as evidenced in Figure 2.5 C depicting dark optical view of interfacial 5CB. Interestingly, the corresponding epifluorescence measurements (Figure 2.5 A) shows lack of interfacial fluorescence clearly due to absence of any fluorescent probe at the interface. Figure 2.5 D describes polarized optical micrograph of LPS decorated aqueous-LC interface, in presence of BSA (mixed with 0.3% FITC-BSA), after 2 hrs of incubation and subsequent three times exchange with Tris buffer at pH 7.4 to remove excess FITC-BSA from the solution. The bright optical appearance clearly shows the planar/tilted orientation of interfacial LC mediated by strong interaction between LPS and BSA at the interface. Interestingly, the corresponding epifluorescence measurement (Figure 2.5 B) shows the presence of strong interfacial fluorescence due to presence of FITC-BSA at the LPS laden aqueous-LC interface. This observation evidently demonstrates that the strong binding of protein with LPS at aqueous-LC interface and further implies that this strong interaction although disturbed the arrangement of interfacial LPS (also evidenced by bright polarized optical micrograph) but it retained at the interface with protein assembled over it.

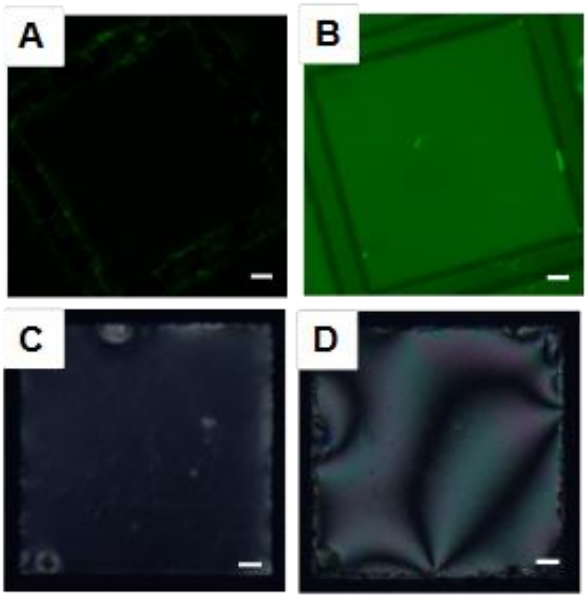

Figure 2.5 Epifluorescence images of LPS decorated aqueous-LC interface after 2 hrs of incubation A) in absence; B) in presence of BSA (mixed with 0.3 mol% FITC–BSA. (C) and (D) Corresponding polarized light micrographs respectively. Scale bar = 40 μm.

2.3.4 Determination of detection limit of these proteins on LPS laden aqueous-LC interface

As noted above, the change in the optical appearance of the LC in the presence of proteins is highly specific towards LPS, and thus, is not present for other lipid–protein interactions. These results inspired us to investigate further in terms of the sensitivity of these protein–LPS interactions through surface-driven ordering transitions in LC. Because the LPS–protein interactions lead to different biological toxicity, therefore, in addition to studying these interactions at aqueous–LC interfaces, determining the sensitivity of these interactions towards LC ordering is crucial and may provide further insight into exploring the LC-based assay as a biosensor to detect different pathogenic interactions. With this in mind, we sought to investigate the limit of detection (LOD) and response time of the system, for which we compared the dynamic response of the LC at different concentrations of these proteins on the LPS-laden aqueous–LC interface. We performed two experiments to establish the above-described response on the lipid-laden aqueous–LC interface to different proteins. First, we sought to determine the minimum concentration required to form the LPS monolayer (at the aqueous–LC interface) that would be sufficient to retain the responsiveness of LC (i.e. after washing excess, free LPS from the aqueous–LC interface). Figure 2.6 shows the optical response of 5CB upon exposure to various concentrations of LPS at the aqueous-LC interface supported on DMOAP-treated glass slides. We found that 60 μg mL^{-1} was the optimum concentration at which LC retained its responsiveness (uniformly dark after washing with Tris buffer followed by 24 h of incubation).

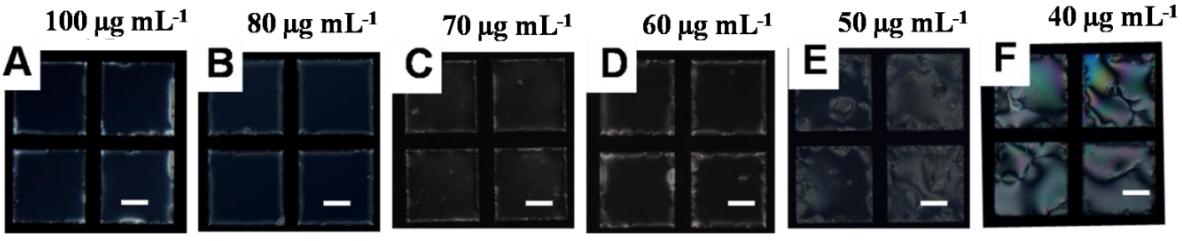

Figure 2.6 Optical micrographs of aqueous-LC interface decorated with A) 100 μg mL^{-1} B) 80 μg mL^{-1} C) 70 μg mL^{-1} D) 60 μg mL^{-1} E) 50 μg mL^{-1} F) 40 μg mL^{-1} concentrations of LPS, after washing with Tris buffer and followed by 24 h of incubation. Scale bar = 40 μm.

Second, we sought to investigate the behavior of the optical response of the LC to various concentrations of proteins within the LPS-laden (optimum concentration, i.e. 60 μg mL^{-1}) aqueous–LC interface. The results shown in Figure 2.7 demonstrate the optical response of the LC at the aqueous-LC interface as a function of different concentrations of proteins. Inspection of Figure 2.7 A–C reveals that, for 50 nM solutions of proteins (Hb, BSA, and LZM) the LC film assumed a bright optical appearance between cross polarizers (all optical images were recorded after 60 min of incubation of each protein at the LPS decorated aqueous-LC interface). The interference colors, however, were bright greens, blues, and yellows, which indicated that LC had assumed a tilted state (i.e. an orientation state distinct from that of pure 5CB) that was more pronounced in the presence of BSA and LZM than that in Hb. Interestingly, with a decrease in the concentration of proteins to 10 nM, an ordering transition was observed in the presence of Hb and BSA, but not with LZM (Figure 2.7 D–F). Upon further decreasing the concentration of the proteins to 5 nM, we observed that the LC exhibited a bright optical appearance only in presence of Hb; this was consistent with an orientational ordering transition (Figure 2.7 G–I). Below 5 nM, no optical change was observed, even after 2 h of incubation of aqueous solutions of Hb, BSA, and LZM at the LPS laden aqueous–LC interface.

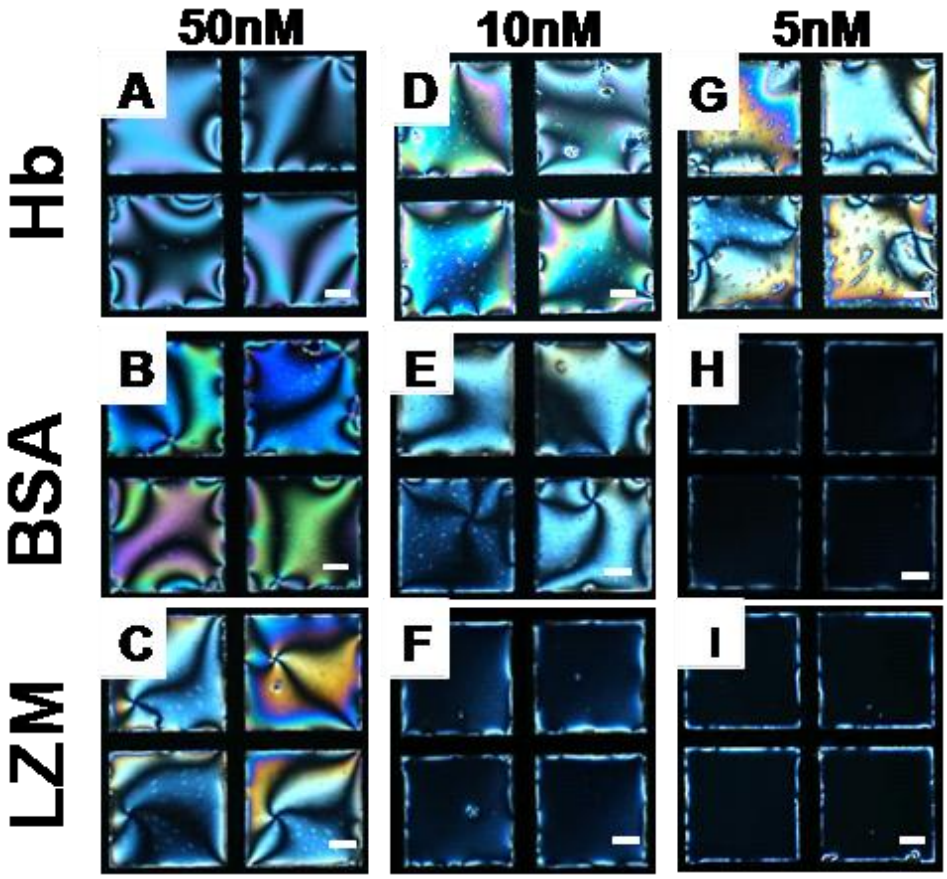

Figure 2.7 Polarizing optical micrographs of 5CB contained in gold grids supported on DMOAP-treated glass slides and placed into contact with the LPS laden aqueous interface followed by incubation for 60 min with 50 nM (A–C), 10 nM (D–F), and 5 nM (G–I) aqueous solutions of Hb (A, D, G), BSA (B, E, H), and LZM (C, F, I).

To determine the minimum concentrations of a particular protein that induces a change in the ordering transition of LC on the LPS-laden interface, we performed similar experiments with other concentrations as well. The detailed study performed for each individual protein at the LPS-laden aqueous– LC interface (Figures 2.8–2.10) confirmed that 5, 10, and 50 nM were the limiting concentrations of Hb, BSA, and LZM, respectively, that induced an ordering transition.

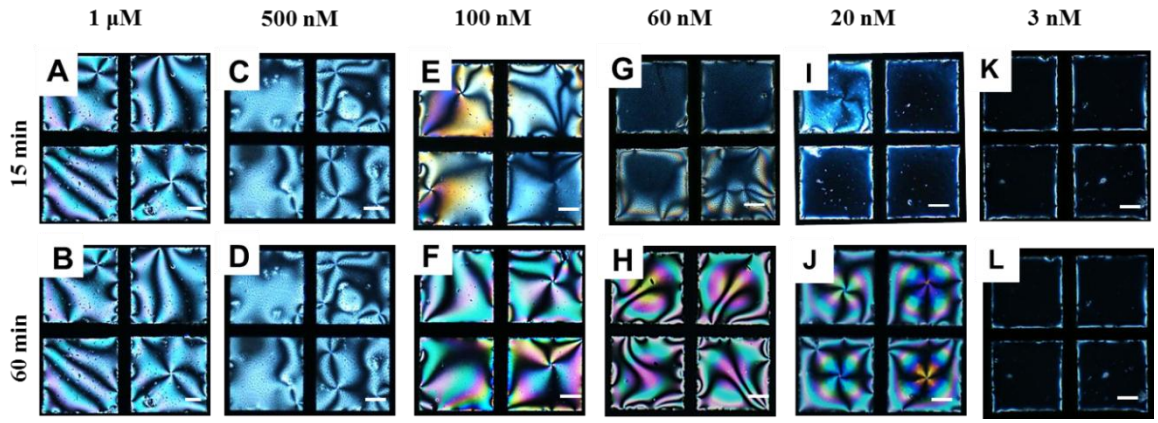

Figure 2.8 Polarized optical micrographs of 5CB films decorated with LPS monolayer after addition of A, B) 1 µM, C, D) 500 nM, E, F) 100 nM, G, H) 60 nM, I, J) 20 nM and K, L) 3 nM concentrations of Hb. Top row and bottom row represent the incubation of LPS laden aqueous-LC interface with above mentioned concentrations of Hb for a period of 15 min and 60 min, respectively. Scale bar = 40 µm.

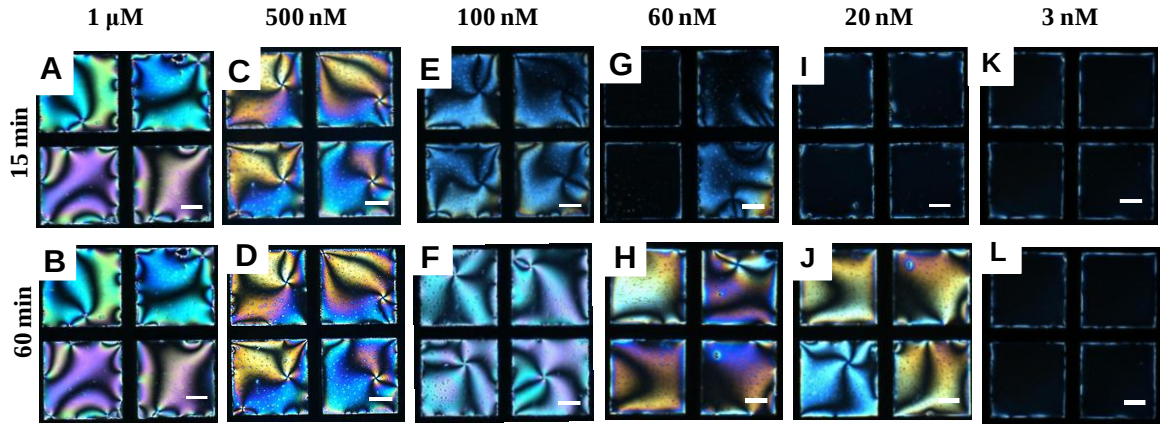

Figure 2.9 Polarized optical micrographs of 5CB films decorated with LPS monolayer after addition of A, B) 1 µM, C, D) 500 nM, E, F) 100 nM, G, H) 60 nM, I, J) 20 nM and K, L) 3 nM concentrations of BSA. Top row and bottom row represent the incubation of LPS laden aqueous-LC interface with above mentioned concentrations of BSA for a period of 15 min and 60 min, respectively. Scale bar = 40 µm.

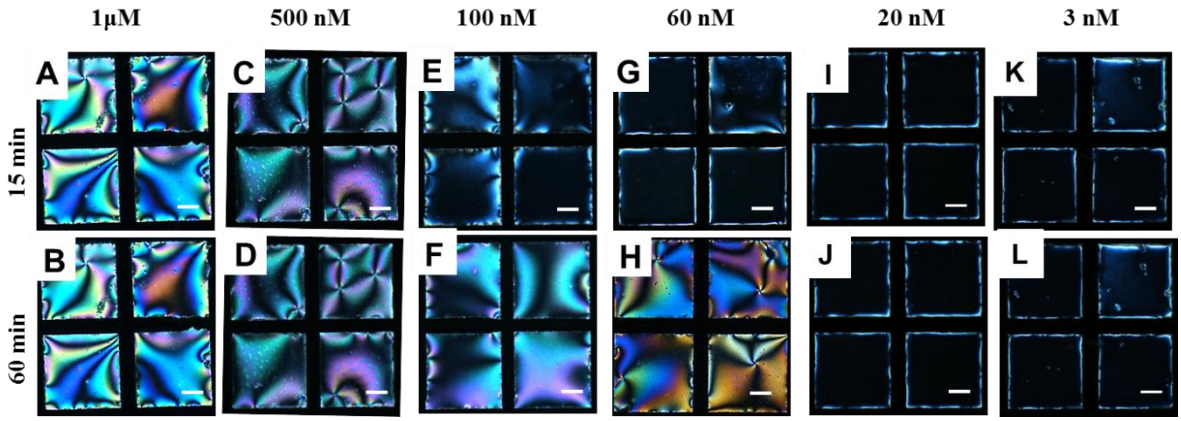

Figure 2.10 Polarized optical micrographs of 5CB films decorated with LPS monolayer after addition of A, B) 1 µM, C, D) 500 nM, E, F) 100 nM, G, H) 60 nM, I, J) 20 nM and K, L) 3 nM concentrations of LZM. Top row and bottom row represent the incubation of LPS laden aqueous-LC interface with above mentioned concentrations of LZM for a period of 15 min and 60 min, respectively. Scale bar = 40 µm.

2.3.5 Average gray scale intensity and tilt angle measurements to quantify the interaction of proteins with LPS at the aqueous-LC interface

Quantification of the intensity of light transmitted through the LC, as shown in Figure 2.11, reveals that the anchoring transition varies as a function of the concentration of proteins. Because the LC was imaged with white light under crossed polarizers, we observed interference phenomena that caused changes in the average grayscale intensity of the optical images. Although the macroscopic appearance (and thus, grayscale intensity) of the LC changes continuously with a decrease in concentration of the proteins, we wish to make two additional observations with regard to ordering of the LC at the LPS-laden aqueous–LC interface. First, careful analysis of the average grayscale intensity of the optical images due to protein–LPS interactions suggest that the comparative changes in the intensity varies drastically at all concentrations. Therefore, the measured grayscale intensity at the aqueous–LC interface can be correlated with the affinity constant values of LPS with Hb, BSA, and LZM for a particular concentration. Second, the measured grayscale intensity (obtained at the LPS–aqueous–5CB interface) has the highest order of magnitude in the case of Hb, followed by BSA and LZM. Interestingly, this trend (Hb>BSA>LZM) is maintained for all concentrations of proteins. More generally, the results in Figure 2.11

suggest that Hb shows the strongest interactions with LPS, and thus, is more sensitive (detection limit reaches 5 nM) among the other protein–LPS (BSA–LPS and LZM–LPS) interactions used in our study.

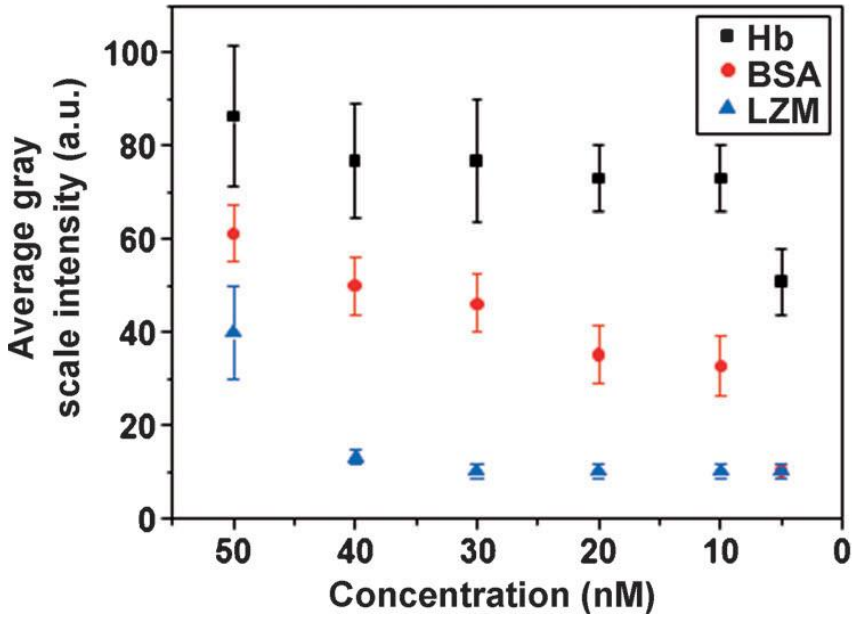

Figure 2.12 Represents the average gray scale intensity of optical images of 5CB films as a function of varying concentrations of Hb, BSA and LZM on LPS decorated aqueous-LC interface.

To further test the proposition that the change in the organization of the adsorbed LPS monolayer at the aqueous–LC interface underlies different orientational behavior in the presence of proteins shown in Figure 2.12, we sought to measure the orientation of 5CB at a particular concentration of proteins as a function of time. Because different proteins have different binding affinities towards LPS, it may be hypothesized that the extent of disruption of a self-assembled monolayer of LPS depends upon the strength of binding of proteins with LPS, leading to different tilts of LC molecules. Therefore, measurement of the tilt angle, by quantifying the retardation of the LC by using a birefringence mapping system, might provide additional insight into the physical phenomena that underlie LPS–protein binding events driven by the ordering transition of LC at aqueous–LC interface. In this experiment, we use 50 nM of each protein (Hb, BSA, and LZM), which was the minimum concentration at which they showed an optical response (change in ordering transition of LC from homeotropic to planar), when binding with LPS. First, we measured the effective birefringence of 5CB immediately after contact with 50 nM of each protein

(Hb, BSA, and LZM) at the LPS-laden aqueous–LC interface. Then, we calculated the tilt angle of 5CB from the above-measured values of effective birefringence by using previously reported procedures (details procedure has been mentioned at the Experimental Section).[37] Figure 2.12 shows the dynamic change in the tilt angle of 5CB after the addition of aqueous solutions of Hb, BSA, and LZM at the LPS-laden aqueous–LC interface. The maximum tilt angles of 5CB obtained after 2 h of incubation for Hb–LPS, BSA–LPS, and LZM–LPS interactions at the aqueous-LC interface were (69.26°±4.3), (35.15°±1.8), and (21.4°±2.5), respectively. This result suggests that Hb, BSA, and LZM bind with LPS with different affinities. With strong binding between LPS and protein, disruption of the interaction of 5CB with LPS will take place to a large extent, leading to a greater change in the tilt angle of 5CB. On this basis, we can predict that the Hb–LPS interaction is the strongest, followed by BSA–LPS, and least for LZM–LPS.

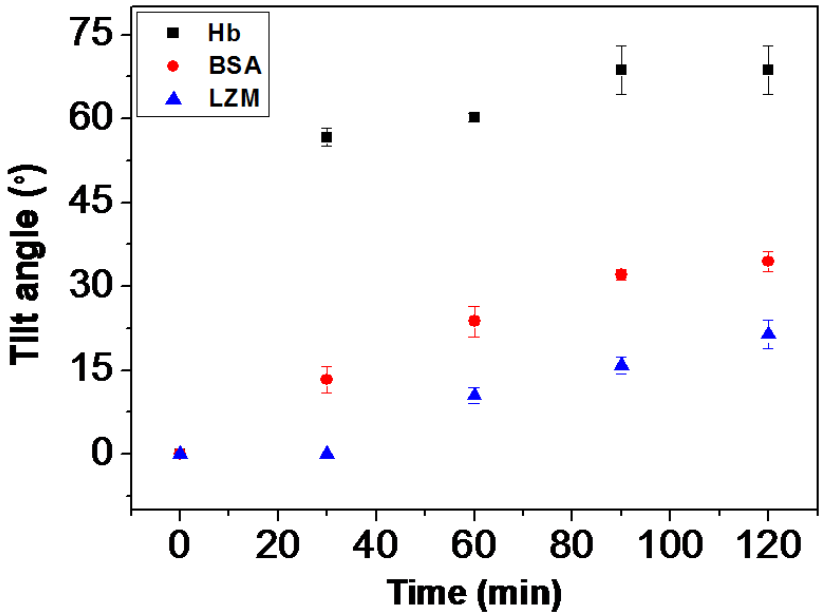

Figure 2.12 Graph showing the change in the tilt angle of the 5CB at LPS laden aqueous-LC interface on exposure to 50 nM aqueous solutions of Hb, BSA and LZM (measured relative to surface normal).

This observation was also supported by previous studies in which the binding constants of these abovementioned interactions were calculated by using the SPR technique.[21] Table 2.1 shows the direct correlation of binding constants obtained by using SPR along with the tilt angles and birefringence values of the LC for LPS interactions with Hb, BSA, and LZM. These results results reveal, for the first time, that in addition to detecting LPS–protein

interactions the LC-based system can quantify these interactions through changes in the ordering transition of LC at the fluid interface.

Biomolecular Interactions	Association constant (K_a L mol^{-1})	Birefringence (Δn)	Tilt Angle(°)
LPS – Hb	2.036×10^8	0.18 ± 0.01	69.26 ± 4.3
LPS –BSA	2.366×10^7	0.06 ± 0.001	35.15 ± 1.8
LPS – LZM	2.826×10^4	0.03 ± 0.004	21.40 ± 2.5

Table 2.1 The correlation of binding constants of interactions between LPS and Proteins with tilt angle and birefringence values of 5CB

Another significant observation reported herein is that the ordering transition of 5CB induced by binding of proteins to LPS-decorated LC interfaces is continuous, as evidenced by the gradual change in the tilt of the LC. Previous studies reported that contact of an aqueous dispersion of DLPC or LPS vesicles with the interface of a micrometer-thick film of nematic LC, such as 5CB, resulted in the spontaneous formation of the lipid monolayer on the interface of LC; this ensured discontinuous ordering transitions of the LC from planar to homeotropic.[22] Herein, however, we observed that the response of LPS monolayer to the solution of protein was a continuous change in the ordering of LC, in which the LC changed in orientation from perpendicular to the interface (prior to protein binding with LPS) to parallel to the interface (after protein–LPS binding). The interpretation of the continuous ordering transition was inspired by previous studies, which reported that heterogeneous interfaces comprised of nanoscopic patches, which caused homeotropic or planar anchoring of LC, could give rise to micrometer-scale tilting of the LC.[38–40] For example, Abbott and co-workers reported that continuous LC ordering transitions induced by binding of vesicles to protein-decorated LC interfaces was consistent with an inhomogeneous LC interface comprised of nanodomains of proteins and

phospholipids.[30, 41] Therefore, we interpret our results from two key interfacial processes. First, it involves the accumulation of proteins near the interfacial region of LC through specific binding of the proteins to the LPS-decorated interface. This is then followed by protein-driven reorientation of LPS on the LC interface. physicochemical phenomena, that LC ordering transitions have the potential to be useful for reporting specific binding events involving proteins.

2.4 Conclusions

The key result reported herein was that thin films of LC could be used to report the adsorption of biological proteins at LPS decorated aqueous–LC interface. We demonstrated that the LPS monolayer formed at the interface of the LC led to an anchoring transition of the LC (from homeotropic to planar) in contact with an aqueous solution of proteins (Hb, BSA, and LZM). We observed, however, that protein–LPS binding affinity changed the nature of the anchoring transitions of the LC significantly; this suggested that manipulation of the interfacial phase state of the LPS monolayer (due to changes in protein–LPS binding affinities) could provide the basis for a general, facile method to tune the LPS-induced responses of the LC to interfacial phenomena. We also observed that the response of the LC, owing to strong coupling between proteins and the LPS monolayer, remained invariant as a function of pH, and therefore, suggested that the ordering of the LC was independent of electrostatic interactions. Our results also demonstrated that protein–LPS binding affinity could be quantified by measuring the optical retardation of the LC. Interestingly, the retardation values were in accordance with the order of the binding constants between LPS and different proteins; a higher binding constant resulted in a greater tilt angle of the LC. Overall, the results presented herein suggested that LC could offer not only the basis of a novel analytical tool for fundamental studies of protein–LPS interactions, but could also be used to quantify specific binding of proteins on LPS-decorated aqueous–LC interfaces.

2.5 Experimental Section

2.5.1 Materials and methods

Lipopolysaccharides (from E.coli 0111:B4), human hemoglobin, lysozyme from chicken egg white, bovine serum albumin, 1,2-dioleoyl-Sn-glycero-3-phospho-rac-(1-glycerol) sodium salt (DOPG), Tris buffered saline (pH 7.4) and N,N-dimethyl-N-octadecyl-3-aminopropyltrimethoxysilyl chloride (DMOAP) were purchased from Sigma-Aldrich (St. Louis, MO). 1,2-Didodecanoyl-Sn-glycerol-3-phosphocholine (DLPC) and lysophosphatidic acid (LPA) were purchased from Avanti Polar Lipids, Inc. (Alabaster, AL). Sulfuric acid and hydrogen peroxide (30% w/v) were purchased from Merck. Ethanol was obtained from Jebsen & Jenssen GmbH and Co., Germany (Sd. fine–chem limited). The 5CB LC was obtained from Merck. Deionization of a distilled water source was performed using a Milli-Q-system (Millipore, bedford, MA). Fischer's Finest Premium Grade glass microscopic slides and cover glass were obtained from Fischer Scientific (Pittsburgh, PA). Gold specimen grids (20 μm thickness, 50 μm wide bars, 283 μm grid spacing) were obtained from Electron Microscopy Sciences (Fort Washington, PA).

2.5.2 Cleaning of Glass Substrates

Glass microscope slides were cleaned according to published procedures using 'piranha' solution [70:30 (% v/v) H_2SO_4:H_2O_2 (30%)], as described in detail elsewhere.[22] Briefly, the glass slides were immersed in a piranha bath at 100 °C for at least 1h and then rinsed in running deionized (DI) water for 5-10 min. Finally, the slides were rinsed sequentially in ethanol and then dried under a stream of nitrogen. The clean slides were stored in an oven at 100 °C for overnight. All other glassware was cleaned prior to use.

2.5.3. Treatment of Glass Microscope Slides with DMOAP

The cleaned glass slides were dipped into 0.1% (v/v) DMOAP solution in DI water for 5 min at room temperature and were then rinsed with DI water to remove unreacted DMOAP from the surface. The DMOAP coated glass slides were dried under a stream of nitrogen gas and kept in oven at 100 °C for 3 h to allow crosslinking of DMOAP.

2.5.4 Preparation of Optical Cells.

The DMOAP coated glass slides were then cut into squares for supporting LC. Then, a gold grid was placed on the slide, and approximately 0.3 μL of 5CB was dispensed onto the grid. Excessive LC was removed by using a capillary tube.

2.5.5 Formation of the Self-Assembled Monolayers of LPS.

LC laden with a LPS monolayer were prepared following procedures published in previous literature.[22] Powdered LPS (endotoxin) was dissolved in Milli-Q water at room temperature to obtain the required concentration. The resulting solutions were then sonicated for 5 min and vortexed for 10 min at room temperature. The LPS monolayer was formed by contacting the gold grid impregnated with 5CB to the LPS solution in the optical cell for a period of 2 h. The LPS monolayer was washed twice with Tris buffer (pH 7.4) prior to use.

2.5.6 Optical characterization of LC films in aqueous solutions.

The grid containing the LC was immersed in Tris buffer (10 mM, pH 7.4). The optical appearance was observed by using a polarizing optical microscope (Nikon ECLIPSE LV100POL, Japan) in the transmission mode. Each image was captured with a Q-imaging digital camera mounted on the microscope with an exposure time of 40 ms.

2.5.7 Tilt Angle Measurements.

The optical retardance of LC was measured using tilting compensator (type 2357 K, equipped with a calcite compensator plate, Leitz, Germany). The retardance values reported in this paper are the average obtained within four squares of the gold specimen grid used to host the LC. For a thin film of nematic LC with strong homeotropic anchoring ($\theta_1 = 0^o$) at the DMOAP-treated glass interface and a tilt of angle of θ_2 away from the surface normal at the aqueous-LC interface, the tilt of LC across the film varies linearly with position so as to minimize the elastic energy of the LC film (assuming splay and bend elastic constants of the LC to be equal). This result permits the establishment of a relationship between optical retardance (Δr) of the film of LC and the tilt of the director at the aqueous-LC interface (θ_S), namely

$$\Delta r \approx \int_0^d \left(\frac{n_e n_o}{\sqrt{n_o^2 sin^2\left(\frac{z}{d}\theta_s\right) + n_e^2 cos^2\left(\frac{z}{d}\theta_s\right)}} - n_o \right) dz$$

Where η_e and η_o are the indices of refraction parallel (so-called extraordinary refractive index) and perpendicular (ordinary refractive index) to the optical axis of the LC, respectively, and θ_S is the tilt angle of LC measured relative to the surface normal.[37] The retardance values measured using the Scope. A1 were used to calculate the tilt angle of LC at the aqueous-LC interface by numerically solving equation (1). The indices of refraction of 5CB were taken to be η_e = 1.71 and η_o = 1.52 (λ= 632 nm at 25 °C). In following the detailed of the procedure has been explained using an example.

After tilting the compensator plate from zero position to both positive and negative directions, two readings for the position of the compensator was observed 7° and 4°. To measure phase difference we need to add up this two values i.e. (2.9°+2.1°) =5°

Now we need to calculate corresponding log f value of 5. From table of log f values we got log f (5) = 19. Next, the value obtained was multiplied with log C value. log C is known as compensator constant. The value of log C is again dependent on wavelength of light used for this experiment. Here log C value will be 4.54 when λ= 632 nm. After multiplying this value with 19 we get (19 x 4.54) = 86.26.

Next to determine optical retardance (Δr), we need to divide the phase difference value from the thickness of the LC. For our experiment thickness of LC is 20000 nm.

Therefore, (Δr) will be (86.26/20000) = 0.004313. Next putting Δr, n_e and n_o values to equation 1 we get

$$.004313 = \frac{1.74 \times 1.52}{\sqrt{(1.52^2 sin^2\,\theta + 1.74^2 cos^2\theta)}} - 1.52$$

$$.004313 = \frac{2.6448}{\sqrt{(1.52^2 sin^2\,\theta + 1.74^2 cos^2\theta)}} - 1.52$$

$$\sqrt{(1.52^2 sin^2\,\theta + 1.74^2 cos^2\theta)} = \frac{2.6448}{1.52 + 0.004313}$$

$$\sqrt{(1.52^2 sin^2\,\theta + 1.74^2 cos^2\theta)} = 1.735$$

$$1.52^2 sin^2\,\theta + 1.74^2(1 - sin^2\,\theta) = 3.01$$

$$0.7172\ sin^2\,\theta = 3.01$$

$$sin\,\theta = 0.1566°$$

$$\theta = 9.009°$$

Therefore the tilt angle (θ) value obtained is 9.009°

2.5.8 Epifluorescence experiment

Fluorescence experiments were performed using Zeiss (Observer. A1) fluorescence microscope. With a fluorescence filter cube having a 480 nm excitation filter and a 534 nm emission filter samples were observed. Images were captured by Axio cam camera.

2.6 References

(1) Ryan, J. L.; Morrison, D. C., Ed.; CRC Press Inc.: Boca-Raton, Florida, **1992**; Vol. *2*; pp 75-104.

(2) Galanos, C.; Freudenberg, M. A. *Mediators Inflamm.* **1993**, *2*, S11-S16.

(3) Chu, L.; Bramanti, T. E.; Ebersole, J. L.; Holt, S. C. *Infect. Immun.* **1991**, *59*, 1932-1940.

(4) Opal, S. M.; Scannon, P. J.; Vincent, J. L.; White, M.; Carroll, S. F.; Palardy, J. E.; Parejo, N. A.; Pribble, J. P.; Lemke, H. *J. Infect. Dis.* **1999**, *180*, 1584-1589.

(5) Tesh, V. L.; Morrison, D. C. *J. Immunol.* **1988**, *141*, 3523-3531.

(6) Roth, R. I.; Kaca, W. *Biomater.Artif.Cells Immobilization Biotechnol*. **1994**, *22*, 387-398.

(7) Machnicki, M.; Zimecki, M.; Zagulski, T. *Int. J. Exp. Path*. **1993**, *74*, 433-439.

(8) Yu, B.; Wright, S. D. *J. Biol. Chem*. **1996**, *271*, 4100-4105.

(9) Brandenburg, K.; Koch, M. H. J.; Seydel, U. *Eur. J. Biochem*. **1998**, *258*, 686-695.

(10) Jurgens, G.; Muller, M.; Koch, M. H. J.; Brandenburg, K. *Eur. J. Biochem*. **2001**, *268*, 4233-4242.

(11) Takayama, K.; Din, Z. Z.; Mukerjee, P.; Cooke, P. H.; Kirkland, T. N. *J. Biol. Chem.* **1990**, *265*, 14023-14029.

(12) Bahl, N.; Du, R.; Winarsih, I.; Ho, B.; Kellogg, L. T.; Tidor, B.; Ding, J. L. *J. Biol. Chem.* **2011**, *286*, 37793-37803.

(13) Freudenberg, M. A.; Galanos, C. *Infect. Immun.* **1988**, *56*, 1352-1357.

(14) Benbarek, H.; Dupont, G. D.; Caudron, I.; Grulke, S.; Deby, C.; Lamy, M.; Serteyn, D. *Veter. Immunol. Immunopathol*. **1998**, *64*, 313-322.

(15) Sano, H.; Chiba, H.; Iwaki, D.; Sohma, H.; Voelker, D. R. *J. Biol. Chem.* **2000**, *275*, 22442-22451.

(16) Ohno, N.; Morrison, D. C. *J. Biol. Chem.* **1989**, *264*, 4434-4441.

(17) Ueda, T.; Tsurumaru, M.; Imoto, T. *J. Biochem.* **1998**, *124*, 712-716.

(18) Kaca, W.; Roth, R. I.; Levin, J. *J. Biol. Chem.* **1994**, *269*, 25078-25084.

(19) Gioannini, T. L.; Zhang, D.-S.; Teghanemt, A.; Weiss, J. P. *J. Biol. Chem.* **2002**, *277*, 47818-47825.

(20) Huber, M.; Kalis, C.; Keck, S.; Jiang, Z.; Georgel, P.; Du, X.; Shamel, L.; Sovath, S.; Mudd, S.; Beutler, B.; Galanos, C.; Freudenberg, M. A. *Eur. J. Immunol.* **2006**, *36*, 701–711.

(21) Yang, F.; Yang, X. *Front. Chem.China* **2008**, *3*, 14-17.

(22) Brake, J. M.; Daschner, M. K.; Luk, Y.-Y.; Abbott, N. L. *Science* **2003**, *302*, 2094-2097.

(23) Woltman, S. J.; Jay, G. D.; Crawford, G. P. *Nat. Mater.* **2007**, *6*, 929-938.

(24) Hartono, D.; Qin, W. J.; Yang, K.-L.; Lanry Yung, L.-Y. *Biomaterials* **2009**, *30*, 843-849.

(25) Hartono, D.; Lai, S. L.; Yang, K.-L.; Lanry Yung, L.-Y. *Biosens. Bioelectron.* **2009**, *24*, 2289-2293.

(26) Park, J.-S.; Abbott, N. L. *Adv. Mater.* **2008**, *20*, 1185-1190.

(27) Agarwal, A.; Sidiq, S.; Setia, S.; Bukusoglu, E.; de Pablo, J. J.; Pal, S. K.; Abbott, N. L. *Small* **2013**, *9*, 2785-2792.

(28) Hu, Q.-Z.; Jang, C. H. *ACS Appl. Mater. Interfaces* **2012**, *4*, 1791−1795.

(29) Hartono, D.; Xue, C. Y.; Yang, K.-L.; Lanry Yung, L.-Y. *Adv. Funct. Mater.* **2009**, *19*, 3574-3579.

(30) Tan, L. N.; Orler, V. J.; Abbott, N. L. *Langmuir* **2012**, *28*, 6364-6376.

(31) Sidiq, S.; Das, D.; Pal, S. K. *RSC Adv*. **2014**, *4*, 18889-18893.

(32) Price, A. D.; Schwartz, D. K. *J. Am. Chem. Soc.* **2008**, *130*, 8188-8194.

(33) Sivakumar, S.; Wark, K. L.; Gupta, J. K.; Abbott, N. L.; Caruso, F. *Adv. Funct. Mater.* **2009**, *19*, 2260-2265.

(34) Lin, I. H.; Miller, D. S.; Bertics, P. J.; Murphy, C. J.; de Pablo, J. J.; Abbott, N. L. *Science* **2011**, *332*, 1297-1300.

(35) Hartono, D.; Hu, Q. Z.; Jang, C. H. *Colloids Surf. B: Biointerfaces* **2013**, *108*, 142-146.

(36) Hu, Q. Z.; Jang, C. H. *Analyst* **2012**, *137*, 567-570.

(37) Lockwood, N. A.; Gupta, J. K.; Abbott, N. L. *Surf. Sci. Rep.* **2008**, *63*, 255-293.

(38) Kwok, H. S.; Li, Y. W.; Yeung, F. S. *Mol. Cryst. Liq. Cryst.* **2009**, *507*, 26– 40.

(39) Yeung, F. S.; Ho, J. Y; Li, Y. W.; Xie, F. C.; Tsui, O. K.; Sheng, P.; Kwok, H. S. *Appl. Phys. Lett.* **2006**, *88*, 051910 – 3.

(40) Tseng, M. C.; Fan, F.; Lee, C. Y.; Murauski, A.; Chigrinov, V.; Kwok, H. S. *J. Appl. Phys.* **2011**, *109*, 083109 –5.

(41) Tan, L. N.; Bertics, P. J.; Abbott, N. L. *Langmuir* **2011**, *27*, 1419 –1429.

(42) Brake, J. M.; Mezera, A. D.; Abbott, N. L. *Langmuir* **2003**, *19*, 8629 –8637.

Chapter 3

Design of bio-molecular interfaces using liquid crystals demonstrating endotoxin interactions with bacterial cell wall components

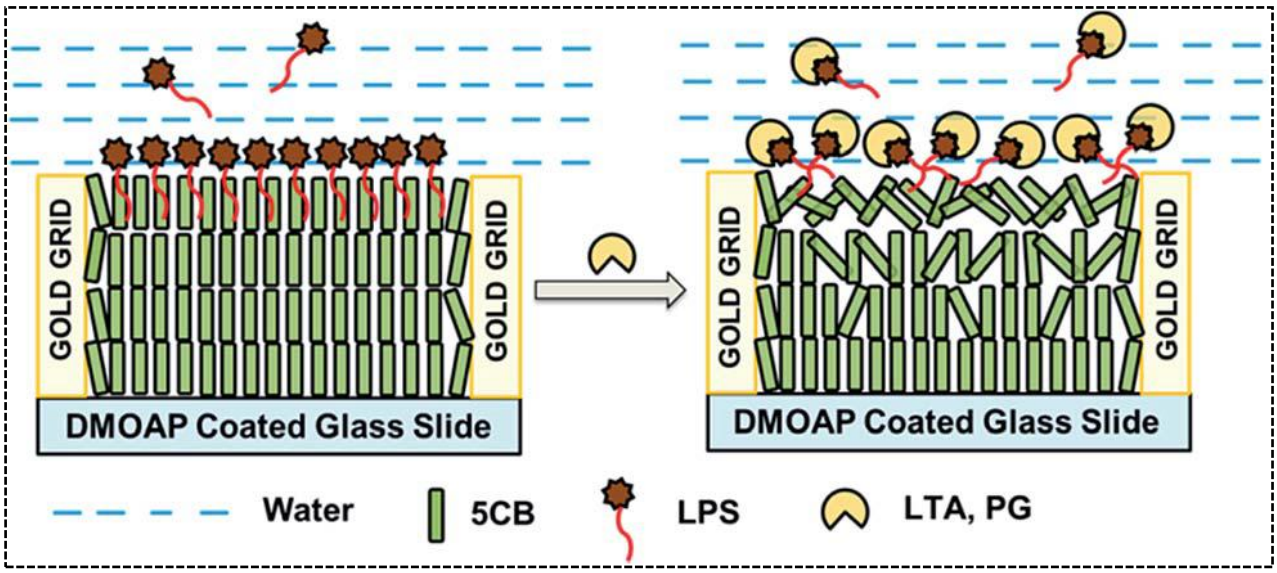

Interaction of different bacterial cell membrane components such as, peptidoglycan (PG) and lipoteichoic acid (LTA) with bacterial endotoxin (LPS) shows diverse consequences on the toxicity of Gram negative bacteria in mammalian hosts, implying the huge importance of studying this interaction for clinical understanding associated with Gram negative bacterial infections. In this advance, herein, we report a liquid crystal (LC) based simple, robust experimental design for rapid and precise recognition of the interaction of LPS with PG and LTA.

3.1 Introduction

In the last two decades, the incidence of Gram negative bacterial infections has progressively increased.[1–4] Currently, among one third of all microorganism mediated infections are caused by Gram negative bacteria and it is expected that these bacterial contagions will continue to rise and predominate in the years to come. Consequently, with increasing concern over Gram negative bacterial infection at present, the substantial medicinal efforts to combat microorganism infections are mainly focused on Gram negative bacteria.[5–7] From the light of vast pathophysiological studies, it has been well approved that the cell membrane components of Gram negative bacteria play as principal mediators in inducing Gram negative bacterial infections in mammalian hosts.[8–14]

Lipopolysaccharide (LPS), also known as bacterial endotoxin, is a major constituent of outer cell membrane of Gram negative bacteria. This amphipathic macromolecule is well recognized as important contributing factors to the pathogenesis of Gram negative bacterial infection. LPS consists of varying length of hydrophilic polysaccharide chains, covalently attached to hydrophobic lipid A moiety which is considered as most active toxic agent during Gram negative bacterial infection leading to high fever, septic shock, multiorgan failure syndrome and even death.[8–10] More recently, several clinical and pathophysiological studies on induced endotoxic behavior of LPS in mammalian cells have revealed and documented very interesting and crucial fact that these severe biological activities caused by LPS are largely intervened by the coexistence of different other bacterial (Gram negative as well as Gram positive) cell membrane components.[11] In this regard, peptidoglycan (PG) and lipoteichoic acid (LTA), two active outer cell membrane components of bacteria, have drawn widespread interest in clinically investigating their influence over the consequence of endotoxicity induced by LPS in mammalian hosts.[15–22]

PG is a glycan polymer containing long sugar chains of two alternating sugar derivatives, *N*-acetylglucosamine (NAG) and *N*-acetylmuramic acid (NAM) which are highly cross-linked through peptide bridges forming 3D mesh like layer. In both Gram negative and Gram positive bacteria PG plays an important role in maintaining structural integrity of bacterial cell membrane, as well as counteracting the osmotic pressure of the cytoplasm. Unlike PG, LTA is only found in the cell wall of Gram positive bacteria. It is a linear

polymer of phosphodiester linked glycerol phosphate and polysaccharide attached to diacylglycerol chains. The main function of LTA is to provide structural rigidity in bacterial cell wall and also regulate the function of auto wall enzymes. The interaction of LPS with these bacterial membrane constituents has been found to result in different effects on LPS endotoxicity, varying from reduction to enhancement. In this context, Thiemermann and his coworkers have reported synergistic behavior of PG towards LPS in mammalian hosts.[18] They have shown that co administration of PG and LPS from pathogenic Gram negative (E. coli) bacteria synergies to cause multiple organ dysfunctions in rat.[18] The presence of PG dramatically amplifies the lethal toxicity of LPS in mammalian host.[15–18] In contrast to this, agonist behavior of PG towards endotoxicity of LPS, LTA exhibits antagonistic influence on the activity of LPS by lowering its lethal toxicity in mammalian cell.[20–22] Hailman and his coworkers reported that LTA prevents LPS induced release of TNF from monocytes into blood serum via CD14 dependent pathway, ensuing in many fold decrease in LPS toxicity.[21] For example, Sugawara et al. have reported that LTA of Gram-positive cocci in the oral cavity may inhibit the action of LPS from periodontopathic Gram-negative bacteria resulting in the inhibition of the initiation of periodontal disease and therefore, LTA can be considered as useful agent for suppressing LPS induced periodontal diseases.[20]

Overall these entire clinical investigations on synergism between bacterial endotoxin and different bacterial cell membrane components (PG and LTA) clearly demonstrate its practical and pathophysiological significance from the aspect of better understanding in Gram negative bacterial infection in mammalian hosts. Interleukine-1 (IL-1),[23] toll like receptor (TLR) expression,[24] tumor necrosis factor (TNF),[25] are major biological assays available to study the interaction of endotoxin with cell membrane components. Although all of these methods provide several essential informations regarding these interactions, but lack of sensitivity, high cost, complex instrumentation and many other drawbacks limit their practical applications.

In this advance, herein, we report a simple, robust liquid crystal (LC) based system for rapid and precise detection of the interaction of LPS with different cell membrane components (PG, LTA). In recent years, the LC-based sensor has become an innovative

and promising tool for transducing and amplifying biomolecular interactions with high sensitivity and spatial resolution at the aqueous-LC interface. Due to its rapid orientational response on chemically functionalized surface, the nematic LC has served as an attractive medium to report chemical/biochemical events occurring at the interfacial biological membranes.[26–38] So far, fluid biometric membrane systems supported on LC have been coupled to the screening of specific protein binding event,[28,29,31–35] DNA hybridization,[39–42] monitoring enzymatic reaction,[30,36,43–45] and different pathogenic toxic detections.[46–49] For example, Abbott and his coworkers reported the specific interaction of immunoglobulin (IgG) antibody to the surface immobilized antigen resulting in a change in optical response of LC.[50] K.-L. Yang *et al*. designed pH sensitive liquid crystal sensor for monitoring enzymatic activities of penicillinase at aqueous–LC interface.[36] Wu *et al*. designed LC biosensor based on target triggering DNA dendrimers for the detection of p53 mutation gene.[51] D. Liu, *et al*. demonstrated the interaction between chitosan, a biopolymer, and lipid membrane at aqueous–LC interface.[52] More recently, C.-H. Jang *et al*. reported LC based detection of coagulating protease thrombin coupled to interactions between a polyelectrolyte and a phospholipid monolayer.[5] To the best of our knowledge, as yet, there is no report regarding the study of interaction of LPS with bacterial cell membrane components, PG and LTA, on LC based sensing platform. The study reported in this chapter is mainly two fold. First, we sought to determine if it is possible to report the interaction of bacterial endotoxin (LPS) with PG and LTA at aqueous–LC interface through surface-driven ordering transition in LC. Second, we sought to demonstrate if it is possible to quantify these interactions that would explore the use of the LC as novel quantitative analytical tool to report bimolecular interaction at aqueous–LC interface.

3.2 Objective

The approach revolves around the formation of LPS laden aqueous–LC interface. Past reports established that the hydrophobic interaction between alkyl chain of lipid A moiety of LPS interact with 5CB leads to the homeotropic orientation of the LC at aqueous-LC interface.[29,31] With this idea keeping in mind, we hypothesized that strong, specific interactions of LPS with cell membrane components, PG and LTA, may attribute to the disruption of LPS resulting in the orientational ordering transition of the LC from

homeotropic to tilted state which can be easily visualized under polarized optical microscopy. Overall, the results of the study served as a promising tool to the design of responsive LC-based system that can report LPS–PG/LTA interactions at aqueous-LC interface.

3.3 Results and discussion

3.3.1. LPS induced ordering transition of liquid crystal at aqueous-LC interface

In order to investigate the interaction of LPS with different cell membrane components, we first studied the interaction of LPS with LC at aqueous–LC interface. Figure 3.1 A represents the optical response of 5CB, confined within a gold grid supported on DMOAP coated glass slides, dipped into an aqueous solution of Tris buffer (pH 7.4). The bright and colorful optical appearance reflects the planar orientation of LC due to its interaction with water at aqueous-LC interface. Here, it is noteworthy that, the orientation of LC at DMOAP coated glass surface still remains homeotropic due to the interaction between alkyl chain of 5CB and DMOAP leading to an orientation of the nematic molecules perpendicular to the surface. Next, we observed a fast change in optical appearance of 5CB from bright to dark (Figure 3.1 B) when 0.1 mg mL^{-1} aqueous LPS solution in Tris buffer (pH 7.4) was introduced on LC interface, as expected. This observation clearly indicates that the homeotropic orientation of the LC mediated by LPS is a consequence of strong hydrophobic interaction of lipid chains of the LPS with the mesogens of the LC.[29–31] Notably, the bright rim observed around the grid circumference in Figure 3.1 B is due to direct interaction of peripheral 5CB with gold surface.

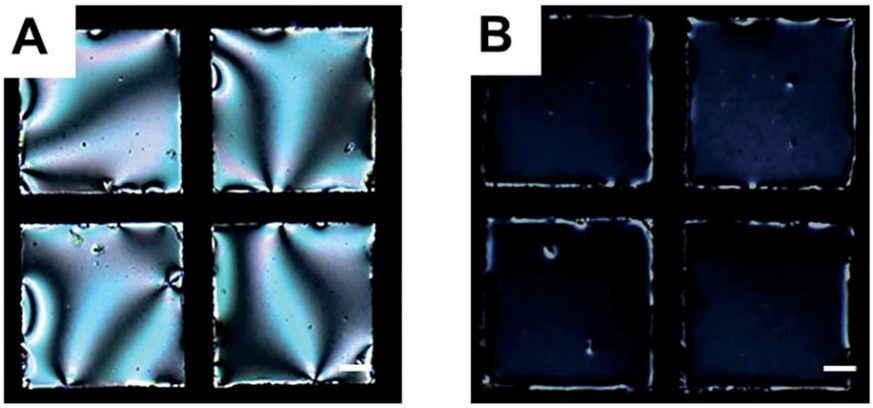

Figure 3.1 Polarized optical micrographs of 5CB films confined in TEM gold grid supported on DMOAP coated glass slides: (A) immersed in Tris buffer of pH 7.4 (10 mM), (B) incubated with LPS of 0.1 mg mL^{-1} for 2 h to form stable LPS laden aqueous-LC interface. Scale bar = 40 µm.

3.3.2. Characterization of LPS decorated aqueous-LC interface

Prior to study the interactions between LPS with cell membrane components at aqueous–LC interfaces, we verified that the surface used in our study was decorated with LPS. For this, first we exploited Langmuir film balance technique[54-56] to preorganize monolayer of LPS molecules at the air–water interface at well-defined densities, followed by transferring this LPS monolayer in a vertical dip fashion to LC–water interfaces stabilized within gold grids supported on DMOAP coated glass slide. Before attempting transfer of LPS from the air–water interface, we verified that the surface pressure (π) *vs* area (A_m) isotherms at the air–water interfaces. Figure 3.2 shows the representative π –A_m isotherm of LPS at the air–water interface. Collapse of the film was observed at surface pressures in the range of 56 mN m^{-1}.

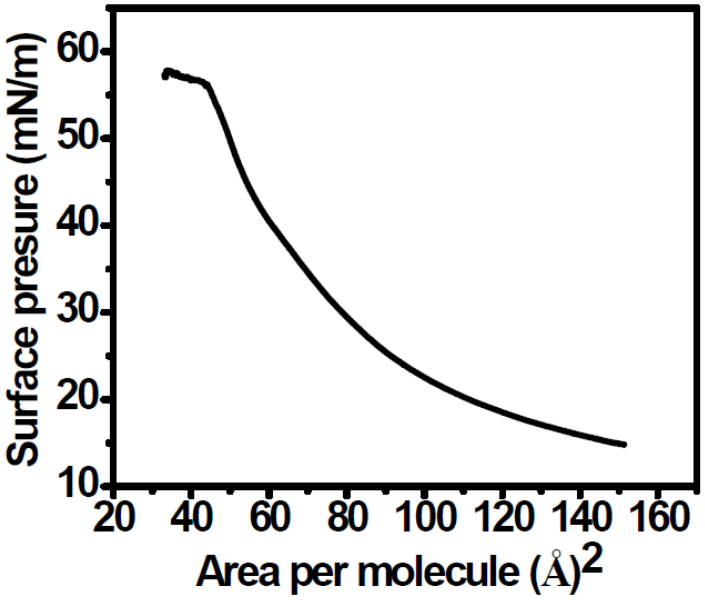

Figure 3.2 Surface pressure (π)-area per molecule (A_m) isotherm for LPS on NaCl based subphase at 25 °C.

Next, we quantitatively transfer LPS/LPS doped with 0.2% FITC–LPS monolayers from the air–water interface to the LC–aqueous interface at different surface pressures. The preparation of LPS monolayers *via* Langmuir transfer from the air–water interface was performed at a surface pressure of 0, 30 and 52 mN m^{-1}. Figure 3.3 shows the polarized optical micrographs and the respective epifluorescence micrographs of LPS monolayers formed *via* Langmuir transfer from the air–water interface at different surface pressures. The lower density of LPS monolayers at the LC interface gave rise to planar orientation of the LC (Figure 3.3 A and B) while the higher area density (higher surface pressure) LPS film transferred gave rise to homeotropic LC orientation as shown in Figure 3.3 C. Interestingly the corresponding epifluorescence measurements (Figure 3.3 D–F) shows the increase in fluorescence intensity indicate the quantitative transfer of LPS from the aqueous–air interface onto the aqueous–LC interface. Figure 3.3 G represents the linear increase of fluorescence intensity of LPS monolayers formed *via* Langmuir transfer from the air–water interface at increasing areal density. These results confirmed that LPS–LC interactions lead to the ordering transition of the LC at aqueous-LC interface.

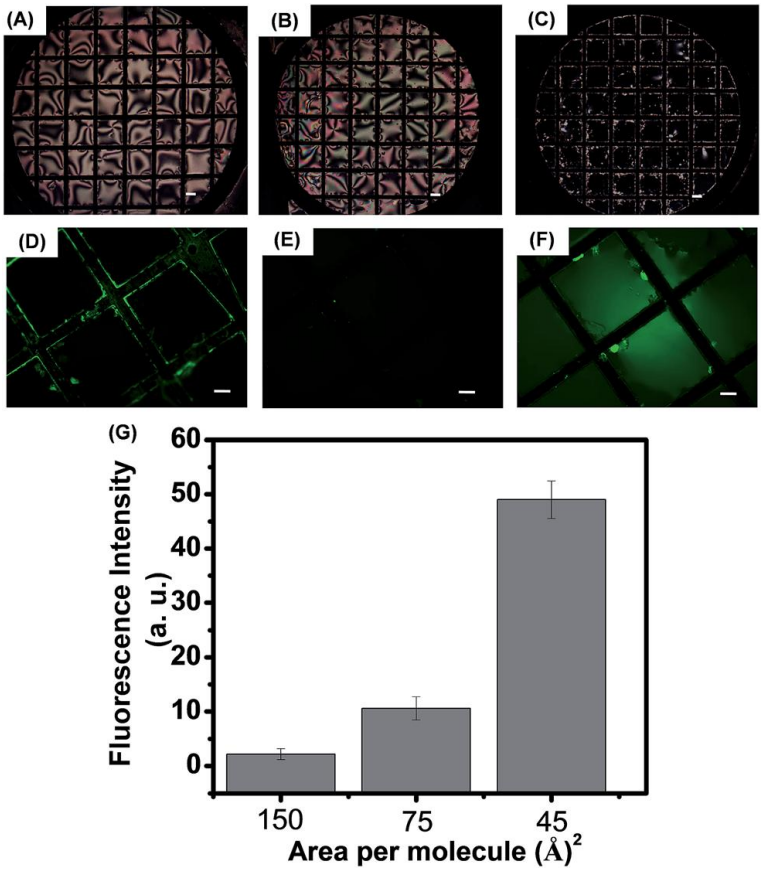

Figure 3.3 Polarized light micrographs of 0.5% (mol) FITC–LPS/LPS monolayers after transfer to the LC–water interface at surface pressure of (A) 0, (B) 30 and (C) 52 mN m^{-1}. (D)–(F) Corresponding fluorescence images of films at the LC–water interface. Scale bar = 40 μm. (G) Represents fluorescence intensity measured for a 0.5% (mol) FITC–LPS doped Langmuir monolayer of LPS at different areal density, measured at 25 °C.

We further characterized the adsorption of LPS on aqueous-LC interface using PM-IRRAS measurements. PM-IRRAS is used to evaluate the structural features of organic films of thickness less than 200 nm.[57] First, we functionalized gold coated micro-pillars (2–3 mm) with DMOAP. The IR spectra using polarization modulation of DMOAP coated surface shows the characteristic peaks of Si–C (1265 cm^{-1}), Si–O (1177 cm^{-1}, 1110 cm^{-1}), C–O (1043 cm^{-1}) and CH_3 and CH_2 stretching (2960 cm^{-1}, 2924 cm^{-1}, 2853 cm^{-1}) as shown in Figure 3.4 A. Next we poured the 5CB into the DMOAP coated micropillars. Figure 3.4 B shows the strong absorption bands of C≡N (2218 cm^{-1}) along with aromatic C–H stretching (3144 cm^{-1}, 3030 cm^{-1}), aliphatic CH_2 and CH_3 stretching (2924 cm^{-1}, 2852 cm^{-1}, 2801 cm^{-1}) and C–H bending (1474 cm^{-1}). Next we incubated 5CB confined in DMOAP coated micro-pillars with an aqueous solution of 0.1 mg mL^{-1} LPS for 6 h and kept this LPS adsorbed on 5CB film under vacuum for complete drying. In PM-IRRAS spectra of this LPS (Figure 3.4 C) absorbed 5CB films, we observed amide carbonyl stretching (1631 cm^{-1}), broad O–H stretching (3441 cm^{-1}), amide N–H stretching (3239 cm^{-1}), sharp amide N–H bending (1556 cm^{-1}), symmetric and anti-symmetric stretching of phosphate (1138 cm^{-1}, 1298 cm^{-1}), CH_2 and CH_3 stretching (2983 cm^{-1}, 2919 cm^{-1}, 2801 cm^{-1}) and C–H bending (1461 cm^{-1}). Overall these peaks strongly support presence of LPS[58] over 5CB film. In addition to this, in this spectrum we also observed aromatic C–H stretching (3108 cm^{-1}) and C≡N stretching (2205 cm^{-1}) correspond to the presence of 5CB film.

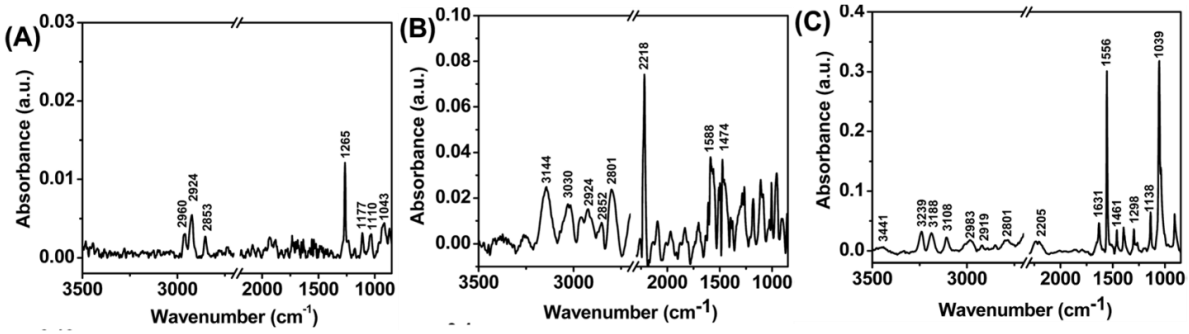

Figure 3.4 PM-IRRAS spectra generated from (A) DMOAP, (B) 5CB and LPS supported on micro-pillars coated with a uniformly deposited film of gold.

3.3.3 Interaction of bacterial cell membrane components (PG and LTA) with LPS at aqueous-LC interface

To study the interactions of LPS with cell membrane components, we first incubated this optical cell containing LPS solution for 2 h. Next, we exchanged the LPS solution with Tris buffer (pH 7.4) three times to remove excess free LPS from bulk solution and then exposed this LPS laden aqueous-LC interface in contact with different cell membrane components. In our first experiment, we added 0.1 mg mL^{-1} solution of PG in Tris buffer (pH 7.4) onto the LPS laden aqueous–LC interface. We observed an immediate change in optical response of the LC from dark to bright indicating an ordering transition of LCs from homeotropic to tilted state (Figure 3.5 A, B). This ordering transformation of LC was construed due to strong interaction between PG and LPS, which, in turn, disturb the ordered arrangement of LPS at aqueous–LC interface leading to the tilted orientation of LC molecules.

Next, we sought to investigate if the interaction of LTA with LPS interface could lead to an ordering transition in the LC. For this, we exposed 0.1 mg mL^{-1} of aqueous LTA solution in Tris buffer (pH 7.4) onto the LPS laden aqueous–LC interface. We observed a rapid change in the optical appearance of the LC from dark to bright (Figure 3.5 C, D) consistent with an ordering transition of 5CB from homeotropic to planar/tilted state. We interpreted the orientational ordering transition of the LC as a result of hydrophobic interaction of LTA with LPS decorated aqueous–LC interface.

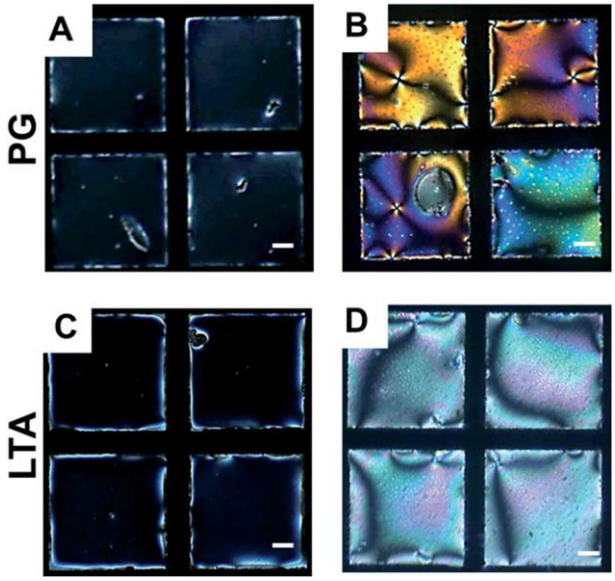

Figure 3.5 Optical images (crossed polars) of 5CB hosted in gold grids supported on DMOAP-coated glass slides in contact with (A and C) LPS for 2 h of incubation. (B and D) after introducing aqueous PG and LTA solution onto LPS laden aqueous-LC interface respectively. Scale bar =40 µm.

To confirm, whether electrostatic interactions play any role in determining ordering transitions of the LC at these interfaces, we performed several control experiments in different pH conditions other than the physiological pH. Interestingly, in all cases the dynamic ordering transitions towards a planar ordering in different pH conditions other than the physiological pH was found to be same. These observations, as a whole, suggest that the interactions between LPS with LTA and PG are not driven by electrostatically. This study also demonstrate that specific and non-specific interactions of different cell membrane components (PG and LTA) with endotoxin leading to changes in the optical appearance of LCs can be attributed to changes in the ordering of LPS molecules at the interface through strong interactions and thus, provide facile approach to study these interactions at aqueous–LC interface.

3.3.4 Control experiments

Next, to provide further insight into the above proposition that strong interaction of LPS with PG and LTA is responsible for the rapid ordering transitions of the LC at aqueous–LC

interface we performed several control experiments. First, we sought to investigate whether direct interaction of PG and LTA with interfacial 5CB molecules could able to alter the orientation of LCs in the absence of LPS membrane at the interface. To validate this, we added 0.2 mg mL^{-1} of aqueous solution of PG, LTA in Tris buffer (pH 7.4) directly onto LPS free aqueous-LC interface. We found that the optical appearance of the LC remained bright (even after 12 h of incubation or more) indicating a planar/tilted orientation of 5CB molecules at aqueous–LC interface (Figure 3.6). This observation clearly demonstrates that there are no direct interactions present between interfacial 5CB molecules and the cell membrane components which could perturb the orientation of LC at the interface.

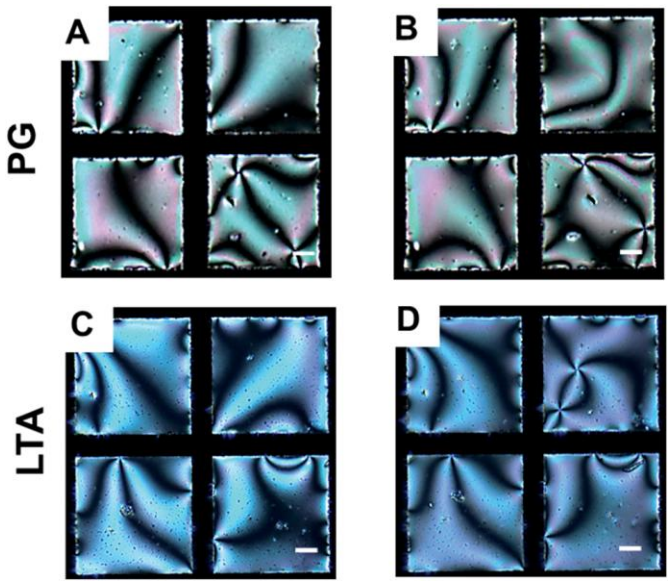

Figure 3.6 Polarized optical images of 5CB contained in gold grids supported on DMOAP-treated glass slides and placed into contact with (A and C) aqueous Tris buffer (pH 7.4) and (B and D) in contact with an aqueous solution of 0.2 mg mL^{-1} of PG and LTA respectively. Scale bar = 40 μm.

Second, we focused to carry out investigations on the specificity of the interactions of LPS with PG and LTA, respectively. For this, we replaced LPS with other three different phospholipids. We chose zwitterionic DLPC and negatively charged LPA and DOPG which can form self-assembled at aqueous–LC interfaces and orient the LC homeotropically. This study was motivated by two goals. First, we wanted to see whether these lipids (in addition to LPS) could able to interact with PG and LTA resulting in an

orientational ordering transition of the LC from homeotropic to tilted/planar at the interface. Second, we sought to find out if any favorable electrostatic interactions between these phospholipids (charged) and PG, LTA are responsible for the LC ordering at those interfaces. Interestingly, we observed that the optical appearance of the LC coupled to DLPC, LPA and DOPG decorated interfacial membrane remained dark (Figure 3.7) after addition of 0.2 mg mL^{-1} aqueous solution of PG, LTA in Tris buffer (pH 7.4) even after 6 h or more incubation. This observation strongly suggests that the interaction of PG and LTA coupled to these phospholipids decorated interfaces is not strong enough, if present, to disrupt the ordering of aqueous- LC interfaces.

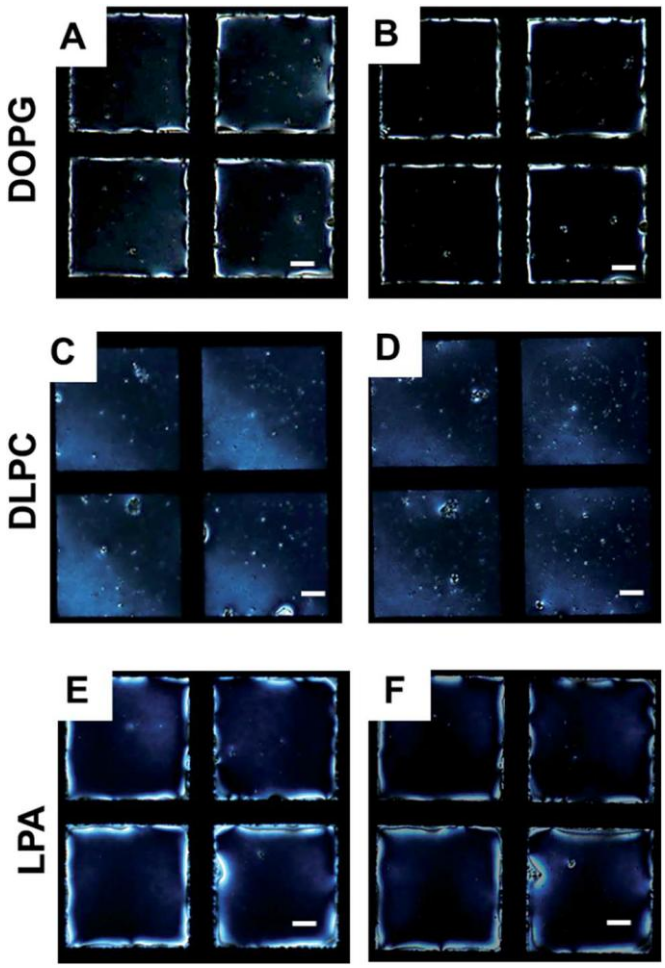

Figure 3.7 Polarized optical micrographs of aqueous-LC interface laden with (A) DOPG (C) DLPC and (E) LPA. (B, D and F) represents the optical response of 5CB decorated with DOPG, DLPC and LPA after adding biomolecules respectively. Scale bar = 40 µm.

In addition, we have measured the zeta potential of LPS, PG and LTA solutions (Tris buffer 20mM, pH 7.4) as shown in Table 3.1. The zeta potential was found to be negative in all cases. This also led us to conclude that the interaction of these cell membrane components (PG and LTA) with LPS is highly specific and not driven by electrostatically but could be through hydrophobic interactions.

Biomolecule	Zeta potential (mV)
LPS	-5.2 ± 1.4
PG	-4.7 ± 0.2
LTA	-11.7 ± 0.9
LPS+LTA	-9.8 ± 2.2
PG+ LPS	-4.4 ± 0.1

Table 1. Zeta potential measurements of different biomolecules used in the study.

To provide further insight into the mode of interaction of PG and LTA with LPS at aqueous–LC interface, we performed another control experiment using aqueous starch solution. This investigation is guided by the proposition from a recent report where Vagenende *et al*. have shown the self-assembly of LPS on allantoin crystals is initiated through hydrogen-bond attachment of hydrophilic LPS regions with amide-groups of allantoin.[59] Therefore, the principle motive behind performing this control experiment with starch was to find out whether hydrogen bonding plays any role in the interaction of these biomolecules (PG and LTA) with LPS self-assembled at aqueous–LC interface. Starch is a polysaccharide based macromolecule. PG and LTA also contain sugar units, having several hydroxyl functionalities, similar to starch. Therefore, we hypothesized that, like PG and LTA, if starch also could able to induce an ordering transition of LPS laden interfacial

5CB, we would be able to confirm that the hydrogen bonding between the polysaccharide moieties of these biomolecules (PG, LTA, starch)and LPS is mainly responsible to induce ordering transition of LPS decorated interfacial 5CB. But when we carried out this experiment, we found that the optical appearance of LPS laden 5CB interface remained dark over 2 hours of observation period after exposing 500 μg mL^{-1} aqueous starch solution onto aqueous-LC interface (Figure 3.8). This result strongly suggests the absence of any interaction between LPS and starch at 5CB interface and hydrogen bonding between LPS and starch does not play any role in inducing ordering transition of interfacial 5CB. In addition to that, from this experiment, we also confirmed that the interaction of these cell membrane components (PG and LTA) with LPS is highly specific and not driven by hydrogen bonding but dominated mostly through hydrophobic interactions.

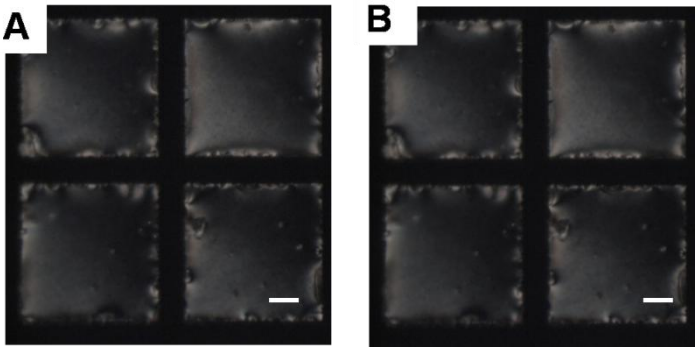

Figure 3.8 Polarized optical microscopic images of 5CB decorated with LPS at aqueous-LC interface, (A) before and (B) after addition of 500 μg/mL aqueous solution of starch respectively. Scale bar =40 μm.

3.3.5. Determination of detection limit of PG and LTA on LPS laden aqueous-LC interface

The above experiments demonstrate that the strong interaction of LPS with PG and LTA results in rapid ordering transition of the LCs from homeotropic to tilted/planar and these interactions are proven to be highly specific towards LPS at those interfaces. As the consequence of these interactions of cell membrane components with LPS in mammalian hosts is highly divergent towards the endotoxic behavior of LPS, therefore, in addition to, studying the interaction of PG, LTA with LPS at these interfaces, it is very important to

determine the sensitivity of the LC based system to the realization of a novel biosensor for detection of such biomolecular interactions. With this idea keeping in mind, we thought to determine limit of detection (LOD) and response time of the LC based system to study biomolecular interactions. For this, we compared the dynamic response of the LC at different concentrations of PG and LTA onto LPS decorated aqueous-LC interface. We first optimized the concentration of LPS (i.e. minimum concentration required) which is required to align the LC homeotropically at aqueous–LC interfaces. After exposing LPS of different concentrations onto aqueous–LC interface followed by removal of excess LPS from the solution, we found that 60 μg mL^{-1} is the optimum concentration at which LPS orients the LC homeotropically and results a uniform dark optical image under crossed polars (Figure 3.9). Second, we varied the concentration of PG and LTA onto LPS laden (at a concentration of 60 μg/mL) aqueous-LC interface.

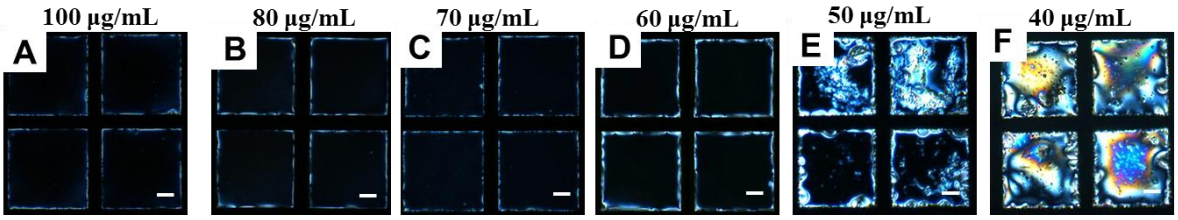

Figure 3.9 Polarized optical micrographs of 5CB supported on DMOAP coated glass slides on exposure to A) 100 μg/mL B) 80 μg/mL C) 70 μg/mL D) 60 μg/mL E) 50 μg/mL F) 40 μg/mL concentrations of LPS at aqueous-LC interface after washing with Tris buffer followed by 24 h of incubation. Scale bar = 40 μm.

Figure 3.10 A and B exhibits the optical appearance of the LC after addition of 60 μg mL^{-1} PG, LTA solutions (for 1 h of incubation)onto LPS laden aqueous-LC interface. We observed a rapid change in the optical appearance of the LC from dark to bright within 5 minutes-a little longer time span compare to the concentration (0.1 mg mL^{-1}) of PG/LTA used previously. After careful observation we revealed that the birefringence colors of 5CB (20 mm thick film) in presence of PG onto LPS laden LC interface was distinct from that of LTA, which clearly indicates the different tilted states of 5CB molecules at aqueous–LC interfaces. On further varying the concentrations of PG and LTA to successive lower concentrations values, we observed an increase in the time span of the change in the optical appearance of the 5CB (from completely dark to bright) (Figure 3.10 and 3.11).We also

observed a faster change in the optical appearance of the LC in presence of LTA in comparison to that of PG. Careful inspection of the LC ordering at different concentrations of PG and LTA, we found that 5CB exhibits only few bright spots (for 1 h of incubation, see Figure 3.10 E, F) at a concentration of 30 μg $mL^{-1}$of PG, whereas, LTA at the similar concentration (same 1 h of incubation) induced bright appearance of the LC (Figure 3.11 C, D).Further lowering the concentration to 28 μg mL^{-1} or below, we found that in presence of PG, the optical appearance of 5CB remained completely dark even after 2 h of incubation (Figure 3.10 G, H and I, J). Therefore, we confirmed that the concentration of 30 μg mL^{-1} as LOD for PG in our LC based sensing system. In contrast, we observed that 20 μg mL^{-1} of LTA could able to alter the optical appearance of the LC from dark to bright (Figure 3.11 E, F) within 1 h of incubation period suggesting higher sensitivity of LTA in comparison to PG. Therefore, we further decreased the concentration of LTA to determine the LOD value. Consequently, we found that 6 μg mL^{-1} is the LOD for LTA (Figure 3.11 I, J) which could induce an ordering transition of the LC at LPS laden aqueous–LC interface. Further decreasing the concentration (<6 μg mL^{-1}), we observed that LC retained its dark optical view, in presence of LTA even after 2 h of incubation period or more (Figure 3.11 K, L). The LOD values found as invariant at different pH (pH 2, pH 9) suggesting these binding events are independent of any electrostatic interaction and mainly driven by hydrophobic forces.

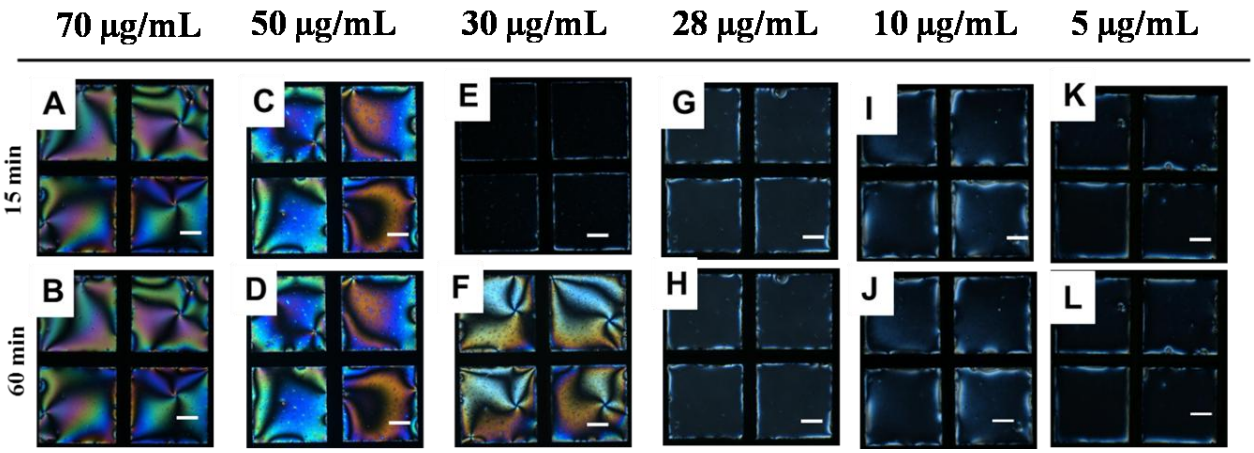

Figure 3.10 Polarized optical micrographs of 5CB decorated with LPS at aqueous/LC interface, after exposing aqueous PG solution with varying concentrations. (A, B) 70 μg/ml, (C, D) 50 μg/ml, (E, F) 40 μg/ml , (G, H) 28μg/ml , (I, J) 10 μg/ml , (K, L) 5 μg/ml.

Top and bottom row represents incubation of PG solution on LPS decorated aqueous-LC interface over period of 15 min and 60 min respectively. Scale bar = 40 μm.

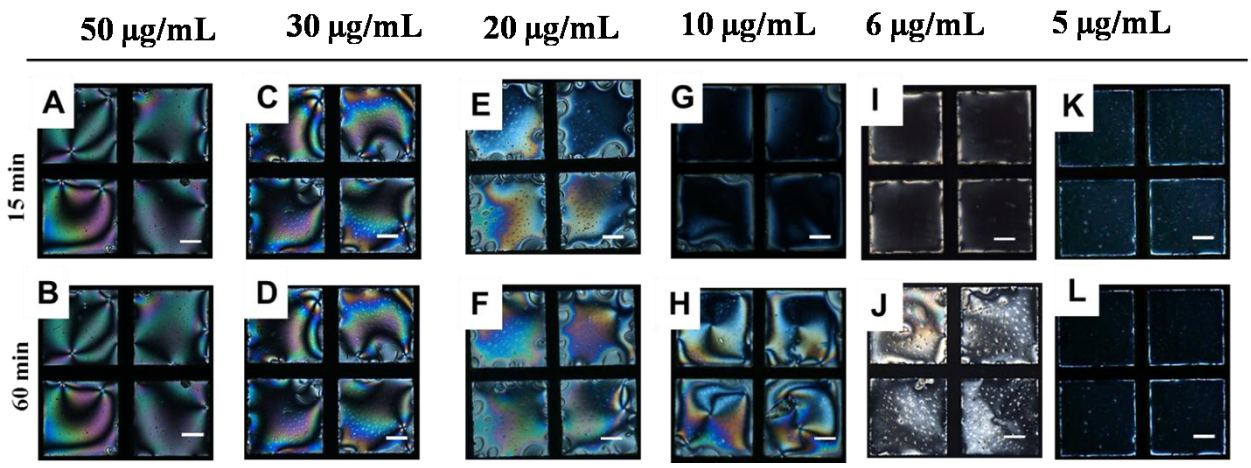

Figure 3.11 Polarized optical images of 5CB laden with LPS at aqueous-LC interface, after exposing aqueous LTA solution with varying concentrations. (A, B) 50 μg/ml, (C, D) 30 μg/ml, (E, F) 20 μg/ml , (G, H) 10 μg/ml , (I, J) 6 μg/ml , (K, L) 5 μg/ml. Top and bottom row represents incubation of LTA solution on LPS laden aqueous-LC interface over period of 15 min and 60 min respectively. Scale bar = 40 μm.

3.3.6 Average gray scale intensity and tilt angle measurements to quantify the interaction of Lf with LPS at the aqueous-LC interface

In a consequence, to report the change in the optical appearance of the LC with varying concentrations of PG and LTA, we measured the average gray scale intensity and quantified the optical response as a function of varying concentration of PG and LTA. Interestingly, we observed a continuous decrease in gray scale intensity with decreasing in concentration on addition of both PG and LTA (Figure 3.12). It is noteworthy; however, the measured gray scale intensity obtained for LTA on LPS laden aqueous–LC interface is higher than that of PG in all concentration range measured. This experiment demonstrates that LTA exhibits stronger binding affinity towards LPS with respect to PG which is also well-supported with their LOD values (6 μg mL^{-1} for LTA, whereas 30 μg mL^{-1} for PG).

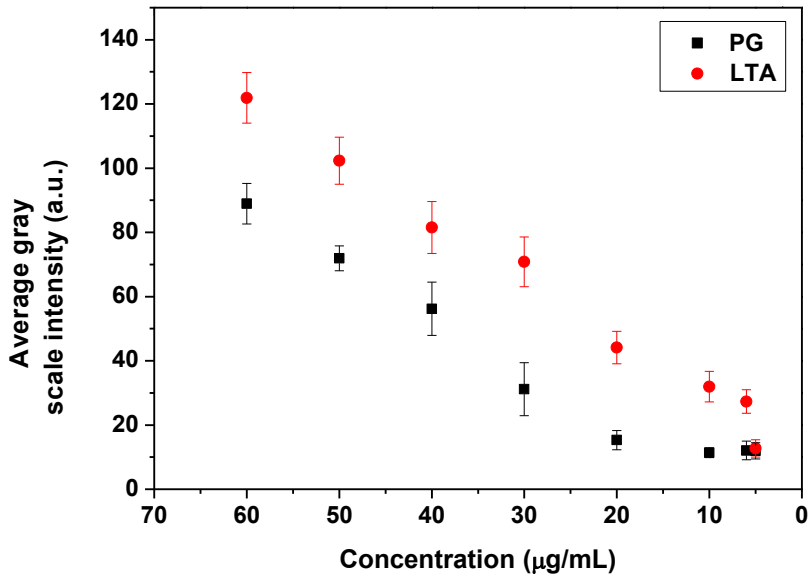

Figure 3.12 Represent the average gray scale intensity of optical images of 5CB films as a function of varying concentrations of PG and LTA on LPS decorated aqueous-LC interface.

In order to further validate our observation that the changes in the organization of the adsorbed LPS at the aqueous–LC interfaces underlie the different orientational behaviors of 5CB in presence of PG and LTA, we measured the tilt angle of LC during LPS–PG/LTA binding event at those interfaces. According to our hypothesis, the extent of disorderness of LPS membrane at aqueous–LC interface solely depends on the strength of binding of these cell membrane components (PG and LTA) with LPS which, in turn, lead to different tilt of LC molecules. Therefore, we thought that by measuring tilt angle at aqueous–LC interfaces (during LPS–PG/LTA binding events) it is possible to quantify the LC ordering at those interfaces. For this experiment, first, we chose 30 μg mL^{-1} of PG and LTA which is the minimum concentration required to show the change in the ordering transition of LC from homeotropic to tilted through interfacial binding with LPS–laden aqueous interface. Next, we calculated tilt angle of 5CB from the measured values of optical retardance using previously reported procedures (see experimental section for details).[37] Figure 3.13 shows the dynamic change in the tilt angle of 5CB coupled to PG and LTA onto LPS decorated aqueous–LC interface, respectively. We observed the (for 3.5 h of incubation or more) maximum tilt angle of 5CB obtained for PG–LPS and LTA–LPS were 26.7°±1.7 and

38.6°±2.5, respectively, at these interfaces. During the experiment, it may be pointed out that the tilt of 5CB is highest (38.6°±2.5) within80 minutes in case of LTA–LPS binding event and the value remained constant in rest of the observation period. In contrast the highest tilt angle (26.7°±1.7) of 5CB observed after 180 min in case of PG–LPS binding event. Consequently, these observations clearly indicate different binding affinity of LTA and PG towards LPS–laden aqueous–LC interface. We have mentioned earlier that stronger binding event could disrupt the LPS arrangement to a greater extent which, in turn, will lead to greater change in the tilt angle of 5CB at aqueous interfaces. Therefore, on this basis from tilt angle measurement we can say that LTA shows greater binding affinity towards LPS compared to PG. These experiments also reveal a quantitative approach to report the interaction of bacterial endotoxin with cell membrane components (PG and LTA) at aqueous–LC interface.

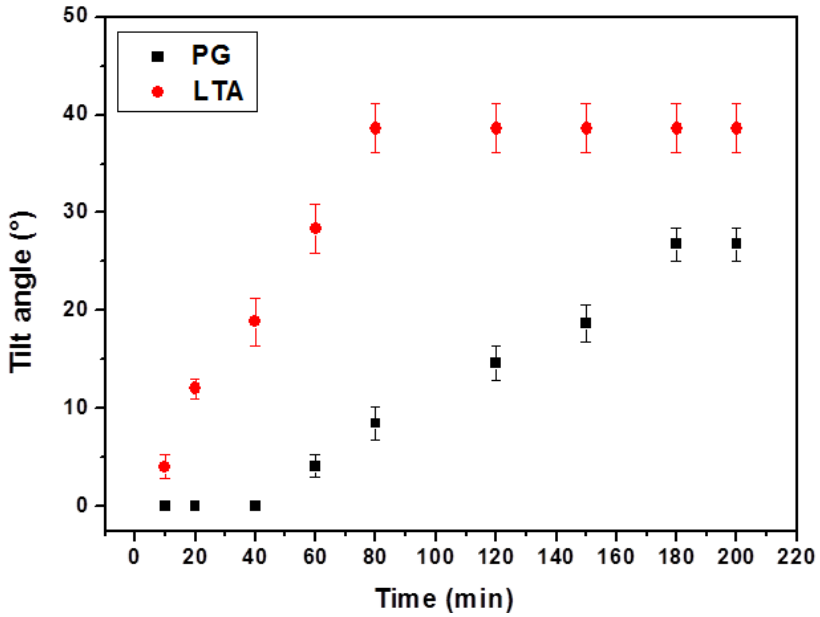

Figure 3.13 The tilt angle of 5CB decorated with LPS at aqueous-LC interface on exposure of 30 µg mL^{-1} aqueous solution of PG and LTA, respectively.

3.4 Conclusions

In summary, we have developed a subtle and robust LC-based sensing platform to study quantitatively the interaction of LPS with bacterial cell membrane components. We have

characterized the LPS laden aqueous-LC interface using Langmuir–Blodgett technique and PM-IRRAS measurement. We also measured hydrodynamic diameter of all the cell membrane components. Strong interaction between the cell membrane components (PG, LTA) and LPS induces the orientational ordering transition of LC at aqueous–LC interfaces through changes in the optical appearance of the LC. These binding events remain invariant as a function of pH and therefore, suggest that the ordering of the LC is independent of electrostatic interactions. We demonstrated that these interactions of PG and LTA are highly specific towards LPS in response to different lipids. The detection limit of our LC based system towards these biomolecular interactions was found 6 μg mL^{-1} and 30 μg mL^{-1} for LTA–LPS and PG–LPS interactions respectively, indicating high sensitivity of our system towards these biomolecular binding events at aqueous-LC interface. From average gray scale intensity measurement, we affirmed that binding affinity of LTA towards LPS is higher compared to PG. Finally, we have shown the quantitative approach of studying different binding affinities of PG and LTA towards LPS in light of tilt angle measurement. Overall, the results presented in this paper suggest that LC offer the basis of a novel analytical tool for fundamental studies of bacterial cell membrane components and endotoxin at interface and, specifically, they offer methods to quantify specific binding of PG and LTA on LPS decorated interface.

3.5 Experimental Section

3.5.1 Materials and methods

Lipopolysaccharides (from E.coli 0111:B4), peptidoglycan (from Micrococcus luteus), lipoteichoic acid (from Staphylococcus aureus), 1,2-dioleoyl-Sn-glycero-3-phospho-rac-(1-glycerol) sodium salt (DOPG), Tris buffered saline (pH 7.4) and N,N-dimethyl-N-octadecyl-3-aminopropyltrimethoxysilyl chloride (DMOAP), FITC conjugated lipopolysaccharides (from E.coli 0111:B4) were purchased from Sigma-Aldrich (St. Louis, MO). 1,2-Didodecanoyl-Sn-glycerol-3-phosphocholine (DLPC) and lysophosphatidic acid (LPA) were purchased from Avanti Polar Lipids, Inc. (Alabaster, AL). Sulfuric acid and hydrogen peroxide (30% w/v) were purchased from Merck. Ethanol was obtained from Jebsen & Jenssen GmbH and Co., Germany (Sd. fine–chem limited). The 5CB LC was obtained from Merck. Deionization of a distilled water source was performed using a Milli-

Q-system (Millipore, bedford, MA). Fischer's Finest Premium Grade glass microscopic slides and cover glass were obtained from Fischer Scientific (Pittsburgh, PA). Gold specimen grids (20 μm thickness, 50 μm wide bars, 283 μm grid spacing) were obtained from Electron Microscopy Sciences (Fort Washington, PA).

3.5.2 Cleaning of glass substrates

Glass microscope slides were cleaned according to published procedures using 'piranha' solution [70:30 (% v/v) H_2SO_4:H_2O_2 (30%)], as described in detail elsewhere.[34] Briefly, the glass slides were immersed in a piranha bath at 100°C for at least 1 h and then rinsed in running deionized (DI) water for 5-10 min. Finally, the slides were rinsed sequentially in ethanol and then dried under a stream of nitrogen. The clean slides were stored in an oven at 100° C for overnight. All other glassware was cleaned prior to use.

3.5.3 Treatment of glass microscope slides with DMOAP

The cleaned glass slides were dipped into 0.1% (v/v) DMOAP solution in DI water for 5 min at room temperature and were then rinsed with DI water to remove unreacted DMOAP from the surface. The DMOAP coated glass slides were dried under a stream of nitrogen gas and kept in oven at 100 °C for 3 h to allow crosslinking of DMOAP.

3.5.4 Preparation of optical cells

The DMOAP coated glass slides were then cut into squares for supporting LC. Then, a gold grid was placed on the slide, and approximately 0.3 μL of 5CB was dispensed onto the grid. Excessive LC was removed by using a capillary tube.

3.5.5 Formation of the LPS decorated LC film

LC laden with a LPS monolayer were prepared following procedures published in previous literature.[34] Powdered LPS (endotoxin) was dissolved in Milli-Q water at room temperature to obtain the required concentration. The resulting solutions were then sonicated for 5 min and vortexed for 10 min at room temperature. The LPS monolayer was formed by contacting the gold grid impregnated with 5CB to the LPS solution in the optical cell for a period of 2 h. The LPS monolayer was washed twice with Tris buffer (pH 7.4) prior to use.

3.5.6 Preparation of Vesicles

Vesicles were prepared according to the published procedures.[35] Briefly, the lipids were dissolved in chloroform (0.5 mL) and dispensed into round bottomed flask. Prior to resuspension, the chloroform was evaporated from the flask under vacuum for at least 2 h until it formed a thin film along the inner walls of the flask. The lipid film formed in the flask was then placed under a stream of nitrogen for 30 min. The dried lipid was then hydrated in the aqueous solution (DI water) for at least 1h and vortexed for 1 min. This results in the cloudy solution indicative of large multilamellar vesicles. Subsequent sonication of lipid suspension using a probe ultrasonicator (1 x 15 min at 25 W) resulted in a clear solution. Vesicles size was determined by DAWN8+ dynamic light scattering instrument. Prior to dynamic light scattering measurements, the solution of DLPC, LPA and DOPG vesicles were filtered twice using 0.22 μm filter. The vesicles were used within 24 h of their preparation.

3.5.7 Optical characterization of LC films in aqueous solutions

The grid containing the LC was immersed in Tris buffer (10 mM, pH 7.4). The optical appearance was observed by using a polarizing optical microscope (Nikon ECLIPSE LV100POL, Japan) in the transmission mode. Each image was captured with a Q-imaging digital camera mounted on the microscope with an exposure time of 40 ms.

3.5.8 Tilt Angle Measurements

The optical retardance of LCs was measured using tilting compensator (type 2357 K, equipped with a calcite compensator plate, Leitz, Germany). The retardance values reported in this paper are the average obtained within four squares of the gold specimen grid used to host the LCs. For a thin film of nematic LCs with strong homeotropic anchoring ($\theta_1 = 0^o$) at the DMOAP-treated glass interface and a tilt of angle of θ_2 away from the surface normal at the aqueous-LC interface, the tilt of LCs across the film varies linearly with position so as to minimize the elastic energy of the LC film (assuming splay and bend elastic constants of the LCs to be equal). This result permits the establishment of a relationship between optical retardance (Δr) of the film of LCs and the tilt of the director at the aqueous-LC interface (θ_S), namely equation 1

$$\Delta r \approx \int_0^d \left(\frac{n_e n_o}{\sqrt{n_o^2 sin^2\left(\frac{z}{d}\theta_s\right) + n_e^2 cos^2\left(\frac{z}{d}\theta_s\right)}} - n_o \right) dz$$

Where n_e and n_o are the indices of refraction parallel (so-called extraordinary refractive index) and perpendicular (ordinary refractive index) to the optical axis of the LCs, respectively, and θ_S is the tilt angle of LCs measured relative to the surface normal.[37] The retardance values measured using the Scope. A1 were used to calculate the tilt angle of LCs at the aqueous-LC interface by numerically solving equation (1). The indices of refraction of 5CB were taken to be n_e = 1.711 and n_o = 1.5296 (λ = 632 nm at 25 °C).In following the detailed of the procedure has been explained using an example.

After tilting the compensator plate from zero position to both positive and negative directions, two readings for the position of the compensator was observed 7° and 4°. To measure phase difference we need to add up this two values i.e. (2.9°+2.1°) =5°

Now we need to calculate corresponding log f value of 5. From table of log f values we got log f (5) = 19. Next, the value obtained was multiplied with log C value. log C is known as compensator constant. The value of log C is again dependent on wavelength of light used for this experiment. Here log C value will be 4.54 when λ= 632 nm. After multiplying this value with 19 we get (19 x 4.54) = 86.26.

Next to determine optical retardance (Δr), we need to divide the phase difference value from the thickness of the LC. For our experiment thickness of LC is 20000 nm.

Therefore, (Δr) will be (86.26/20000) = 0.004313. Next putting Δr, n_e and n_o values to equation 1 we get

$$.004313 = \frac{1.74 \times 1.52}{\sqrt{(1.52^2 sin^2\,\theta + 1.74^2 cos^2\theta)}} - 1.52$$

$$.004313 = \frac{2.6448}{\sqrt{(1.52^2 sin^2\,\theta + 1.74^2 cos^2\theta)}} - 1.52$$

$$\sqrt{(1.52^2 sin^2\,\theta + 1.74^2 cos^2\theta)} = \frac{2.6448}{1.52 + 0.004313}$$

$$\sqrt{(1.52^2 sin^2\,\theta + 1.74^2 cos^2\theta)} = 1.735$$

$$1.52^2 sin^2\,\theta + 1.74^2(1 - sin^2\,\theta) = 3.01$$

$$0.7172\ sin^2\,\theta = 3.01$$

$$\sin\theta = 0.1566$$

$$\theta = 9.009°$$

Therefore the tilt angle (θ) value obtained is 9.009°

3.5.9 Epifluorescence imaging of aqueous–LC interface

The LC-filled grid was incubated under LPS solution containing FITC-conjugated LPS. After incubation the solution was then exchanged with distilled water thrice to remove the excess of FITC-LPS from the bulk solution. The LC-filled grid supported on DMOAP coated surfaces was then removed from the solution and placed over a glass slide. Fluorescence imaging was performed with Zeiss (Observer.A1) fluorescence microscope. The samples were viewed using a fluorescence filter cube with a 460 nm excitation filter and a 534 nm emission filter. Images were obtained with Axio cam camera.

3.5.10 Fluorimetric measurement

Fluorescence intensity of the sample was measured with a SHIMADZU RF-5301PC SPECTROFLUROPHOTOMETER (Shimadzu Corp., Kyoto, Japan). For the detection

FITC fluorescent probe an excitation wavelength 490 nm (0.5 nm excitation slit) and an emission wavelength range of 500–534 nm (5 nm emission slit) was selected.

3.5.11 Preparation of LPS monolayer

Surface pressure (p)–area per molecule (A_m) isotherm experiments were carried out in an Langmuir Blodgett (LB) trough.LPS monolayers were prepared at the air–water interface. The surface pressure was measured using the standard Wilhelmy plate technique in a trough (MINITROUGH, KSV, Finland) enclosed in a Plexiglas box to reduce surface contamination. The subphase of the trough was filled with 1 M NaCl. Using a microsyringe, 50 µL of lipid (LPS and LPS doped with 0.2%FITC–LPS) solution (1 mg mL^{-1}) in chloroform: methanol (3:1) was carefully spread onto the aqueous subphase. After spreading, the film was left for 20 min, allowing the solvent to evaporate. The p–A_m isotherms were obtained by symmetric compression of the barriers with a constant compression rate of 10 mm min^{-1}. Surface pressure and trough area were recorded simultaneously using Nima software. Based upon the volume deposited, the average molecular weight, and concentration of solution, the average area per molecule was calculated. All the measurements were performed at a room temperature of 25° C. Once deposited and transferred onto the 5CB confined in gold grid supported on DMOAP coated glass slide supported on gold films at a surface pressure of 56 mN m^{-1}, these supported LPS monolayers were kept under vacuum.

3.5.12 Polarization modulation infrared reflection absorption spectroscopy

The gold films with thicknesses of 2000 Å were deposited onto micropillars (array of nickel (Ni) micropillars electroplated on a glass substrate) mounted on rotating planetaries (no preferred direction or angle of incidence) by using thermal evaporator (Excel Instruments, India). These gold coated micropillars were dipped into 0.1%(v/v) DMOAP solution in DI water for 5 min at room temperature and were then rinsed with DI water to remove unreacted DMOAP from the surface. The DMOAP coated micropillars were dried under a stream of nitrogen gas and kept in oven at 100° C. Then, 5CB was dispersed onto the micropillars. Deposited LPS onto a5CB immobilized on DMOAP supported on micro-pillars coated with a uniformly deposited film of gold (2000 Å) were examined by using PM-IRRAS. A Bruker PMA 50 connected to the external beam port of a Bruker Tensor 27

FT-IR spectrometer was used for PM-IRRAS measurements. The deposited LPS on a gold sample was mounted on an attachment for PM-IRRAS measurements within the PMA 50 compartment. After reflection of the polarized light incident on the substrate at an angle of incidence of 82 from the surface normal, the IR beam was focused on a liquid nitrogen-cooled photovoltaic MCT detector in the PMA 50 cabinet. A photoelastic modulator (Hinds, PEM 90) was used to modulate the polarization of the light at a frequency of 50 kHz. Demodulation was performed with a lock-in-amplifier (Standford Research Systems, SR830 DSP). Before measurements, the spectrometer was allowed for a complete purge with nitrogen for at least 30 min. Each spectrum is the sum of 100 individual spectra collected at a resolution of 4 cm^{-1} with photoelastic modulator (ZnSe, 42 kHz, AR-coated) set to 1600 cm^{-1}. Data was collected as differential reflectance (DR/R)/absorbance versus wavenumbers.

3.5.13 Dynamic light scattering

(DLS) Hydrodynamic size (diameter) measurements of bacterial cell wall components and LPS were performed on a Malvern Zetasizer Nano ZS90 (Malvern Instruments, Southborough, Massachusetts). The DLS instrument was operated under the following conditions: temperature: 25° C, detector angle: 90° incident laser wavelength: 632 nm, and laser power: 4 mW. Samples were prepared in Tris buffer (pH 7.4) followed by equilibration typically 5 minutes.

3.5.14 Zeta potential measurement

A Malvern Zetasizer Nano ZS instrument (Malvern Instruments, Southborough, Massachusetts) was used to measure zeta potential at 25° C for bacterial cell wall components. Samples prepared for the DLS measurements were loaded into a pre rinsed polystyrene cuvette for the zeta potential measurements. An applied voltage of 100 V was used for the measurement. A minimum of three measurements were made per sample.

3.6 References

(1) Giske, C. G.; Monnet, D. L.; Cars, O.; Carmeli, Y. *Antimicrob. Agents Chemother.* **2008**, *52*, 813-821.

(2) Engel, L. S. *Emerg. Med.* **2009**, *41*, 18-27.

(3) Wright, G. D. *Nat. Rev. Microbiol.* **2007**, *5*, 175-186.

(4) Turhan, V.; Mutluoglu, M.; Acar, A.; Hatipoglu, M.; Onem, Y.; Uzun, G.; Ay, H.; Oncul, O.; Gorenek, L. *J. Infect. Dev. Citries.* **2013**, *7*, 707-712.

(5) Beutler, B.; Rietschel, E. T. *Nat. Rev. Immunol.* **2003**, *3*, 169-176.

(6) Tesh, V. L.; Morrison, D. C. *J. Immunol.* **1988**, *141*, 3523-3531.

(7) Roth, R. I.; Kaca, W. *Immobilization Biotechnol*. **1994**, *22*, 387-398.

(8) Galanos, C.; Freudenberg, M. A. *Mediators Inflamm.* **1993**, *2*, S11-S16.

(9) Chu, L.; Bramanti, T. E.; Ebersole, J. L.; Holt, S. C. *Infect. Immun.* **1991**, *59*, 1932-1940.

(10) Opal, S. M.; Scannon, P. J.; Vincent, J. L.; White, M.; Carroll, S. F.; Palardy, J. E.; Parejo, N. A.; Pribble, J. P.; Lemke, H. *J. Infect. Dis.* **1999**, *180*, 1584-1589.

(11) Myhre, A. E.; Aasen, A. O.; Thiemermann, C.; Wang, J. E. *Shock* **2006**, *25*, 227-235.

(12) Daziarski, R. *J. Biol. Chem*. **1991**, *266*, 4719-4725.

(13) Natanson, C.; Danner, R. L.; Ellin, R. J.; Hosseini, J. M.; Peart, K. W.; Banks, S. M.; Macvitte, T. J.; Walker, R. I.; Parrillo, J. E. *J. Clin. Inves.* **1989**, *83*, 243-251.

(14) Takayama, K.; Din, Z. Z.; Mukerjee, P.; Cooke, P. H.; Kirkland, T. N. *J. Biol. Chem.* **1990**, *265*, 14023-14029.

(15) Wang, J. E.; Jorgensen, P. F.; Ellingsen, E. A.; Almiof, M.; Theimermann, C.; Foster, S. J., Aasen, A. O.; Solberg, R. *Shock* **2001**, *16*, 178-182.

(16) Takada, H.; Galanos, C. *Infect. Immun.* **1987**, *55*, 409-413.

(17) Parant, M.; Parant, F.; Vinit, M. A.; Jupin, C.; Noso, Y.; Shedid, L. *J. Leukoc. Biol.* **1990**, *47*, 164-169.

(18) Wary, G. M.; Foster, S. J.; Hinds, C. J.; Theimermann, C. *Shock* **2001**, *15*, 135-142.

(19) Wolfert, M. A.; Murray, T. F.; Boons, G. J.; Moore, J. N. *J. Biol. Chem.* **2002**, *277*, 39179-39186.

(20) Sugawara, S.; Arakaki, R.; Rikiishi, H., Takada, H. *Infect. Immun.* **1999**, *67*, 1623-1632.

(21) Kusunoki, T.; Hailman, E.; Juan, T. S.-C.; Lichenstein, H. S.; Wright, S. D. *J. Exp. Med.* **1995**, *182*, 1673-1682.

(22) Nisengard, R. J.; Newman, M. G. Ed. *Oral microbiology and immunology*, The W.B. Saunders Co., Philadelphia, Pa., **1994**, *2*nd ed., pp- 360-384.

(23) Lichtman, S. N.; Wang, J. J.; Schwab, H.; Lemasters, J. J. *Hepatology* **1994**, *19*, 1013-1022.

(24) Hadley, J. S.; Wang, J. E.; Foster, S. J.; Theimermann, C.; Hinds, C. J. *Infect. Immun.* **2005**, *73*, 7613-7619.

(25) Mattsson, E.; Verhage, L.; Rollof, J.; Fleer, A.; Dijk, H. V. *FEMS. Immunol. Med. Microbiol.* **1993**, *7*, 281-287.

(26) Hartono, D.; Qin, W. J.; Yang, K.-L.; Lanry Yung, L.-Y. *Biomaterials* **2009**, *30*, 843-849.

(27) Hartono, D.; Lai, S. L.; Yang, K.-L.; Lanry Yung, L.-Y. *Biosens.Bioelectron.* **2009**, *24*, 2289-2293.

(28) Park, J.-S.; Abbott, N. L. *Adv. Mater.* **2008**, *20*, 1185-1190.

(29) Agarwal, A.; Sidiq, S.; Setia, S.; Bukusoglu, E.; de Pablo, J. J.; Pal, S. K.; Abbott, N. L. *Small* **2013**, *9*, 2785-2792.

(30) Hu, Q.-Z.; Jang, C. H. *ACS Appl. Mater. Interfaces* **2012**, *4*, 1791−1795.

(31) Brake, J. M.; Daschner, M. K.; Luk, Y.-Y.; Abbott, N. L. *Science* **2003**, *302*, 2094-2097.

(32) Tan, L. N.; Orler, V. J.; Abbott, N. L. *Langmuir* **2012**, *28*, 6364-6376.

(33) Sidiq, S.; Das, D.; Pal, S. K. *RSC Adv*. **2014**, *4*, 18889-18893.

(34) Woltman, S. J.; Jay, G. D.; Crawford, G. P. *Nat. Mater.* **2007**, *6*, 929-938.

(35) Luk, Y.-Y.; Tingey, M. L.; Dickson, K. A.; Raines, R. T.; Abbott, N. L. *J. Am. Chem. Soc.* **2004**, *126*, 9024-9032.

(36) Bi, X.; Hartono, D.; Yang, K.-L. *Adv. Funct. Mater.* **2009**, *19*, 3760-3765.

(37) Das, D.; Sidiq, S.; Pal, S. K. *ChemPhysChem* **2015**, *16*, 753–760.

(38) Sidiq, S.; Verma, I.; Pal, S. K. *Langmuir* **2015**, *31*, 4741–4751.

(39) Price, A. D.; Schwartz, D. K. *J. Am. Chem. Soc.* **2008**, *130*, 8188-8194.

(40) Yang, S.; Wu, C.; Tan, H.; Wu, Y.; Liao, S.; Yu, Z.; Shen, G.; Yu, R. *Anal.Chem.* **2013**, *85*, 14−18.

(41) Tan, H.; Yang, S. Y.; Shen, G. L.; Yu, R. Q.; Wu, Z. Y. *Angew.Chem. Int. Ed.* **2010**, *49*, 8608−8611.

(42) Yang, S. Y.; Liu, Y. M.; Tan, H.; Wu, C.; Wu, Z.; Shen, G. L.; Yu, R. *Chem. Commun.* **2012**, *48*, 2861−2863.

(43) Chen, C.-H.; Yang, K.-L. *Sens. Actuators, B* **2013**, *181*, 368– 374.

(44) Hu, Q.-Z.; Jang, C.-H. *J. Biotechnol.* **2012**, *157*, 223– 227.

(45) Hu, Q.-Z.; Jang, C.-H. *Colloids Surf. B: Biointerfaces* **2011**, *88*, 622-626.

(46) Lin, I. H.; Meli, M. V.; Abbott, N. L. *J. Colloid Interface Sci.* **2009**, *336*, 90–99.

(47) Espinoza, L. A. T.; Schumann, K. R.; Luk, Y.-Y.; Israel, B. A.; Abbott. N. L. *Langmuir* **2004**, *20*, 2375-2385.

(48) Cheng, L.-L.; Luk, Y.-Y.; Murphy, C. J.; Israel, B. A.; Abbott, N. L. *Biomaterials* **2005**, *26*, 7173-7182.

(49) Jang, C.-H.; Cheng, L.-L.; Olsen, C. W.; Abbott, N. L. *Nano.Lett.* **2006**, *6*, 1053-1058.

(50) Skaife, J. J.; Abbott, N. L. *Langmuir* **2001**, *17*, 5595-5604.

(51) Tan, H.; Li, X.; Liao, S.; Yu, R.; Wu, Z. *Biosens.Bioelectron.* **2014**, *62*, 84-89.

(52) Liu, D.; Hu, Q. Z.; Jang, C. H. *Colloids Surf. B: Biointerfaces* **2013**, *108*, 142-146.

(53) Zhang, M.; Jang, C.-H. *Anal.Biochem.* **2014**, *455*, 13-19.

(54) Cheng, D.; Sridharamurthy, S. S.; Hunter, J. T. Park, J.-S.; Abbott, N. L.; Jiang, H. *J. Microelectromech. Syst.* **2009**, *18*, 973–981.

(55) Meli, M. V.; Lin, I. H.; Abbott, N. L. *J. Am. Chem. Soc.* **2008**, *130*, 4326–4333.

(56) Lin, I. H.; Miller, D. S.; Bertics, P. J.; Murphy, C. J.; de Pablo, J. J.; Abbott, N. L. *Science*, **2011**, *332*, 1297–1300.

(57) Frey, B. L.; Corn, R. M.; Weibel, S. C., ed. Chalmers, J.; Griffins, P. R. John Wiley & Sons, Chichester, U.K., **2001**, vol. *2*, p. 1042.

(58) Bradenburg, K. *Biophys. J.* **1993**, *64*, 1225–1231.

(59) Vagenende, V.; Ching, T.-J.; Chua, R.-J.; Jiang, Q. Z.; Gagnon, P. *Colloids Surf. B* **2014**, *120*, 8–14.

Chapter 4

Liquid crystal based interfacial study demonstrating the interaction of bacterial endotoxin with milk protein lactoferrin

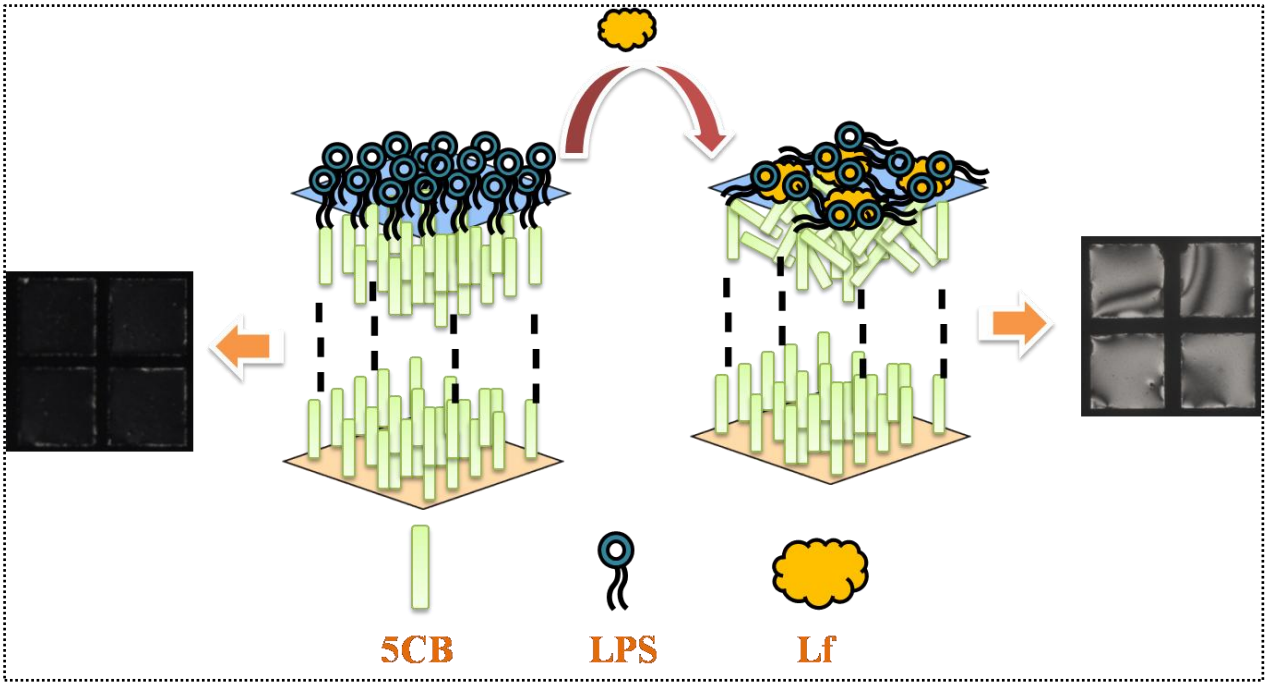

Immune active milk protein lactoferrin (Lf) exhibits antibacterial property due to its interaction with Gram negative bacterial lipopolysachcharide (LPS). This chapter reports an approach to build up a Liquid crystal (LC) based biosensonsors to study the interaction between Lf and LPS and also illustrates the conformational behavior of Lf in the environment of bacterial endotoxin.

4.1 Introduction

Gram negative bacterial infection has been considered as potential threat to human health.[1] Lipopolysaccharide (bacterial endotoxin), the major phospholipid presents on exterior of gram negative bacterial cell membrane, is strongly responsible for inducing several lethal pathogenesis related to bacterial infections such as cardiovascular attack, organ failure, septic shock etc. Moreover the lipid moiety of endotoxin, lipid A, is considered as potent contributor to severe endotoxic injuries.[2,3] Interestingly the adversities of endotoxin on mammalin hosts are strongly regulated by varieties of proteins present in body fluids. For instance, the interaction LPS with of serum proteins enhance the binding of LPS on neutrophil receptor.[4] On the other hand, interaction of LPS with immune-responsive lysozyme results in diminishing the endotoxic activity and followed by lysis of bacterial cell membrane.[5] Therefore, a thoughtful perspective of synergy between LPS and various proteins is immense important to battle gram negative bacterial infection. Incidentally, lactoferrin, a cationic globular glycoprotein of molecular mass about 80 KDa, has become point of interest due to its strong synergistic influence over the endotoxicity of LPS in mammalian hosts.

Lf, the glycoprotein of transferrin family, is broadly found in secretory fluids, such as milk, saliva, tears. Among these human milk is the most abundant source of Lf with concentration of 150 mg mL^{-1}. Apart from other nutritional value, potent contribution towards antimicrobial activity of human milk for infants is due to the presence of Lf. The role of Lf in building human innate immune system is very crucial. Clinical studies have shown that Lf strongly binds with LPS and destabilize the integrity of the outer cell membrane of Gram negative bacteria leading to the lysis of bacterial cells.[6] Furthermore, Lf also has been found effective in modulation of immune response triggered by LPS.[7] For instance; Lf decreases LPS stimulated Interleukin (IL)-1, IL-2 secretion. Lf also diminishes LPS induced monocyte cytotoxicity to a significant extent. Therefore, on a whole these entire clinical investigations on antimicrobial activities of Lf towards bacterial endotoxin are highly important from the aspect of exploring the possibilities to battle Gram negative bacterial infection in mammalian hosts.

Mostly, the characterization of this interaction between LPS and Lf has been carried out using the following biological assays such as,. Interleukine-1 (IL-1),[8] tumor necrosis factor (TNF).[9] In addition to that some spectroscopic techniques, Fourier-transform infrared (FTIR) spectroscopy,[6] Radioisotope labeling method,[10] have been employed to study this interaction these interactions. But their practical usages are limited due to lack of sensitivity, high cost, complex instrumentation, requirement of radio labeling of protein and many other drawbacks. From this viewpoint, in this paper, we aim to report an uncomplicated, sensitive liquid crystal (LC) based sensing system for quick and accurate recognition of the interaction between Lf and LPS.

In recent years, LC–aqueous interface has been employed as sensing platform for the recognition of several biomolecular interactions.[11-13] Ordering transition of LC molecules in micrometer range is responsive towards external stimuli and able to amplify the interfacial events into optical read-out that are visible through naked eye. Till now several biological interactions including protein recognition,[14,15] DNA sensing,[16] characterization of enzymetic catalysis,[17] different pathogenic toxic detections [18,19] and many more [20;21] have been characterized using aqueous- LC interface. But, till now, no work has been done to exploit the interaction of Lf with bacterial endotoxin by using aqueous-LC interface.

4.2 Objective

In this study reported in this chapter our goals are as follows. First, we sought to study the interaction of bacterial endotoxin (LPS) with Lf at aqueous–LC interface. Second, we planned to quantify these interactions in terms of measuring the alteration of tilt of LCs during this interfacial event. Third, we wanted to find out the conformational behaviour of Lf, in addition, how this conformational arrangement gets influenced in regard of LPS environment and impose potential impact on the sensitivity of our designed LCs based system. For this, our first approach was to study the self-assemble behaviour of LPS at aqueous–LC interface. Strong hydrophobic interaction between alkyl chain of lipid A moiety of LPS interact with 5CB known to orient LC homeotropically at aqueous-LC interface.[22] Therefore, we assume that strong, interaction between LPS and Lf, may rattle the LPS assembly and resulting in the orientational switch of the interfacial LCs from homeotropic to tilted fashion that can be well envisaged under polarized optical

microscopy. Therefore, aqueous-LC interface could be represented as sensing tool for the recognition of LPS–Lf interactions.

4.3 Results and discussion

4.3.1. LPS mediated ordering transition of liquid crystal at aqueous-LC interface

First we envisaged self-assemble behavior of LPS at the aqueous-LC interface. In contact with Tris buffer solution, LC confined within a gold grid supported on DMOAP coated glass slides appeared with bright texture when viewed under polarized optical microscope (Figure 4.1. A). The bright appearance of 5CB is indicative of its planar/tilted orientation on interaction with water at aqueous-LC interface. Upon exposure of 0.1 mg mL^{-1} aqueous solution of LPS (pH 7.4) onto aqueous-LC interface, the appearance of LC promptly changed to dark from bright (Figure 4.1. B). The dark appearance of LCs is associated with homeotropic orientation of LCs at aqueous-LC interface as a result of hydrophobic interaction of lipid moieties of LPS and the interfacial LC. The LPS-laden aqueous-LC interface was incubated for 2 h and followed by washing thrice with Tris buffer at pH 7.4 to remove excess LPS.

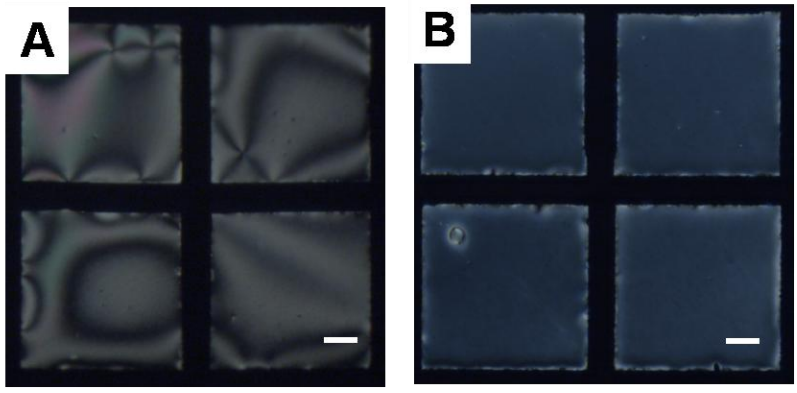

Figure 4.1 Polarized optical images of 5CB film dispensed in TEM gold grid supported on DMOAP coated glass slides: A) immersed in Tris buffer (pH 7.4) , B) incubated with an aqueous solution of 0.1 mg mL^{-1} LPS in Tris buffer (pH 7.4) for 2 h. Scale bar = 40 μm.

4.3.2. Interaction of Lf with LPS at aqueous-LC interface

Next, LPS laden aqueous-LC interface was brought in contact with 5 μM aqueous solution of Lf in Tris buffer (pH 7.4). A rapid change (within 10 sec) in optical appearance of the LC from dark to bright was viewed under POM. This observation suggested that LCs underwent an ordering switch from homeotropic to planar/tilted state (Figure 4.2. A, B). The alteration in the orientation of LC is consequence of strong binding of Lf with self-assembled LPS molecules. Due to this strong interfacial association of Lf and LPS, the arrangement of LPS at interface got disturbed and resulted in tilted orientation of LC aqueous-LC interface.

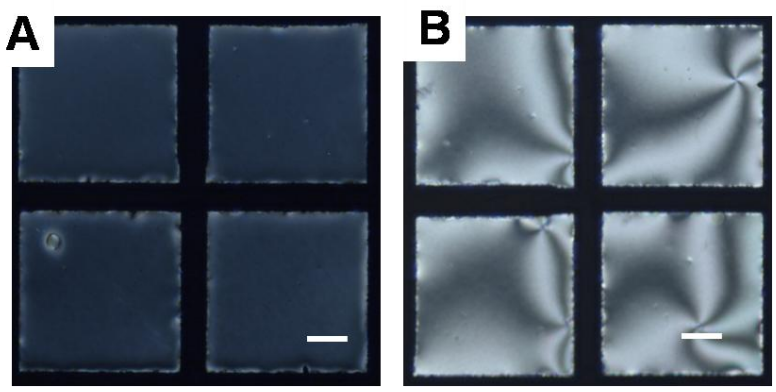

Figure 4.2 Polarized optical micrographs of 5CB immobilized in gold grids placed on DMOAP-coated glass slides. A) in presence of LPS at aqueous-LC interface B) after introducing 5 μM aqueous solution of Lf on the exposure of LPS decorated aqueous-LC interface. Scale bar = 40 μm.

To put detailed insight into the mode of interaction of Lf with LPS we planned to perform zeta potential experiment (Figure 4.3). We found that Lf is positively charged at neutral pH having zeta potential ξ=9.3±0.8 mV and LPS is negatively charge with ξ value -4.3±1.7. Interestingly, when we mixed 5 μM Lf with 0.1 mg mL^{-1} aqueous solution of LPS, we observed small change in the ξ value -3.1±1.2 which is close to value LPS. From this experiment we can conclude that hydrophobic interaction predominates over electrostatic interaction during the binding of Lf with LPS.

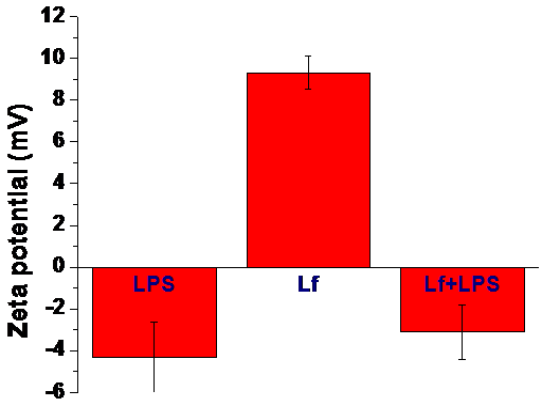

Figure 4.3 Zeta potential of aqueous solution of 0.1 mg.mL^{-1} LPS, 5 μM Lf and mixture of 5 μM Lf in 0.1 mg mL^{-1} LPS.

4.3.3. Control Experiments

After observing that the aqueous-LC interface is responsive towards binding of Lf with LPS, we planned several control experiments to reconfirm our proposition drawn from the above experiment. In first control experiment, we wanted to observe the direct effect of Lf onto LPS free aqueous-LC interface. On exposing 10 μM of aqueous solution of Lf directly onto LPS free aqueous-LC interface, we observed no alteration of the bright appearance of LC even after 6h period of incubation (Figure 4.4. A, B). From this we can conclude that there is no direct interaction between interfacial 5CB molecules and Lf which could change the orientation of LC. Therefore, interfacial LC remained in planar/tilted state showing bright appearance.

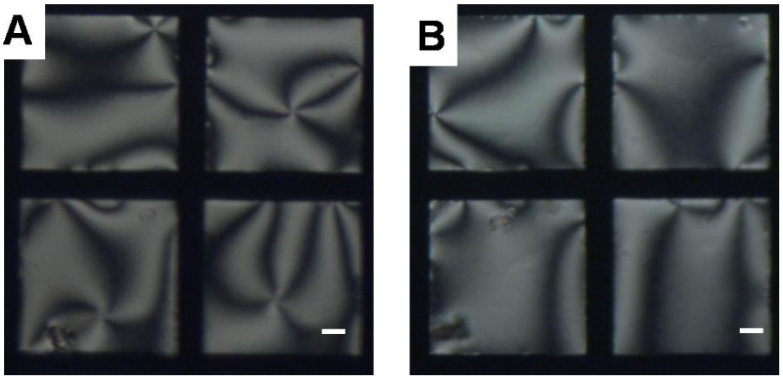

Figure 4.4 Optical micrographs of 5CB immobilized gold grids supported on DMOAP-coated glass slides. A) in presence of aqueous Tris buffer (pH 7.4) and B) on exposing 10 μM Lf solution onto aqueous-LC interface. Scale bar 40 μm.

In our second control experiment, we determined the specific interaction of Lf with LPS compared to other milk proteins, namely, Casein and β-lactoglobulin (β-lg) After replacing Lf with casein and β-lg and followed by coupling to LPS laden aqueous-LC interface, we found that in presence of any of these proteins the optical appearance of LPS laden interfacial 5CB, remained dark (Figure 4.5) even after 3h period of incubation. From this observation we can conclude that binding of Lf with LPS is highly specific compared to other milk proteins to bring about the ordering transition of LC at aqueous-LC interface.

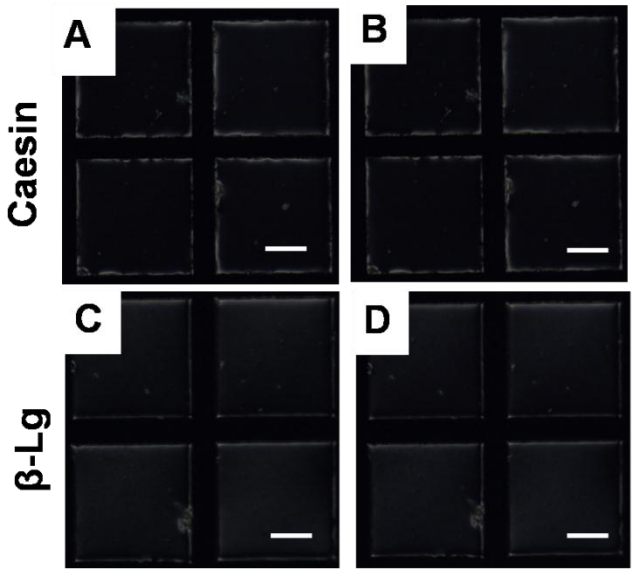

Figure 4.5 Polarized optical micrographs of A), C) 0.1 mg mL^{-1} LPS laden aqueous-LC interface A) after 2 hrs of incubation of LPS laden aqueous-LC interface in presence of B) 20 μM Casein and D) 20 μM β-Lg. Scale bar = 40 μm.

In third control experiment, we planned to find out the specificity of Lf towards binding LPS compared to other biologically relevant phospholipids, which also can able to orient the interfacial LC homeotropically. In three different sets of experiments, when we introduced 10 μM aqueous solution of Lf onto aqueous-LC interface laden with, three

different phospholipids, namely, 1,2-Didodecanoyl-Sn-glycerol-3-phosphocholine (DLPC), 1,2-dioleoyl-Sn-glycero-3 phospho-rac-(1-glycerol) (DOPG) and Lysophosphatidic acid (LPA), the optical appearance of LCs under POM remained dark (Figure 4.6 A-B, C-D, E-F) even after 6 h or more incubation. These results firmly demonstrate the absence of any interaction between Lf and these phospholipids that can cause ordering switch of LC at aqueous-LC interface. Therefore, binding of Lf is highly specific towards LPS at aqueous-LC interface to bring about homeotropic LC into planar/tilted state.

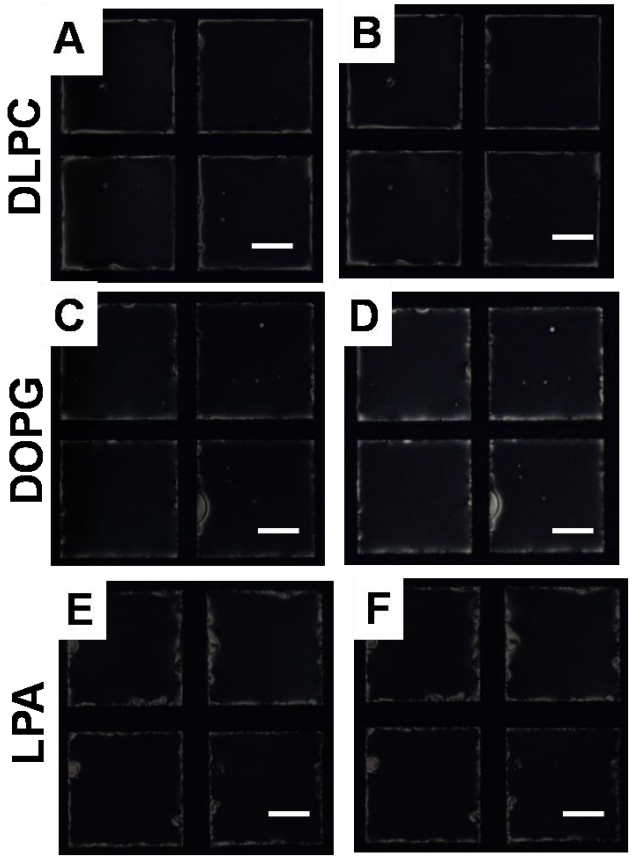

Figure 4.6 Optical images of (A) DLPC (C) DOPG and (E) LPA decorated aqueous-LC interface. (B, D and F) depicts micrographs of 5CB after exposing Lf onto DOPG, DLPC and LPA laden aqueous-LC interface respectively. Scale bar = 40 µm.

In addition to these control experiments, we further envisage the interfacial binding activity of Lf onto self-assembled LPS through exploiting epifluorescence measurements with FITC tagged Lf as a fluorescence probe. From this experiment, first, we thought to observe

fluorescence density of FITC-Lf on the 5CB containing grid surface decorated with LPS which could stronghold our LC based detection of Lf-LPS interaction. Second, depending on the interfacial fluorescence density we could also explain the integrity of assembling Lf over self-assembled interfacial LPS during this LPS-Lf binding event at interface. In epifluorescence experiment, we coupled 500 nM of Lf mixed with 0.3 mol% FITC–Lf onto LPS laden aqueous-LC interface and kept for 2 hrs period of incubation. We also run a parallel control experiment where we kept incubation of Lf free LPS laden aqueous-LC interface for 2 hrs period. Figure 4.7 shows the epifluorescence micrographs and the respective polarized optical micrographs of LPS decorated aqueous-LCs interface in absence and presence of Lf (mixed with FITC-Lf) respectively. In absence of Lf, interfacial LC laden with LPS remained in homeotropic orientation as evidenced in figure 4.7. C depicting dark optical view of interfacial 5CB. Interestingly, the corresponding epifluorescence measurements (Figure 4.7 A) shows lack of interfacial fluorescence clearly due to absence of any fluorescent probe at the interface. Figure 4.7. D describes POM of LPS decorated aqueous-LC interface, in presence of Lf (mixed with 0.3% FITC-Lf), after 2 hrs of incubation and subsequent three times exchange with Tris buffer at pH 7.4 to remove excess FITC-Lf from the solution. The bright optical appearance clearly shows the planar/tilted orientation of interfacial LC mediated by strong interaction between LPS and Lf at the interface. Interestingly, the corresponding epifluorescence measurement (Figure 4.7. B) shows the presence of strong interfacial fluorescence due to presence of FITC-Lf at the LPS laden aqueous-LC interface. This observation evidently demonstrates that the strong binding of Lf with LPS at aqueous-LC interface and further implies that this strong interaction although disturbed the arrangement of interfacial LPS (also evidenced by bright polarized optical micrograph) but it retained at the interface with Lf assembled over it. To gain further support to the above interpretation we planned to measure fluorescent intensity. Figure 4.7 E represents the difference of fluorescence intensity, obtained from fluorimetric measurement, between LPS laden aqueous-LC interface in presence and in absence of Lf (mixed with 0.3% FITC-Lf). As expected, we obtained large fluorescence intensity for LPS laden interface coupled to Lf (mixed with 0.3% FITC-Lf). In contrast, negligible fluorescence intensity observed for Lf free aqueous-LC interface. As a whole, the entire fluorescence experiments strongholds our assumptions based on the previous

experiments that the strong interaction of Lf with interfacial LPS results in rapid ordering transition of the LC from homeotropic to tilted/planar at aqueous-LC interface and furthermore during this interfacial binding event Lf retained over disordered LPS assembly at aqueous-LC interface.

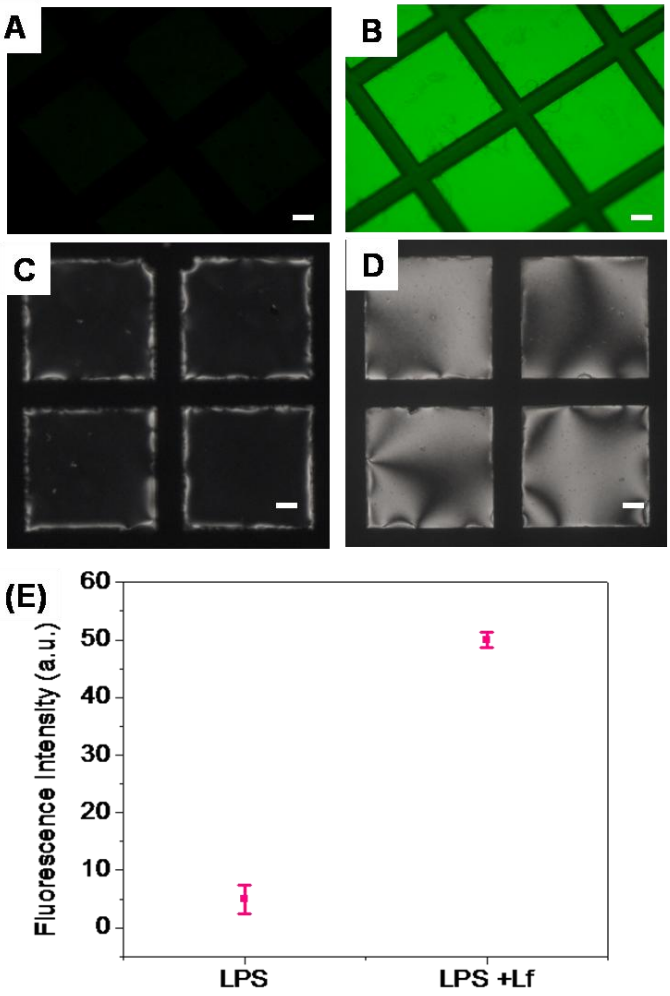

Figure 4.7 Epifluorescence images of LPS decorated aqueous-LC interface after 2 hrs of incubation A) in absence; B) in presence of 500 nM Lf (mixed with 0.3 mol% FITC–Lf. (C) and (D) Corresponding polarized light micrographs respectively. Scale bar = 40 µm. (E) fluorescence intensity graph measured for LPS laden aqueous-LCs interface in absence and in presence of Lf (mixed with 0.3 mol% FITC-Lf), measured at 25 °C.

4.3.4. Determination of detection limit of Lf on LPS laden aqueous-LC interface

In our next experiment, we focused on investigating the detection limit (LOD) of this interaction at aqueous-LC interface. We measured response time of LC at different concentrations of Lf on the LPS-laden aqueous–LC interface. At first, we determined the minimum concentration of LPS sufficient enough to orient LC in homeotropic fashion at aqueous–LC interfaces. On varying concentrations of LPS onto aqueous–LC interface (followed by washing off excess LPS) 0.06 mg mL^{-1} has been found to be the optimum concentration for LPS to orient interfacial LCs homeotropically and to get a homogeneous dark optical image. (Figure 4.8)

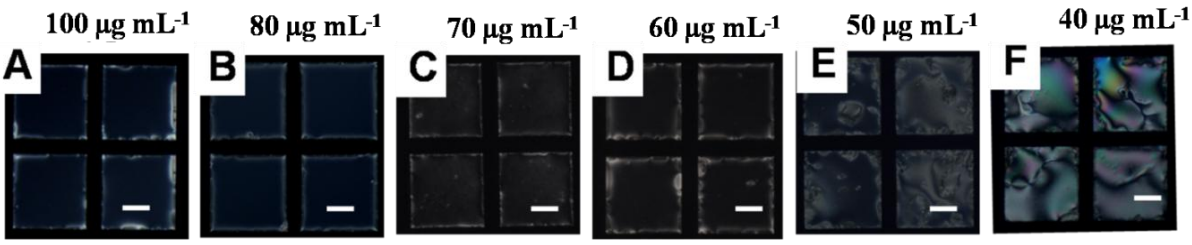

Figure 4.8 Optical micrographs of aqueous-LC interface decorated with A) 100 µg mL^{-1} B) 80 µg mL^{-1} C) 70 µg mL^{-1} D) 60 µg mL^{-1} E) 50 µg mL^{-1} F) 40 µg mL^{-1} concentrations of LPS, after washing with Tris buffer and followed by 24 h of incubation. Scale bar = 40 µm.

When we varied concentrations of Lf in contact with LPS decorated aqueous–LC interfaces (with concentration of LPS 0.06 mg mL^{-1}) we found gradual increase in response time of LCs with respect to decreasing concentrations of Lf. In presence of 500 nM of Lf solutions onto LPS laden aqueous-LC interface the optical appearance of the 5CB changed within 1 min (Figure 4.9 A, B). Whereas at consecutive lower concentration of Lf, 100 nM, we found response time of LC further delayed to 10 min to appear as complete bright (Figure 4.9 C, D). At further lower concentrations of Lf, 10 nM, partial bright appearance of LC after 30 min. (Figure 4.9 G, H), and within 1 hr it turned into complete bright. At the concentration of 5 nM of Lf, only partial bright appearance of 5CB emerged within 1 h of incubation time. The complete bright appearance of 5CB at this concentration level was achieved after 2 h of period of incubation (Figure 4.9 I, J). To the following lower concentrations of Lf, 3 nM (Figure 4.9 K, L), we found 5CB remained as dark even after 3

h of incubation period. As a whole, from this experiment 5 nM concentration of Lf was determined as LOD for Lf to study this interaction in our LC based sensing system.

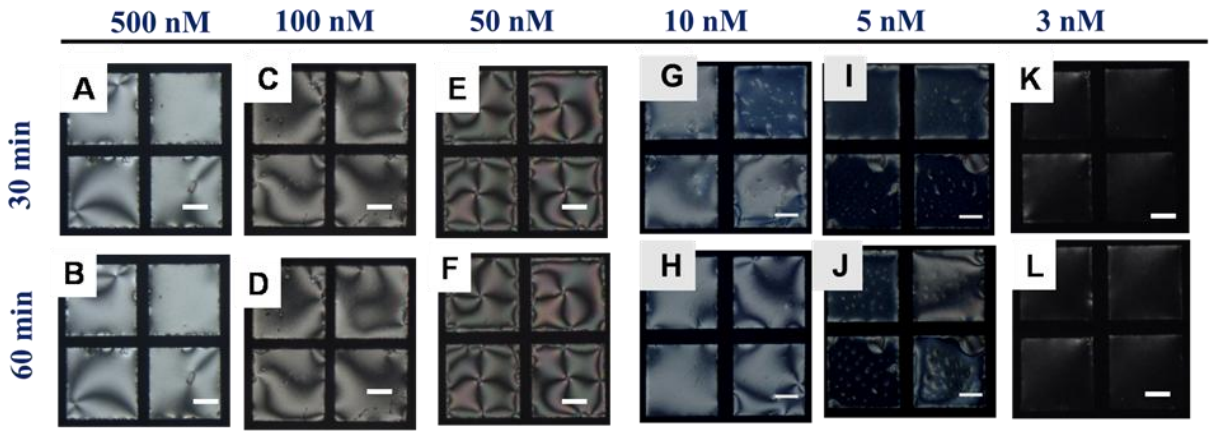

Figure 4.9 Optical images of LPS decorated aqueous-LC interface on the exposure of aqueous Lf solution of varying concentrations. (A, B) 500 nM, (C, D) 100 nM, (E, F) 50 nM, (G, H) 10 nM , (I, J) 5 nM, (K, L) 3 nM. Top row represents images after 30 min of incubation period and bottom row represents images after 60 min of incubation period. Scale bar = 40 μm.

4.3.5 Average gray scale intensity and tilt angle measurements to quantify the interaction of Lf with LPS at the aqueous-LC interface

In the previous experiment, we found that response time of the LC to change in the orientation is dependent on the concentration of Lf exposed on LPS laden aqueous-LC interface. Therefore we planned to measure the average gray scale intensity of the optical images of 5CB during this interfacial binding event and quantify the optical response of LC with respect to different concentrations of Lf. As expected, we observed a regular decline in gray scale intensity with decreasing concentrations of Lf (Figure 4.10), implying direct correlation between the brightness of optical images of 5CB (during Lf–LPS interactions) and concentration of Lf exposed on LPS membrane. Additionally, from this experiment, we can also able to correlate the binding affinity of Lf and interfacial LPS and ordering transition of LC at the interface.

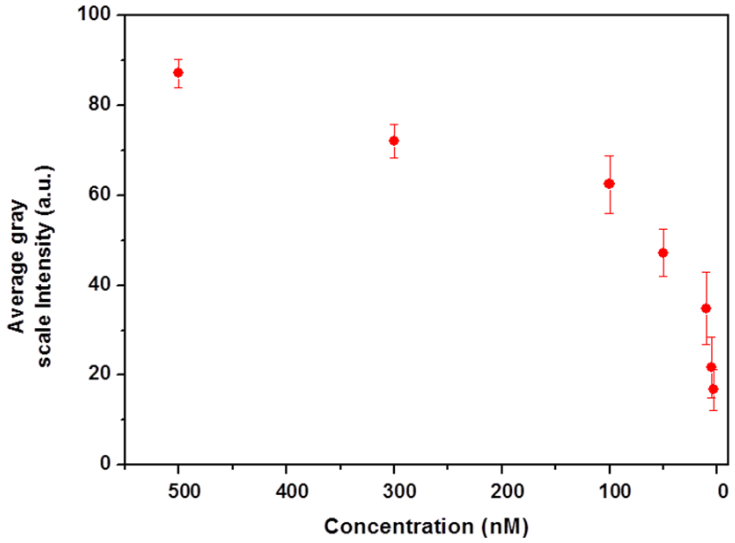

Figure 4.10 Average grey scale intensity graph of optical micro-graphs of LPS decorated 5CB interface plotted against varying concentrations of Lf exposed onto LPS laden aqueous-LC interface.

To provide further quantitative insight into the LPS-Lf binding event at the aqueous-LC interface, we aimed to measure the tilt angle of 5CB during this interfacial event. The extent of tilt in the interfacial LC is directly dependent on the level of Lf mediated disorderness of LPS self-assembly at aqueous–LC interface. Consequently, measuring tilt angle of interfacial 5CB during LPS–Lf binding events at interface we can be able to establish the quantitative correlation between this interfacial interaction and ordering transition of LCs at the interface. During this experiment, we exposed 5 nM concentration of Lf (the limiting concentration to bring about the change in orientation of LPS laden interfacial LC) onto LPS decorated aqueous-LC interface and measured optical retardance of 5CB in regular time interval. From the values of optical retardance, we calculated tilt angles of LC using the methods described in experimental section. Next, we plotted the tilt angle values of LC with incubation period and observed a gradual rise in the tilt angle of 5CB with increasing incubation time (Figure 4.11). The highest tilt angle value of 5CB for 3 h of incubation period was 47.6° ± 3.5. As a whole, this tilt angle experiment established the quantitative correlation between Lf-LPs interfacial binding and anchoring transition of LCs at interface. In addition to that, from the observation of gradual rise of tilt angle of

5CB with increasing incubation period we can conclude that the ordering switch of interfacial LCs during LPS-Lf interfacial binding event took place in a continuous manner.

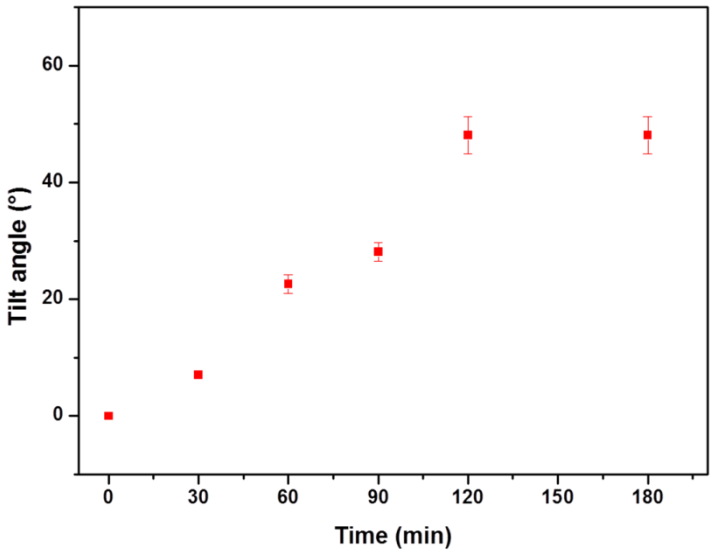

Figure 4.11 Periodical variation of tilt angle of LPS laden interfacial 5CB in presence of 5 nM aqueous solution of Lf at the interface.

4.3.6 Conformational analysis of Lf in aqueous environment as well as in presence of LPS

Following the quantification of Lf-LPS binding event at aqueous-LC interface, our next experiment was to find out conformational behavior of Lf in aqueous environment as well as in presence of LPS. The interaction of lipids with proteins imposes potent impact on the conformations of proteins. Moreover, the activities of proteins are highly dependent on their conformations in solution. conformational alteration of proteins also play key role in lipid infusion into protein network[23,24] and also lead to thermodynamic stability of proteins arrangements across the lipid bilayers[25,26]. Previous reports also mentioned that strong binding of bacterial endotoxin with several membrane proteins results in conformation switch in that proteins.[24] Therefore, we aimed to look into the influence of LPS on the conformational integrity of Lf. Figure 4.12 illustrates the CD Spectra of Lf at different conditions. In aqueous Tris buffer solution (pH 7.4) Lf adopts alpha helical conformation which can be confirmed with two characteristic minima at 210 nm and 223 nm and a sharp maxima towards positive ellipticity range around 202 nm (red line). Whereas, in presence of LPS, we observed Lf to adopt less ordered random coil like conformation exhibiting

only one sharp minima at around 207 nm (black line) and no minima has been observed around 223 nm. From this observation we can reach into the conclusion that strong interaction between Lf and LPS rattles the stable helical structure adopted by Lf in buffer solution and results in more open and less ordered random coil like arrangement.

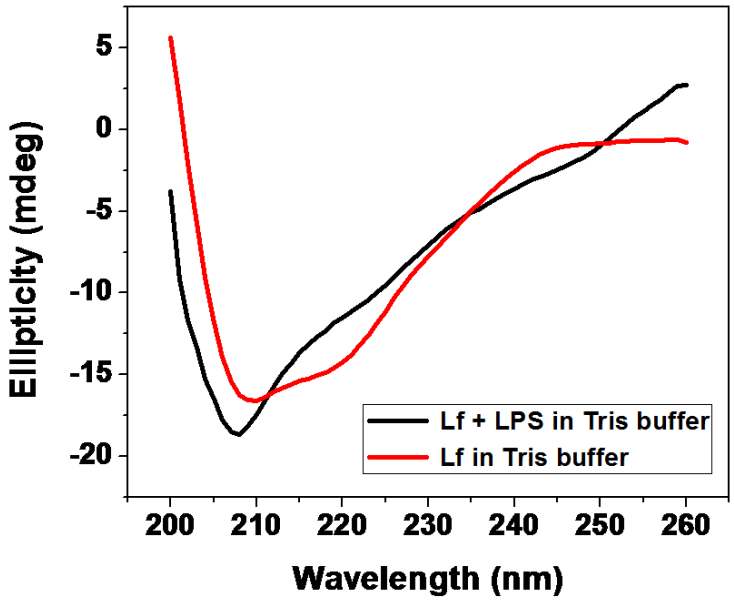

Figure 4.12 Ellipticity measurements of 200 nM Lf in Tris buffer (red line), B) Lf in presence of 0.06 mg mL^{-1} LPS solution (black line).

To provide further insight into the conformational aspect of Lf in aqueous environment as well as its consequence in presence of LPS, we performed VCD experiment. VCD is considered as a sensitive assay to determine the conformational arrangements in proteins and peptides.[27,28] In our VCD experiment, we observed Lf in Tris buffer (pH 7.4) exhibit a strong maxima-minima couplet around 1654 cm^{-1} and 1668 cm^{-1}, respectively (Figure 4.13 A). The maxima in the range of 1645-1655 cm^{-1} along with minima at higher wavenumber region (1662-1670 cm^{-1}) are, commonly, considered as characteristic amide l peaks for alpha helical configuration of protein or peptide.[29,30] This observation correlates well with previously shown CD spectra where Lf in Tris buffer (pH 7.4) also found to be exhibited alpha helical configuration. Figure 4.13 B reveals the VCD spectra of Lf in presence of LPS. In this spectrum, we observed a minima-maxima couplet, exactly reverse to the 4.13 A spectra, with peak positions at 1654 cm^{-1} and 1668 cm^{-1} respectively. This kind of peak

positions around these wavenumbers commonly assigned to less ordered random coil like conformation of Proteins.[27,28] This result further supports the CD experiment where we found spectra in accord with random coil conformation of Lf in presence of LPS. As a whole, on combining results obtained from both CD and VCD experiments we can conclude that Lf adopts alpha helical arrangement in Tris buffer probably to attain maximum thermodynamic stability in aqueous medium. While in presence of LPS, Lf espouses a less ordered random coil confirmation. The strong interaction interplayed between Lf and LPS, possibly, ruptured the helical confirmation of Lf and results in open random coil confirmation in which it could bind more extensive way with LPS and leading to faster dynamic response through orientational switching of LC.

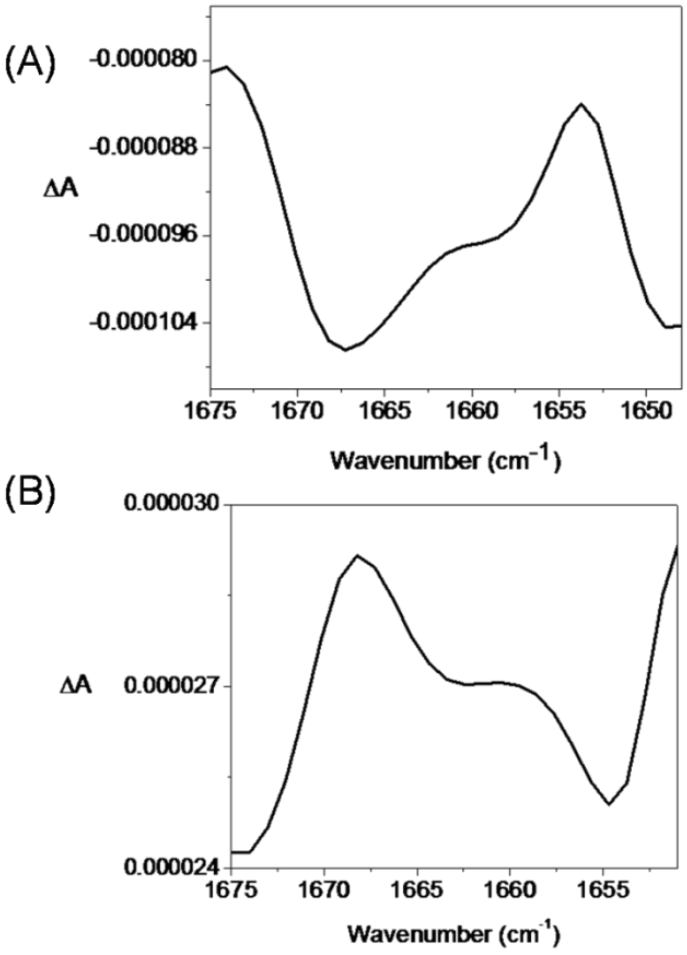

Figure 4.13 VCD spectra of A) 20 mg mL^{-1} aqueous solution of Lf in Tris buffer, B) Lf in presence of 10 mg mL^{-1} LPS solution.

4.4 Conclusions

Overall, the entire results reported in this paper reflect a successful design of LC based sensor to study the interaction between Lf and bacterial endotoxin. The LPS laden aqueous-LC interface was found to be responsive towards binding with Lf, leading to alteration in optical appearance of LCs from dark to bright. The interaction of Lf with LPS was highly specific compared other milk proteins. In other way, compared to several biologically active phospholipids, LPS was found to be solely responsible to interact with Lf and resulting in orientational transition in LCs. From epifluorescence experiment and fluorimetric measurements, we further confirmed this interfacial binding event and also revealed the retention of Lf over LPS assembly during this interaction at the interface. The sensitivity level of this system was reached upto 5 nM concentration level of Lf, to show ordering transition of LPS laden interfacial LCs. Furthermore, we have quantified the anchoring transition of 5CB with this interfacial binding event with help of average grey scale intensity and tilt angle measurement. Finally, we have investigated the conformational behavior of Lf in aqueous Tris buffer solution as well as after incubating with LPS using CD spectroscopy, where we observed that in Tris buffer medium (pH 7.4) Lf adopts a more ordered alpha helical conformation. While in LPS environment, upon strong interaction between LPS and Lf, Lf adopted less ordered random coil conformation possibly to attain extensive interaction with LPS. We further affirmed the results obtained from CD measurements with VCD spectroscopy. In conclusion, the results reported in this paper hold a promising approach in designing a robust LCs based biosensor to study the interaction of milk protein Lf and bacterial endotoxin.

4.5. Experimental Section

4.5.1. Materials and methods

Lactoferrin (from bovine colostrums), Tris buffered saline (pH 7.4), 1,2-dioleoyl-sn-glycero-3-phospho-rac-(1-glycerol) sodium Salt (DOPG), N,N-dimethyl-N-octadecyl-3-aminopropyltrimethoxysilylchloride (DMOAP), Deuterium oxide (99.9 atom % D), Casein (from bovine milk), β-Lactoglobulin (from bovine milk) and lipopolysaccharides (from E. coli 0111:B4) were purchased from Sigma-Aldrich (St. Louis, MO). FITC conjugated

lactoferrin was purchased from Molecular Probes (Oregon, United States) 1,2-Didodecanoyl-sn-glycerol-3-phosphocholine (DLPC), lysophosphatidic acid (LPA) was purchased from Avanti Polar Lipids, Inc. (Alabaster, AL). Sulfuric acid and hydrogen peroxide (30% w/v) were purchased from Merck. Ethanol was obtained from Jebsen&Jenssen GmbH and Co., Germany (Sd. fine-chem limited). The 5CB LC was obtained from Merck. Deionization of a distilled water source was performed using a Milli-Q-system (Millipore, bedford, MA). Fischer's Finest Premium Grade glass microscopic slides and cover glass were obtained from Fischer Scientific (Pittsburgh, PA). Gold specimen grids (20 mm thickness, 50 mm wide bars, 283 mm grid spacing) were obtained from Electron Microscopy Sciences (Fort Washington, PA).

4.5.2 Cleaning of glass slides

The glass microscopes slides were cleaned using piranha solution [70:30 (% v/v) H_2SO_4:H_2O_2 (30%)]. In a brief, piranha solution was poured in to glass slide kept in a coplin jar and heated at 100° C for 1 h. Then the glass slides are rinsed with deionized (DI) water for several times. After that, the glass slides were rinsed sequentially with ethanol and methanol. Then the glass slides were dried under a stream of nitrogen gas. Followed by the cleaned glass slides were kept in an oven at 100° C for 12h.

4.5.3 Coating of glass slides with DMOAP

The pirhana cleaned glass slides were immersed into 0.1% (v/v) DMOAP solution in DI water for 5 min at room temperature. Followed by glass slides were rinsed with DI water to remove excess DMOAP from the glass surface. The DMOAP coated glass slides were dried under flow of nitrogen gas and kept in oven at 100°C for 3 h to allow crosslinking of DMOAP for adhering with glass surface.

4.5.4 Preparation of optical cells

The DMOAP coated glass slides were cut with diamond tipped knife into small squares. Then, a gold grid was kept on the slide, and roughly 0.3 mL of 5CB was spread onto the grid carefully. Excessive LC was removed by using a capillary syringe.

4.5.5 Formation of LPS laden aqueous-LC interfaces

First, required concentration of LPS was prepared by dissolving powdered LPS into Milli-Q water at room temperature. Then the LPS solution was sonicated for 5 min and vortexed for 10 min at room temperature. The size of LPS vesicle was found to be 174.01 ± 2.88 nm. The LPS laden aqueous-LC interface was formed by bringing the gold grid dispensed with 5CB in contact to the LPS solution in the optical cell and kept for 2 h of incubation period. The LPS decorated interface was washed twice with Tris buffer (pH 7.4) prior to use to remove excess LPS.

4.5.6 Preparation of Phospholipids vesicles

First, the phospholipids were taken in a round bottom flask and dissolved into chloroform (0.5 mL) followed by slowly evaporating chloroform under vacuum for at least 2 h until it formed a thin layer along the inside bottom of the flask. The lipid film inside the flask was then kept under flow of nitrogen for 30 min. Then dried lipid film was dissolved into DI water and vortexed for 1 min. The cloudy solution obtained was sonicated for 15 min using a probe ultrasonicator (25 W) resulted in a clear solution.

4.5.7 Characterization of LC films in aqueous solutions using polarizing optical microscope

The gold grid dispensed with 5CB was immersed in Tris buffer (10 mM, pH 7.4). The optical characterizan of 5CB films was performed by using a polarizing optical microscope (Zeiss Axioscope. A1, Germany) in the transmission mode. All the images were captured with a Axiocam digital camera mounted on the microscope with an exposure time of 40 ms.

4.5.8 Tilt angle measurements

With help of tilting compensator (type 2357 K, equipped with a calcite compensator plate, Leitz, Germany) optical retardance of LCs was measured. On averaging the retardance values of 5CB hosted within four squares of the gold specimen grid, we calculated tilt angle of LCs. For homeotropic orientation of nematic LCs at the DMOAP-treated glass interface $\theta_1 = 0°$ and a tilt of angle of θ_2 away from the surface normal at the aqueous–LC interface. The linear variation of the tilt of LCs across the film is to minimize the elastic

energy of the LC film (assuming splay and bend elastic constants of the LCs to be equal). This relationship between optical retardance (Δr) of the film of LCs and the tilt of the director at the aqueous–LC interface (θ_s), is

$$\Delta r \approx \int_0^d \left(\frac{n_e n_o}{\sqrt{n_o^2 sin^2\left(\frac{z}{d}\theta_s\right) + n_e^2 cos^2\left(\frac{z}{d}\theta_s\right)}} - n_o \right) dz$$

Where η_e and η_o are the indices of refraction parallel (so-called extraordinary refractive index) and perpendicular (ordinary refractive index) to the optical axis of the LC, respectively, and θ_s is the tilt angle of LC measured relative to the surface normal.[11]From measured retardance values and solving eqn (1). Tilt angle of LCs was calculated. The indices of refraction of 5CB are η_e =1.711 and η_o =1.5296 (λ= 632 nm at 25 °C).
In following the detailed of the procedure has been explained using an example.

After tilting the compensator plate from zero position to both positive and negative directions, two readings for the position of the compensator was observed 7° and 4°. To measure phase difference we need to add up this two values i.e. (2.9°+2.1°) =5°

Now we need to calculate corresponding log f value of 5. From table of log f values we got log f (5) = 19. Next, the value obtained was multiplied with log C value. log C is known as compensator constant. The value of log C is again dependent on wavelength of light used for this experiment. Here log C value will be 4.54 when λ= 632 nm. After multiplying this value with 19 we get (19 x 4.54) = 86.26.

Next to determine optical retardance (Δr), we need to divide the phase difference value from the thickness of the LC. For our experiment thickness of LC is 20000 nm.

Therefore, (Δr) will be (86.26/20000) = 0.004313. Next putting Δr, n_e and n_o values to equation 1 we get

$$.004313 = \frac{1.74 \times 1.52}{\sqrt{(1.52^2 sin^2\,\theta + 1.74^2 cos^2\theta)}} - 1.52$$

$$.004313 = \frac{2.6448}{\sqrt{(1.52^2 sin^2\,\theta + 1.74^2 cos^2\theta)}} - 1.52$$

$$\sqrt{(1.52^2 sin^2\,\theta + 1.74^2 cos^2\theta)} = \frac{2.6448}{1.52 + 0.004313}$$

$$\sqrt{(1.52^2 sin^2\,\theta + 1.74^2 cos^2\theta)} = 1.735$$

$$1.52^2 sin^2\,\theta + 1.74^2(1 - sin^2\,\theta) = 3.01$$

$$0.7172\ sin^2\,\theta = 3.01$$

$$sin\ \ \theta = 0.1566°$$

$$\theta = 9.009°$$

Therefore, the tilt angle (θ) value obtained is 9.009°

4.5.9 Dynamic light scattering (DLS) experiment

Using Malvern Zetasizer Nano ZS90 DLS instrument (Malvern Instruments, Southborough, Massachusetts) hydrodynamic size (diameter) of LPS was measured. For this experiment temperature was maintained: at 25 °C, with incident laser wavelength: 632 nm, and laser power: 4 mW. Detector angle was kept at 90°. All samples for this experiment were prepared in Tris buffer (pH 7.4). Hydrodynamic diameter of LPS was found to be 46.5±2.1 nm.

4.5.10 Epifluorescence experiment

Fluorescence experiments were performed using Zeiss (Observer. A1) fluorescence microscope. With a fluorescence filter cube having a 480 nm excitation filter and a 534 nm emission filter samples were observed. Images were captured by Axio cam camera.

4.5.11 Fluorimetric measurement

Fluorescence intensity of the sample was measured with a SHIMADZU RF-5301PC SPECTROFLUROPHOTOMETER (Shimadzu Corp., Kyoto, Japan). For the detection FITC fluorescent probe an excitation wavelength 490 nm (0.5 nm excitation slit) and an emission wavelength range of 500–534 nm (5 nm emission slit) was selected.

4.5.12 Circular dichorism (CD) measurements

The CD spectra were acquired using a Chirascan Spectrophotometer (Applied Photophysics, UK) in a 1 mm path length quartz cell with a scan range of 190–260 nm and 1 nm as step size.

4.5.13 Vibrational circular dichroism (VCD) measurements

The VCD spectra were measured using a Bruker FT-IR spectrometer. The IR range was used from 1800 to 800 cm^{-1}The spectrometer is connected with the Bruker polarization modulation accessory PMA 50. The light beam in PMA 50 module, focused onto the sample and passed through an optical low pass filter (blocking wavenumbers >1800 cm^{-1}), which is fabricated with a KRS-5 wire grid polarizer, and a ZnSe photoelastic modulator (PEM) with an oscillation frequency of 42 kHz. ZnSe lens focuses the light to a MCT detector. The detector signal consists of two components: a low-frequency modulation which corresponds to the IR absorption bands, i.e., the A signal, and a high-frequency modulated signal (42 kHz) corresponding to the dichroic absorptions, i.e., the ΔA signal. Additionally, the reference signal direct from the PEM (42 kHz) is mixed to the high-frequency modulated detector signal. Now these two high-frequency modulated signals get demodulated by an internal synchronous demodulator integrated in the electronic units of the TENSOR and VERTEX series FTIR spectrometers. The sample was held inside a

demountable cell with BaF_2 windows and a 100 μm spacer. Spectra were measured in D_2O solvent. For all measurements, the intensity calibration factor was obtained using a multiple-wave retardation plate combined with the second wire grid polarizer, whereby the system tuning was exactly the same as for the sample measurement. The spectra were corrected by subtracting the absorption (or VCD) of the corresponding solvent and were plotted in Origin 8 software.

4.6 References

(1) Vasoo, S.; Barreto, J. N.; Tosh, P. K. *Mayo Clin. Proc.* **2015**, *90*, 395-403.

(2) Amersfoot, E. S. V.; Berkel, T. J. C. V.; Kuiper, J. *Clin. Microbiol. Rev*. **2003,** *16*, 379-414.

(3) Asari, Y.; Majima, M.; Sugimoto, K.; Katori, M.; Ohwada, T. *Shock* **1996**, *5*, 208-212.

(4) Gioannini, T. L.; Zhang, D.; Teghanemt, A.; Weiss, J. P. *J. Biol. Chem.* **2002**, *277*, 47818-47825.

(5) Ohno, N.; Morrison, D. C. *J. Biol. Chem*. **1989**, *264*, 4434-4441.

(6) Kruzel, M. L.; Harari, Y.; Mailman, D.; Actor, J. K.; Zimecki, M. *Clin. Exp. Immunol.* **2002**, *130*, 25-31.

(7) Rochard, E. E.; Legrand, D.; Salmon, V.; Roseanu, A.; Trif, M.; Tobias, P. S.; Mazurier, J.; Spik, J. *Infect. Immun.* **1998**, *66*, 486-491.

(8) Arnold, R. R.; Cole, M. F.; McGhee, J. R. *Science* **1977**, *197*, 263-265.

(9) Bortner, C. A.; Miller, R. D.; Arnold, R. R. *Infect. Immun*. **1986**, *51*, 373-377.

(10) Machnicki, M.; Zimecki, M.; Zagulski, T. *Int. J. Exp. Pathol*. **1993**, *74*, 433-439.

(11) Tan, L. N.; Orler, V. J.; Abbott, N. L. *Langmuir* **2012**, *28*, 6364-6376.

(12) Sidiq, S.; Das, D.; Pal, S. K. *RSC Adv.* **2014**, *4*, 18889-18893.

(13) Agarwal, A.; Sidiq, S.; Setia, S.; Bukusoglu, E.; de Pablo, J. J.; Pal, S. K.; Abbott, N. L. *Small* **2013**, *9*, 2785-2792.

(14) Popov, P.; Honaker, L. W.; Kooijman, E. E.; Mann, E. K.; Jákli, A. I. *Sens. Biosensing Res.* **2016**, *8*, 31-35.

(15) Das, D.; Sidiq, S.; Pal, S. K. *ChemPhysChem* **2015**, *16*, 753–760.

(16) Munir, S.; Park, S. Y. *Sens. Actuator B-Chem.* **2016,** *233*, 559-565.

(17) Bi, X.; Hartono, D.; Yang, K. L. *Adv. Funct. Mater.* **2009**, *19*, 3760–3765.

(18) Das, D.; Sidiq, S.; Pal, S. K., *RSC Adv*. **2015**, *5*, 66476–66486.

(19) Hartono, D.; Bi, X.; Yang, K. L.; Yung, L. Y. L. *Adv. Funct. Mater*. **2008**, *18*, 2938-2945.

(20) Sidiq, S.; Verma, I.; Pal, S. K. *Langmuir* **2015**, *31*, 4741–4751.

(21) Verma, I.; Sidiq, S.; Pal, S. K. *Liq. Cryst*. **2016**, *43*, 1126-1134.

(22) Brake, J. M.; Daschner, M. K.; Luk, Y. Y.; Abbott, N. L. *Science* **2003**, *302*, 2094–2097.

(23) Eliezer, D.; Kutluay, E.; Bussell, Jr. R.; Browne, G. *J. Mol. Biol.* **2001**, *307*, 1061-1073.

(24) Epand, R. M. *Biochim. Biophys.Acta* **1998**, *1376*, 353-368.

(25) Ladokhin, A. S.; Vidal. M. F.; White, S. H. *J. Membrane Biol.* **2010**, *236*, 247-253.

(26) Seelig. J. *Biochim.Biophys.Acta* **2004**, *1666*, 40-50.

(27) Keiderling, T. A.; Silva, R. A.; Yoder, G.; Dukor, R. K. *Bioorg. Med. Chem.* **1999**, *7*, 133−141.

(28) Ma, S.; Freedman, T. B.; Dukor R. K.; Nafie, L. A. *Appl. Spectrosc*. **2010**, *64*, 615−626.

(29) Giugliarelli, A.; Sassi, P.; Paolantoni, M.; Morresi, A.; Dukor, R.; Nafie, L. *J. Phys. Chem. B* **2013**, *117*, 2645−2652.

(30) Keiderling, T. A., *Curr. Opin. Chem. Biol.* **2002**, *6*, 682-688.

Chapter 5

Liquid crystal revealed interactions between melittin and phospholipids at aqueous-liquid crystal interface

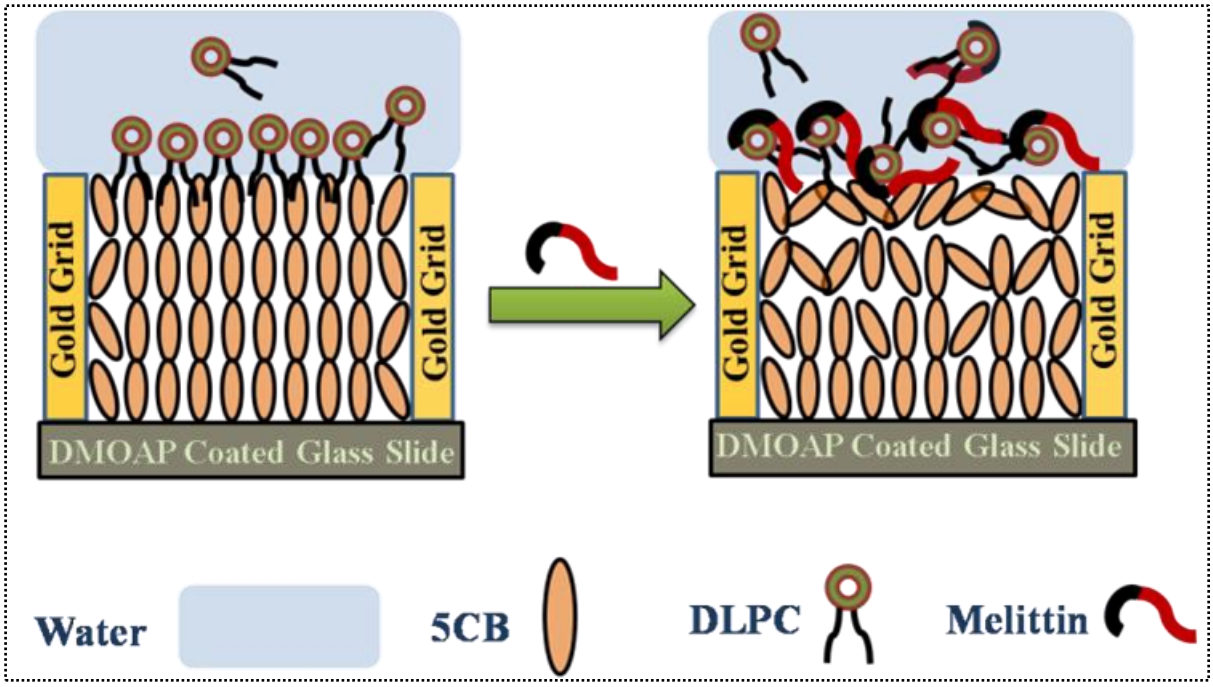

The interaction of honeybee apitoxin (melittin) with phospholipid membrane is very crucial to unveil the mechanistic details of the interaction of peptide with phospholipid membrane. In this regard, herein, our work advances the design of a liquid crystal (LC)-based sensor for precise and quantitative imaging of melittin–phospholipid interaction through interfacial ordering transition. We have investigated the conformational behavior of the melittin in solution as well as in the phospholipid environment.

5.1 Introduction

The interactions between peptides and lipids hold immense importance in regulating several cellular functions.[1,2] Among the wide range of peptides, membrane-active peptides are of great importance as they exhibit several biological activities.[3,4] Furthermore, the functionalities of these peptides related to alteration or permeation of phospholipid bilayers in cellular membrane may be exploited for therapeutic applications.[5] In this regard, melittin has been noticed widely as a model peptide for membrane active proteins which is capable of pore formation on phospholipid decorated cellular membrane.[6,7]

Melittin, a small linear peptide composed of 26 amino acids, is the major toxic substance present in the venom of the European honey bee *Apis mellifera*. Melittin can permeate cellular membrane due to the strong binding affinity towards phospholipid bilayer present at the membrane and thus brings about leakage of cellular components across the phospholipid bilayers.[8,9] However, the mechanistic details related to the activities of melittin on phospholipids bilayers still remain obscure. Moreover, conformational behaviour of melittin is another crucial aspect that actually helps it to permeate phospholipid bilayers via pore formation.[10,11] In a molecular level, under lipid rich environment, melittin monomers self-associate to adopt a α-helical conformation in which hydrophilic and hydrophobic moieties of melittin keep away from each other. Interestingly, the phenomenon of melittin induced disruption of phospholipid bilayer barriers followed by collapse of cell membrane is exhibited for both mammalian as well as bacterial cells. Therefore, melittin is considered as potential antimicrobial peptides to battle with several bacterial infections and also expected to be a useful peptide in designing future anti-bacterial drugs.[12]

To date, only a few biological assays, namely isothermal titration calorimetry,[13] fluorescence quenching,[14] calcein release assay,[15] circular dichroism[16] are on hand to recognize the mellitin-phospholipid interaction. But requirement of labeled melittin, complex sample preparation and lack of sensitivity limits their widespread use. Recently, several spectroscopic methods such as, nuclear magnetic resonance (NMR),[17] fourier-transform infrared (FTIR) spectroscopy,[18] electron spin resonance (ESR),[19] surface plasmon resonance (SPR)[20] have been introduced to exploit the behaviour of melittin on

the phospholipid membrane. In this chapter, we report a simple LC-based system for precise recognition of the interactions between melittin and cellular phospholipids.

Recently, aqueous-LC interface has been introduced as a fascinating sensing tool for various biomolecular interactions.[21-27] Micrometer range communication in the orientation of LC molecules makes it sensitive to target external stimuli which allow the amplification of the interfacial events into optical read-out visible to naked eye. Various biomolecular interactions such as, lipid-protein binding event,[28,29] protein recognition,[30,31] enzymatic reactivity,[32] DNA sensing,[33] toxin detections,[34,35] cholesterol detection[36] and many others[37,38] have been investigated using LC as a sensing platform. But, till now there is no report regarding the investigation of interactions between melittin and membrane phospholipids at aqueous-LC interfaces.

5.2 Objective

The study reported in this chapter is based on the following goals. First, we sought to design a robust LC-based technique that could recognize melittin–phospholipid interactions through surface driven ordering transitions in LC. Second, we wanted to find out the conformational switch of melittin in presence of phospholipid, in particular, how this conformational alteration gets influenced in regard of different chemical environment and impose potential impact on the sensitivity of our designed LC-based system. Finally, we sought to determine if it would be possible to quantify these interactions by measuring the tilt angle (associated with ordering of the LC phase) at the aqueous-LC interface. For our experiment, we chose 1,2-didodecanoyl-*sn*-glycero-3-phosphocholine (DLPC) as model phospholipid. DLPC molecules were known to self-assemble at aqueous-LC interfaces and could trigger an ordering transition of the LC through hydrophobic interactions.[28,39] Motivated by this, we thought that strong interaction between melittin and DLPC could able to disorganize self-assembled DLPC molecules at aqueous-LC interface and may lead to an ordering transition of the LC.

5.3 Results and discussions

5.3.1. Phospholipid mediated ordering transition of liquid crystal at aqueous-LC interface

Our first set of experiments was to image the behaviour of DLPC molecules at aqueous-LC interface. As reported earlier, LC (such as 5CB) appeared bright when immersed into Tris buffer (pH 7.4) and viewed under crossed polars (Figure 5.1 A). The bright optical appearance of the LC in contact with water indicates a planar/tilted orientation at those interfaces. The bright appearance of the LC turned dark immediately after exposure of 0.1 mM aqueous solution of DLPC (Figure 5.1 B). This is due to strong hydrophobic interaction between alkyl chains of DLPC with LC molecules leading to dark optical appearance.[30] For our experiments, DLPC- laden aqueous-LC interface was incubated for 2 h to stabilize the lipid self-assembly at the interface. Excess DLPC from the solution was removed by exchanging with Tris buffer (pH 7.4) three times.

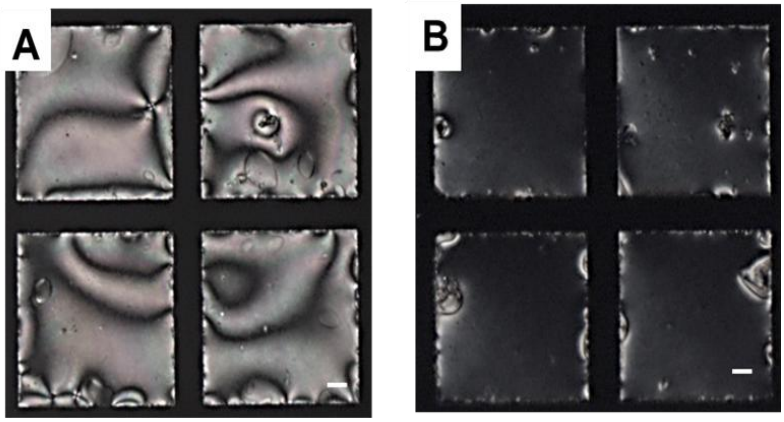

Figure 5.1 Optical images of 5CB confined in gold grid placed on DMOAP coated glass slides: A) in Tris buffer (pH 7.4), B) in contact with 0.1 mM DLPC vesicles. Scale bar = 40 μm.

5.3.2. Interactions of melittin with self-assembled DLPC at aqueous-LC interface

Our next experiment was to investigate the behavior of melittin onto DLPC-laden aqueous-LC interface. For this, DLPC-laden aqueous-LC interface was placed in contact with an aqueous solution of 10 μM melittin in Tris buffer (pH 7.4). We observed a gradual change

in the optical image of the LC molecules from dark to bright within 1 min (Figure 5.2 A, B). This observation indicates an ordering transition of the LC from homeotropic to a planar/tilted state. The result also implies that strong interaction between melittin and DLPC is responsible to trigger the self-assembly of the DLPC molecules at aqueous–LC interface that resulted in ordering transition of the LC.

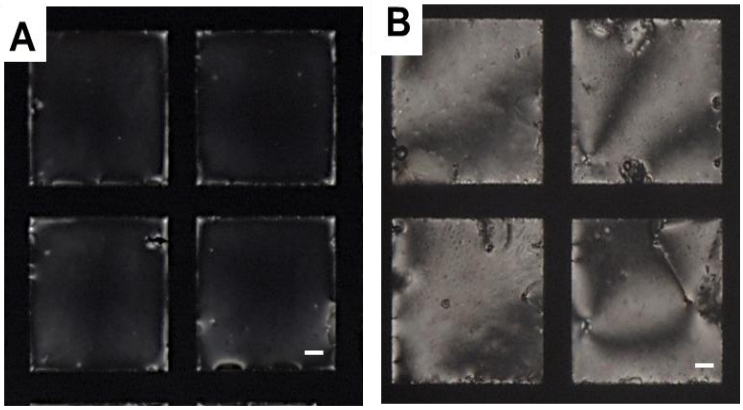

Figure 5.2 Polarized optical appearances of aqueous-LC interface A) in presence of DLPC after 2 h of incubation. B) After exposing 10 μM aqueous solution of melittin onto DLPC decorated aqueous-LC interface. Scale bar = 40 μm.

5.3.3. Control Experiment

To provide further insight into the proposition that the orientational transition of 5CB is only due to the interaction of DLPC with melittin, we performed a control experiment. Here, we sought to investigate whether direct interaction of melittin with interfacial 5CB molecules could able to alter the orientation of the LC in the absence of DLPC vesicles at the interface. To validate this, we added 10 μM of aqueous solution of melittin in Tris buffer (pH 7.4) directly onto the DLPC free aqueous-LC interface. We found that the optical appearance of the LC remained bright (even after 6 h of incubation or more) indicating a planar/tilted orientation of 5CB molecules at aqueous–LC interface (Figure 5.3 A, B). This observation clearly indicates that there are no direct interactions present between interfacial 5CB molecules and the melittin which could disturb the orientation of the LC at those interfaces.

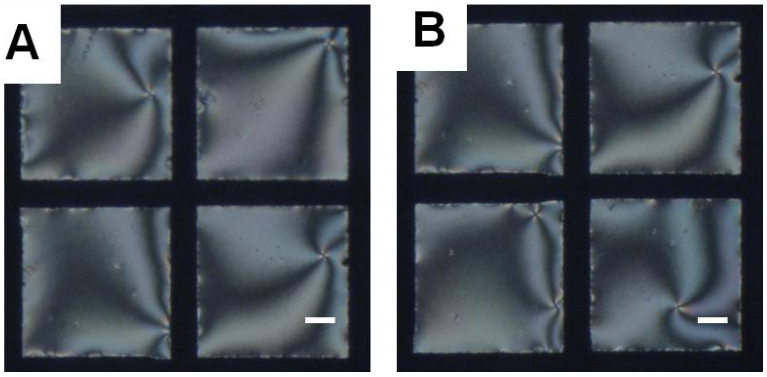

Figure 5.3 Optical micrograph of aqueous-LC interface A) in Tris buffer (pH 7.4) and B) after exposing an aqueous solution of 10 µM melittin onto DLPC free aqueous-LC interface. Scale bar = 40 µm.

5.3.4. Determination of detection limit of melittin on DLPC laden aqueous-LC interface

After confirming that LC is able to recognize the interactions between melittin and phospholipid through orientational transition of the LC, we aimed to investigate the sensitivity of the LC based system for the realization of a novel biosensor for detection of such biomolecular interactions. For this, we sought to investigate the limit of detection (LOD) and response time of the system, for which we compared the dynamic response of the LC at different concentrations of melittin on the DLPC-laden aqueous–LC interface. The results shown in Figure 5.4 demonstrate the optical response of the LC at the DLPC-laden aqueous-LC interface as a function of different concentrations of melittin. Inspection of Figure 5.4 A–D reveals that the dynamic response period of LC significantly increases with decreasing concentrations of melittin (all optical images were recorded after 60 min of incubation of melittin at the DLPC decorated aqueous-LC interface). Figure 5.4 A exhibits the optical appearance of the LC after addition of 5 µM melittin solution onto DLPC laden aqueous-LC interface. We observed a gradual change in the optical appearance of LC from dark to bright within 15 minutes which is longer time span compare to the concentration (10 µM) of melittin used previously. On further varying the concentrations of melittin to successive lower value, 1 µM, we found response time of LC further increased to 40 min to show complete bright appearance

(Figure 5.4 B). At the concentration of 500 nM of melittin, we found partial bright appearance of the LC after 1 h period of incubation (Figure 5.4 C). On further decreasing the concentration of melittin to 300 nM, the optical appearance of 5CB remained dark after 1 h (Figure 5.4 D) or even longer period. Overall, from the above experiment we can conclude that LC is able to recognize the interaction between melittin and phospholipid at higher concentration of melittin but, towards lower concentration of melittin LC remain scarcely responsive. This could be due to slow dynamics of melittin-phospholipid interactions at lower concentration of the melittin at the interface.

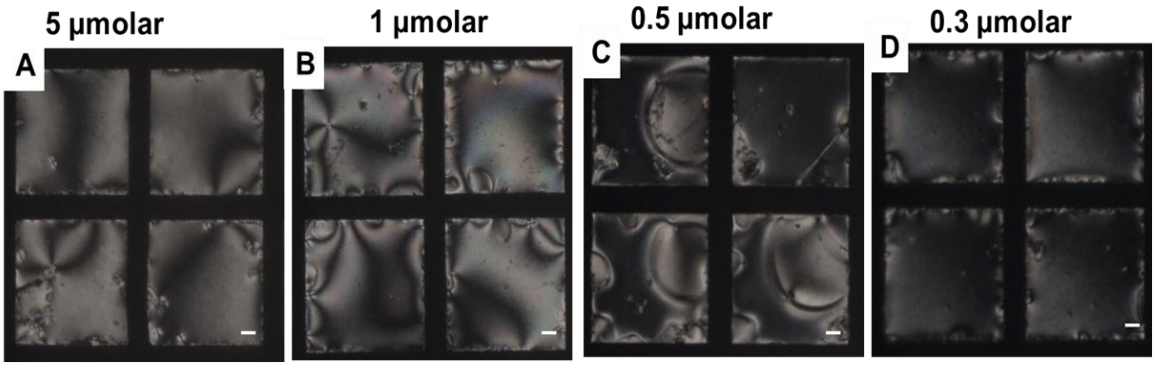

Figure 5.4 Optical images of DLPC laden aqueous-LC interface after 60 min incubation with varying concentrations of melittin A) 5 µM, B) 1 µM, C) 0.5 µM, D) 0.3 µM respectively. Scale bar = 40 µm.

5.3.5. Determination of detection limit of melittin on DLPC-laden aqueous-LC interface in presence of Ca^{2+}

In order to improve the sensitivity level of our LC based sensor, we planned to investigate the chemical condition which would be favorable for faster binding of melittin on DLPC laden aqueous-LC interface. In literature, we found that activities of melittin get highly influenced by Ca^{2+}. For example, melittin inhibits the function of Ca^{2+} dependent protein kinase II by sequestering Ca^{2+} from protein core which, in turn, indicates strong affinity of melittin toward Ca^{2+}.[40] According to another report, the binding of melittin with cell membrane phospholipid increases the permeability of Ca^{2+} across cell membrane to many fold compared to monovalent ions like Na^{+} and K^{+}.[41] Therefore, we thought that in presence of Ca^{2+}, melittin would interact with DLPC rapidly and therefore, sensitivity of the system could be improved. To prove our hypothesis we investigated the response time

of the LC at different concentrations of melittin exposed to DLPC-laden aqueous–LC interface pre-incubated with 5 mM Ca^{2+}. As shown in Figure 5A-F, we observed faster response time of the LC toward recognizing this interaction than before (in absence of Ca^{2+}). Detailed inspection of figure 5.5 A-F also revealed that in presence of Ca^{2+}, 5CB became responsive towards lower melittin concentrations (<500 nM). For the varying concentrations of melittin such as, 500 nM, 300 nM, 100 nM and 50 nM (Figure 5.5 A-D) the response times of LC (to appear complete bright from dark) were 5 min, 15 min, 40 min and 60 min, respectively. On further lowering the concentration to 20 nM, we observed only partial bright appearance of the LC after 1h period of incubation (Figure 5.5 E). After extending incubation period to 2h, 5CB appeared as complete bright at this concentration. On successive lower concentration of melittin to 10 nM the optical appearance of 5CB remained dark after 2 h (Figure 5.5 F) or even longer incubation period. Overall, from this experiment we found that 20 µM concentration as LOD for melittin (in presence of Ca^{2+}) based on our LC based sensor. In summary, we observed faster response time of 5CB towards interfacial binding of melttin on DLPC in presence of Ca^{2+} LC became responsive towards this interaction at further lower concentration of melittin in presence of Ca^{2+} than before (in absence of Ca^{2+}).

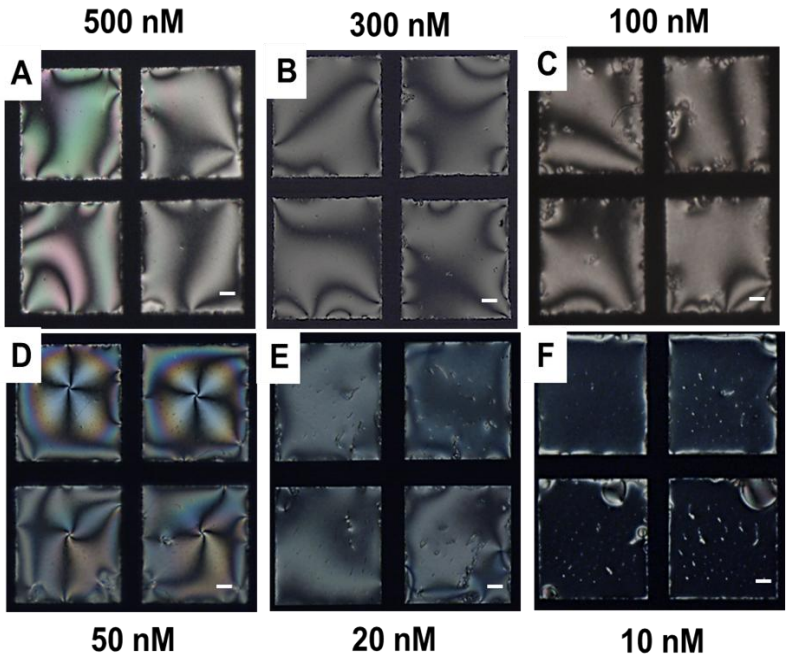

Figure 5.5 Polarized optical images of 5 mM Ca^{2+} pre-incubated DLPC-laden aqueous LC interface after 60 min incubation with A) 500 nM, B) 300 nM, C) 100 nM, D) 50 nM, E) 20 nM, F) 10 nM concentrations of melittin. Scale bar = 40 μm.

To reconfirm our proposition that Ca^{2+} assists in faster binding of melittin on phospholipid decorated aqueous-LC interface, we planned to perform three control experiments. First, we wanted to check whether direct interaction of Ca^{2+} with interfacial DLPC molecules could lead to an ordering alteration of the LC. For this, we exposed 5 mM of aqueous solution of Ca^{2+} directly onto DLPC decorated aqueous-LC interface. We found that the optical appearance of the LC remained dark as before even after 2 h of incubation (Figure 5.6 A, B). This observation clearly implies the absence of any interaction between Ca^{2+} and interfacial DLPC molecules.

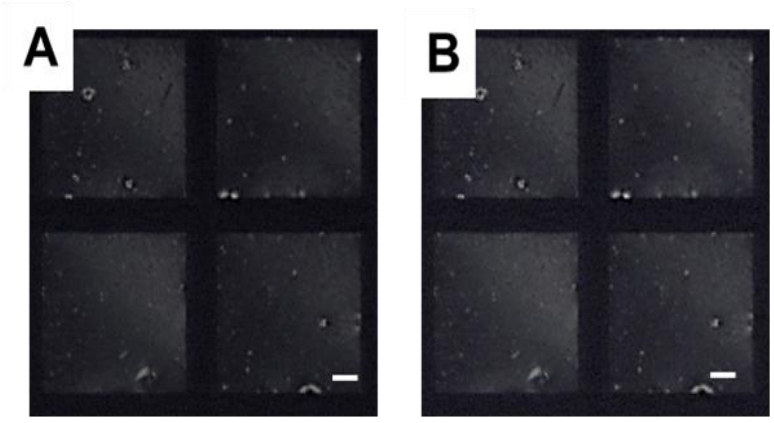

Figure 5.6 Optical images of aqueous-LC interface laden with A) 0.1 mM DLPC. B) the optical response of the same DLPC decorated aqueous-LC interface after 60 min incubation with of 5 mM Ca^{2+} solution. Scale bar = 40 μm.

In our next experiment, we pre-incubated DLPC laden aqueous-LC interface with 5 mM Ca^{2+} in presence of 5 mM EDTA and exposed this interface towards 100 nM concentration of melittin (at this concentration of melittin optical response of 5CB remained dark in absence of Ca^{2+}). As expected, we observed no change in the optical appearance of 5CB. It remained dark even after 1 hr period of incubation (Figure 5.7 A, B). The strong binding affinity of Ca^{2+} towards EDTA resulted in formation of 1:1 EDTA-Ca^{2+} complex. Therefore, no Ca^{2+} was essentially left to facilitate this melittin-DLPC interactions at this

low concentration of melittin. Therefore, from this experiment, we can conclude that free Ca^{2+} ions play a significant role in recognizing these interfacial interactions at low concentration of melittin.

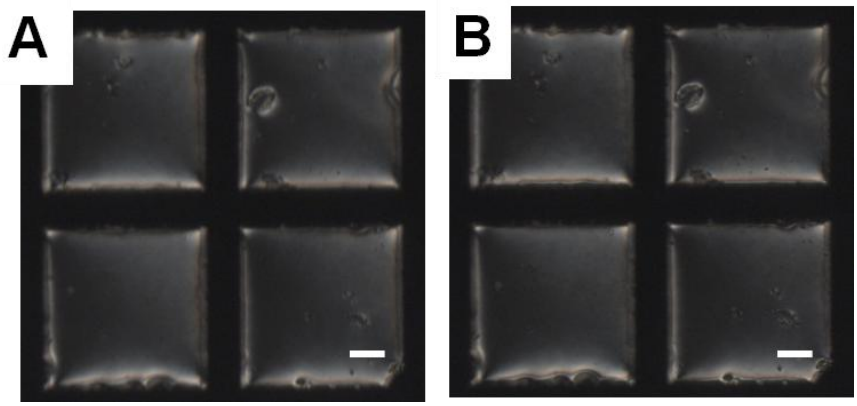

Figure 5.7 Optical micrographs of aqueous-LCs interface A) in presence of 0.1 mM DLPC in presence of 5 mM Ca^{2+} pre incubated with 5 mM EDTA B) represents same DLPC-laden aqueous-LC interface after 30 min incubation with 300 nM of melittin. Scale bar = 40 μm.

Third, we planned to investigate the specific behaviour of Ca^{2+} towards the melittin-DLPC interaction compared to other metal ions (in a same group of Ca^{2+}). For this, we replaced Ca^{2+} with Mg^{2+}, Sr^{2+} and Ba^{2+}. We observed that in presence of these metal ions the optical appearance of the LC remained dark (incubated with 100 nM melittin Figure 5.8 A-C). This observation clearly indicates the specific role of Ca^{2+} towards binding of melittin and DLPC at aqueous-LC interface.

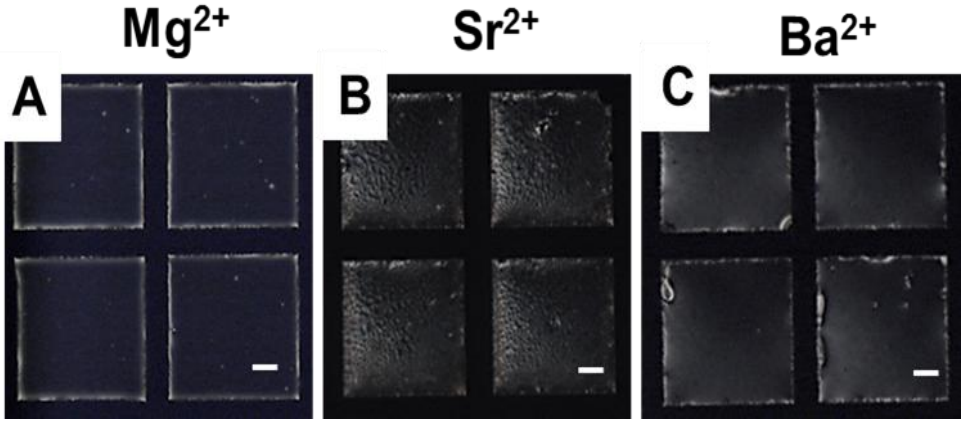

Figure 5.8 Polarized optical micrographs Optical aqueous-LC interface on exposing DLPC-laden aqueous-LC interface for 60 min incubation with 300 nM aqueous solution of melittin in presence of 10 mM aqueous solution of A) Mg^{2+} , B) Sr^{2+} and C) Ba^{2+} respectively. Scale bar = 40 μm.

5.3.6. Average gray scale intensity and tilt angle measurements to quantify the interaction of melittin with DLPC at the aqueous-LC interface

After providing thorough insights into the dynamic response of LC towards melittin-DLPC interactions at aqueous-LC interface, next, we planned to correlate this interaction with anchoring transition of 5CB in a quantitative way. For this, we measured the average gray scale intensity of (pre-incubated with Ca^{2+}) DLPC-5CB films in presence of varying concentrations of melittin. Figure 5.9 shows the variation of average gray scale intensity as a function of the concentrations of melittin. Here, we observed a gradual decrease in gray scale intensity of 5CB films with decreasing concentrations of melittin. This observation confirms that gray scale intensity LC films during this interfacial event can be correlated with the concentration of melittin.

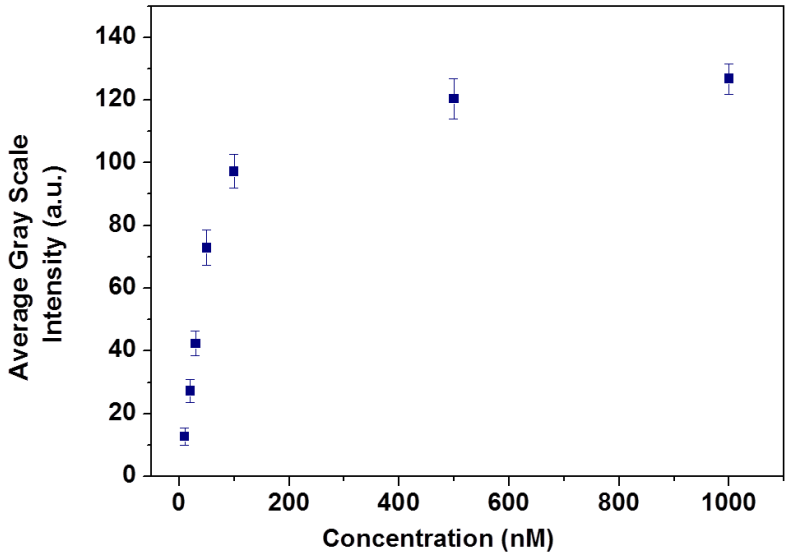

Figure 5.9 Represents the variation of average gray scale intensity of optical images of 5CB films with varying concentrations of melittin on Ca^{2+} pre-incubated DLPC decorated aqueous-LC interface.

Moreover, we found that in absence of Ca^{2+}, the value of average gray scale intensity at all concentration range is lower compared to that observed in presence of Ca^{2+}(Figure 5.10).

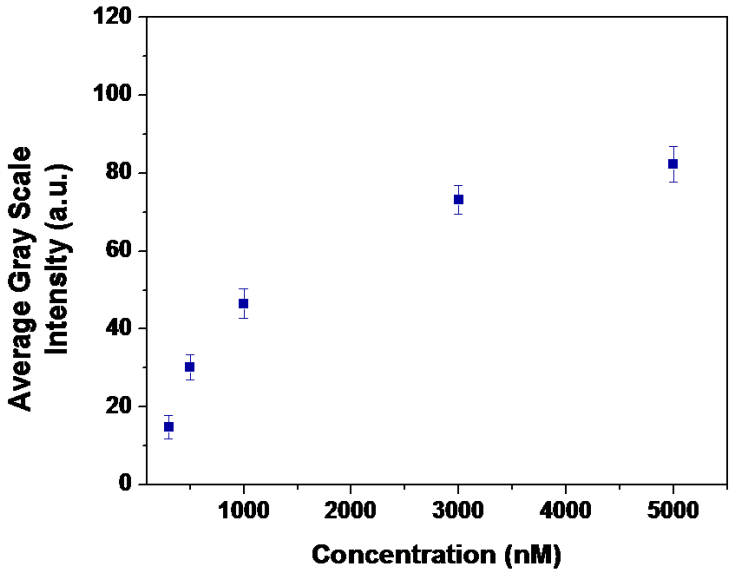

Figure 5.10 Represents the average grey scale intensity of 5CB films associated with lipid-melittin binding event in absence of Ca^{2+}at different concentrations of melittin.

We also plotted average gray scale intensity with respect to time for a particular concentration of melittin (in absence and presence of Ca^{2+}). After introducing 500 nM concentration of melittin on DLPC-laden aqueous-LC interface (in presence of Ca^{2+}), when measured the change in average gray scale intensity of LC during the optical transition of 5CB from black to bright. We found very fast increase in average gray scale intensity and within 20 min it reaches to the maximum value 107.2±2.5 (Figure 5.11).

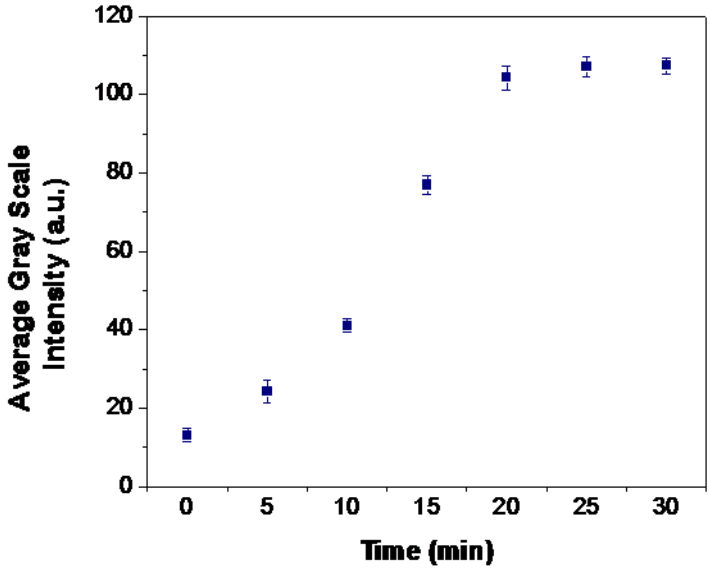

Figure 5.11 Represents the average gray scale intensity vs time graph of 5CB films associated with DLPC-melttin binding event in presence of Ca^{2+} at 500 nM concentration of melittin.

But when the same experiment was repeated without Ca^{2+} we found very slow increase in average gray scale intensity and reaches to maximum value 77.5±1.8 after 2 h period of incubation (Figure 5.12).

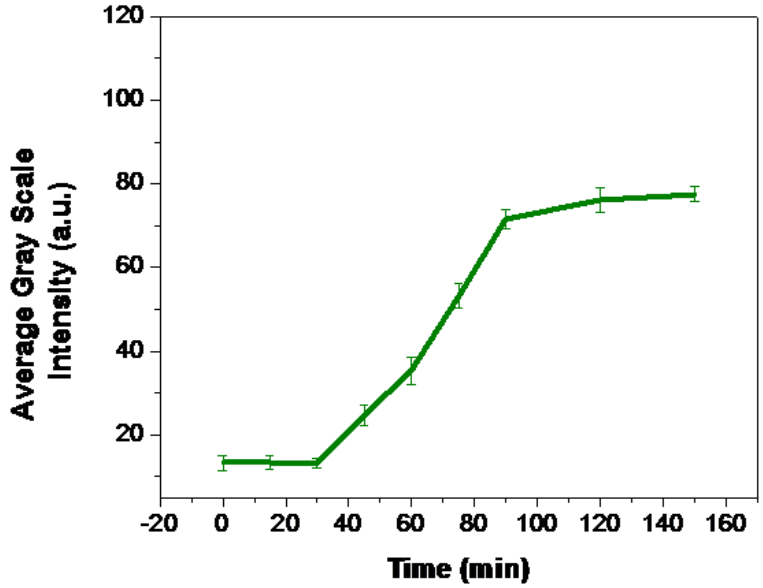

Figure 5.12 Represents the average grey scale intensity vs time graph of 5CB films associated with DLPC-melttin binding event in absence of Ca^{2+}at 500 nM concentration of melittin

Next we planned to check the influence of other divalent metal ion except Ca^{2+} on the average gray scale intensity of 5CB films associated with interaction of DLPC-melittin interactions. We again observed slow increase in the gray scale intensity along the 2 h period of incubation (Figure 5.13). This result is similar to that we got in case of melittin incubated with DLPC without Ca^{2+}. This experiment further confirms only Ca^{2+} has catalytic influence on the interaction of melittin and DLPC at the aqueous-LC interface.

In other way, this observation also led to a quantitative correlation between melttin-DLPC binding affinity (in presence and absence of Ca^{2+}) and orientational anchoring of LC at the interface.

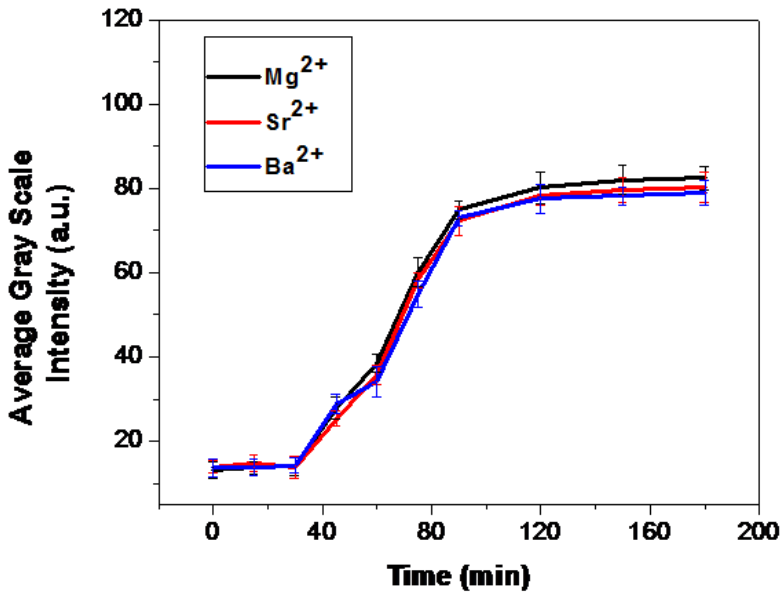

Figure 5.13 Represents the average grey scale intensity vs time graph of 5CB films associated with DLPC-melttin binding event in presence of Ba^{2+}(blue line), Sr^{2+}(red line) and Mg^{2+}(black line) respectively at 500 nM concentration of melittin.

To put further quantitative insight into the melttin-DLPC interactions, we plan to measure the tilt angle of LC during the interaction in presence of Ca^{2+}. The tilt of the LC depends on the change of self-assembly behaviors of interfacial DLPC molecules in presence of melittin. To establish this, first, we exposed 20 nM melittin (the limiting concentration of melittin for our system in presence of Ca^{2+}) onto DLPC-laden aqueous-LC interface in presence of Ca^{2+}. Then, we measured optical retardance of 5CB films during this interfacial event in a regular interval. We calculated tilt angle of 5CB from the measured optical retardance values using the procedures reported in experimental section. When we plot the tilt angle values with different time period, we observed a regular increase in the tilt angle of 5CB with increasing time. Over an observation period of 3h, the maximum tilt angle of 5CB was found to 48.24°±1.5 (Figure 5.14). These experiments established a direct quantitative correlation between melittin-DLPC interfacial interactions (in presence of Ca^{2+}) and anchoring transitions of the LC at the interface. We also observed gradual rise of tilt angle of 5CB with increasing incubation period. This confirms that the ordering switch of interfacial LC during melittin-DLPC interfacial interactions took place in a continuous manner.

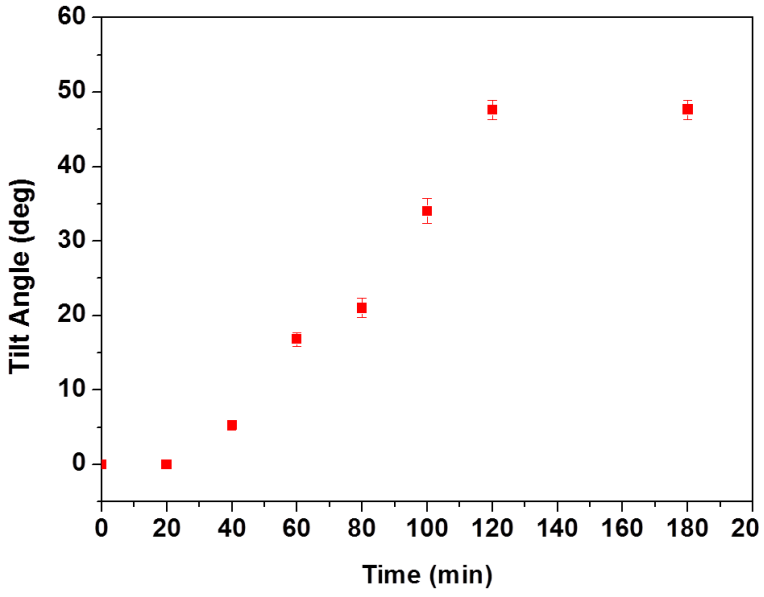

Figure 5.14 Represents the gradual change of tilt angle of Ca^{2+} pre-incubated DLPC laden 5CB films in presence of 20 nM aqueous solution of melittin.

In addition to that we also measured the tilt angle of the LC during this interfacial interaction in absence of Ca^{2+}. We found gradual increase in the tilt angle of 5CB with increasing time but the magnitude of increasing tilt angle of 5CB is less than that of associated with lipid-melttin binding event in presence of Ca^{2+} (Figure 5.15).

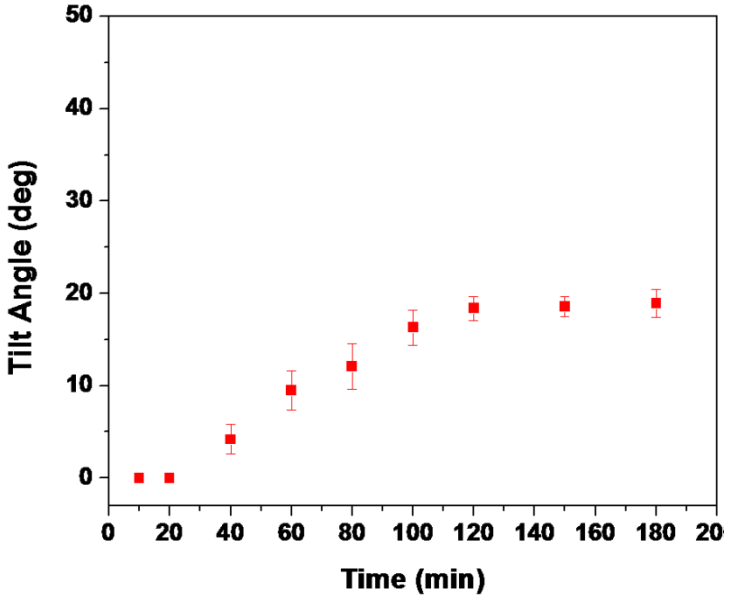

Figure 5.15 Represents tilt angle variation of 5CB associated with lipid-melttin binding event in absence of Ca^{2+}

5.3.7 Conformational analysis of melittin in aqueous environment as well as in presence of Phospholipid and Ca^{2+}

After providing quantitative insights into the interaction of melittin and DLPC decorated aqueous-LC interface, next we aimed to investigate the conformational behavior of melittin in solution as well as in presence of DLPC vesicles. Previous reports describe that the binding of lipids with peptides or proteins highly influence their conformations.[42] Furthermore, the activities of peptides are highly dependent on their conformational arrangement. Binding of peptides on lipid bilayers starts with alteration of the conformations of peptides which, in turn, facilitates the infusion of peptides into lipid bilayers and also leads to thermodynamic stability of peptide arrangements across the lipid bilayers.[43-46] Therefore, determining conformation state of melittin could provide additional insight into understanding the binding with phospholipid vesicle. Keeping this end in view,

we planned to characterize conformations of melittin in Tris buffer, as well as in presence of Ca^{2+} and DLPC. Figure 5.16 illustrates the CD Spectra of melittin at different conditions. In aqueous Tris buffer solution (pH 7.4) melittin adopts α helical conformation which can be confirmed with two characteristic minima at 208 nm and 223 nm (blue line). In presence of Ca^{2+}, we observed two broadened minima around 208 nm and 223 nm with a sharp decrease in the ellipticity value of melittin helices from -80 mdeg to -48 mdeg (black line). This observation suggests that, in presence of Ca^{2+}, melittin retains its alpha helical conformation but with less helical arrangement, which, in turn, depicts less rigid structure of the melittin compared to that in Tris buffer solution. In our previous experiments, we found faster dynamic response of the LC towards melittin-DLPC binding event in presence of Ca^{2+}. This is probably due to such less helical conformation of melittin (adopted in presence of Ca^{2+}) in which it becomes more exposed to interact with phospholipid vesicle efficiently and thus, resulted a rapid ordering transition. However, in presence of DLPC vesicles, we found the CD spectra of melittin exhibiting two sharp minima around 208 nm and 223 nm with increased ellipticity value (Compared to that in presence of only Ca^{2+}) to -55 mdeg (red line). This observation indicates that upon binding with DLPC vesicles, melittin adopts more ordered α helix conformation which, possibly, could lead to more thermodynamic stability of melittin in phospholipid environment.

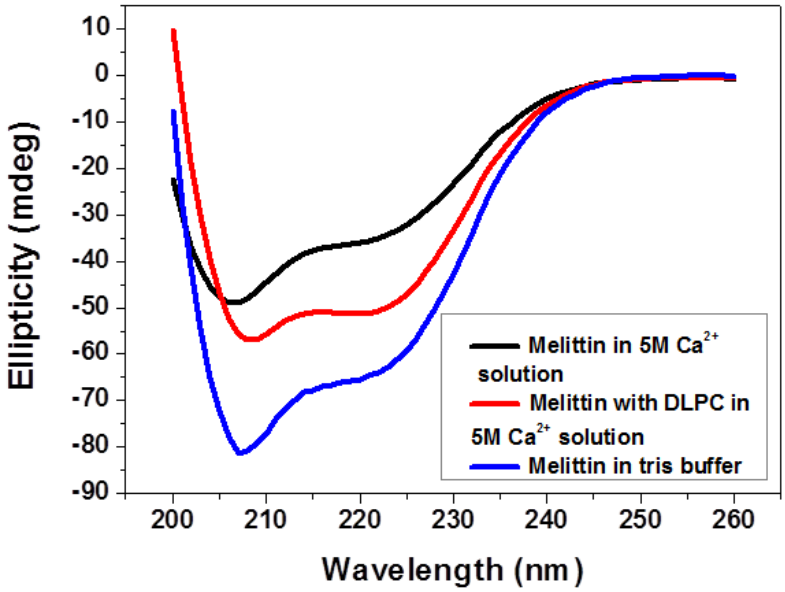

Figure 5.16 Ellipticity graph of A) 100 nM melittin in Tris buffer, B) melittin in presence of 5 mM Ca^{2+} solution and C) 100 nM melittin with 0.1 mg mL^{-1} DLPC in 5 mM Ca^{2+} solution.

We have also done CD experiments to determine the influence of other divalent metal ions (Mg^{2+}, Sr^{2+} or Ba^{2+}) on the conformation of melittin in solution. We found that except Ca^{2+}, for all other three ions, the ellipticty value of melltin remains same as that in Tris buffer solution (Figure 5.17). This observation implies that Mg^{2+}, Sr^{2+} and Ba^{2+}don't have strong influence on altering the conformation of melittin towards less ordered structure. As a whole, from this CD experiment we can reach into two conclusions. First, Ca^{2+} induced melittin adopt a less ordered α helix conformation which, possibly, could facilitate its interaction with phospholipid and leading to faster orientational ordering of the LC. Second, we observed in phospholipid environment melittin adopted more ordered α helical conformation to attain maximum thermodynamic stability on binding with DLPC.

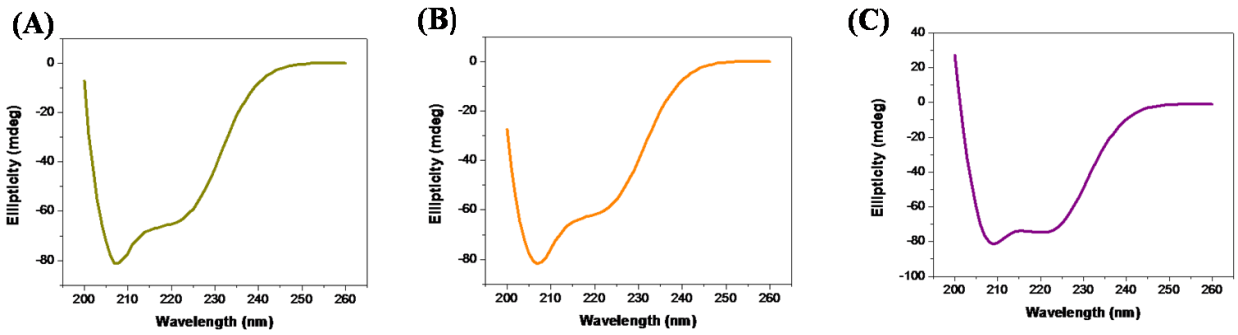

Figure 5.17 Represents ellipticity graph of A) 100 nM melittin in presence of 5 mM Mg^{2+} solution, B) in presence of 5 mM Sr^{2+} solution and C) in presence of 5 mM Ba^{2+} solution.

To provide further insight into the Ca^{2+} induced conformational behaviour of melittin and its consequence in presence of phospholipid vesicles, we performed VCD experiment. VCD shows high sensitivity to the conformational rearrangements of the protein and peptide system.[47, 48] In fact, VCD exhibits an enhanced sensitivity to protein secondary structure due to combination of structural sensitivity of infrared and stereospecificity of circular dichroism. In our VCD experiment, we observed melittin in Tris buffer (pH 7.4) exhibit a maxima around 1643 cm^{-1} with ΔA value about 0.00015 (Figure 5.18 A, black line). The maxima around 1643 cm^{-1} are, commonly, considered as characteristic amide ll

peak for α helical configuration of protein or peptide. This observation correlates well with previously shown CD spectra where melittin in Tris buffer (pH 7.4) also found to be exhibited alpha helical configuration. Figure 5.18 B (red line) reveals the VCD spectra of melittin in presence of Ca^{2+}. In this spectrum, we again observed the maxima around 1643 cm^{-1} indicating α helical arrangement of melittin. On the contrary to the spectra (Figure 5.18 C), here we found decrease in the intensity of the characteristic maxima with ΔA value 0.00005 as well as little broadening of that peak implying melittin with less ordered α helical configuration. This observation further supports the CD spectra where we found decreased ellipticity of α helical arrangement of melittin in presence of Ca^{2+} resulting in less ordered α helical configuration. However, in presence of DLPC vesicles in Ca^{2+} solution, we found the VCD spectra of melittin exhibiting maxima around 1645 cm^{-1} (Figure 5.18 C, blue line) implying α helical configuration of melittin retained on binding with phospholipids. Additionally, we also observed an increase in the intensity of the characteristic maxima with ΔA value close to 0.00015 (similar to the Figure 5.18 A spectra) as well as sharpening of that peak (compared to the Figure 5.18 B spectra) implying melittin goes back to more ordered alpha helical configuration in presence of DLPC. This observation is in accord with the result obtained from CD experiment where we found that upon binding with DLPC vesicles, the ellipticity value of melittin increased indicating melittin adopts more ordered α helix conformation in presence of DLPC. As a whole, on combining results obtained from both CD and VCD experiments, we can conclude that melittin adopts alpha helical arrangement in Tris buffer, while in presence of Ca^{2+} melittin espouses a less ordered α helical conformation which, possibly, could ease its interaction with phospholipid and leading to faster dynamic response through orientational switching of LCs. But, upon binding with DLPC, we observed in phospholipid environment melittin adopted more ordered alpha helical conformation to attain maximum thermodynamic stability on its interaction with phospholipid.

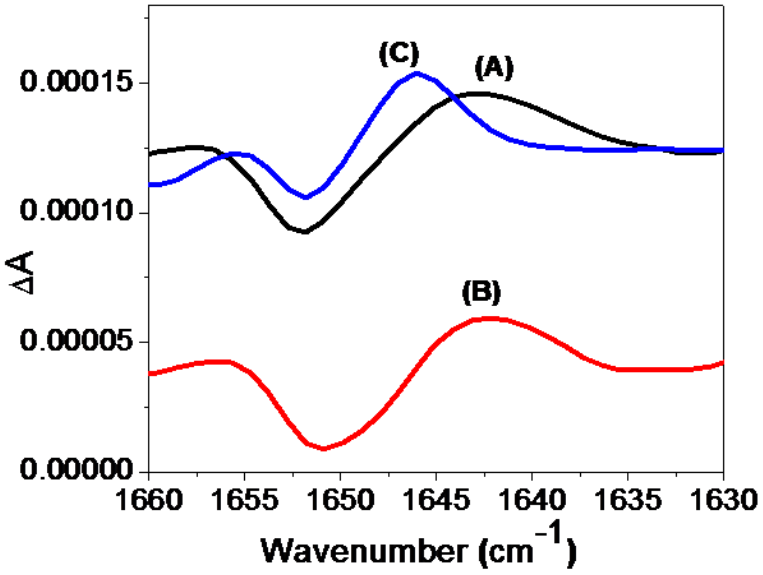

Figure 5.18 VCD spectra of A) 10 mg mL^{-1} aqueous solution of melittin in Tris buffer, B) melittin in presence of 10 mM Ca^{2+} solution and C) melittin with 0.5 mM DLPC in 10 mM Ca^{2+} solution.

5.4 Conclusions

Overall, we have designed LCs based sensor to study the interaction of honey bee venom melittin with cell membrane phospholipid (DLPC). We have shown that DLPC-laden interfacial LC flipped from homeotropic to plannar/titlted state (visualized as dark to bright under POM) on exposure of an aqueous solution of melittin onto this interface. Strong interaction between melittin and DLPC induces the ordering transition of LC at aqueous–LC interfaces. Our experiment also revealed that Ca^{2+} plays crucial role for faster response time of DLPC decorated interfacial LC in presence of melittin. The assistance of Ca^{2+} towards kinetics of melittin-DLPC binding was highly specific compared to other alkaline earth metal ions. The sensitivity level of our system towards recognizing these interactions was found to be 500 nM concentration of melittin (in absence of Ca^{2+}) and 20 nM concentration of same (in presence of Ca^{2+}) respectively. Furthermore, we also have demonstrated quantitative correlation between anchoring transition of 5CB associated with this interfacial interaction with help of average gray scale intensity and tilt angle measurement. Finally, we have investigated the conformational behavior of melittin in aqueous Tris buffer solution, in presence of Ca^{2+} and after incubating with DLPC vesicles

using CD spectroscopy, where we observed that Ca^{2+} induced melittin to adopt a less ordered α helix conformation which could facilitate its interaction with phospholipid. In phospholipid environment melittin adopted more ordered α helical conformation to attain thermodynamic stability on binding with DLPC. We further affirmed our observations with VCD spectroscopy. Overall, the results offer a promising approach in designing a robust LCs based biosensor to study the interaction of melittin with phospholipid at aqueous-LC interface. This LCs based sensor is more sensitive, without having complex instrumentation and results in simple optical read-out compared to conventional biological and spectroscopic assays.

5.5 Experimental Section

5.5.1 Materials and methods

Melittin (from Apis Mellifera venom), Tris buffered saline (pH 7.4), Calcium chloride, magnesium chloride, N,N-dimethyl-N-octadecyl-3-aminopropyltrimethoxysilylchloride (DMOAP), Deuterium oxide (99.9 atom % D) and Ethylenediaminetetraacetic acid (EDTA) were purchased from Sigma-Aldrich (St. Louis, MO). 1,2-Didodecanoyl-sn-glycerol-3-phosphocholine (DLPC) was purchased from Avanti Polar Lipids, Inc. (Alabaster, AL). Sulfuric acid and hydrogen peroxide (30% w/v), barium chloride and Strontium chloride were purchased from Merck. Ethanol was obtained from Jebsen & Jenssen GmbH and Co., Germany (Sd. fine-chem limited). The 5CB LC was obtained from Merck. Deionization of a distilled water source was performed using a Milli-Q-system (Millipore, bedford, MA). Fischer's Finest Premium Grade glass microscopic slides and cover glass were obtained from Fischer Scientific (Pittsburgh, PA). Gold specimen grids (20 mm thickness, 50 mm wide bars, 283 mm grid spacing) were obtained from Electron Microscopy Sciences (Fort Washington, PA).

5.5.2 Cleaning of glass slides using piranha solution

All Glass slides were cleaned using 'piranha' solution. [Composed of 70:30 (% v/v) H_2SO_4:H_2O_2 (30%)]. At first, all the glass slides were taken in a coplin jar. Then piranha solution was poured into the coplin jar and heated at 100 °C for 1 h. After that, the coplin

jar containing glass slides was allowed to cool down. The glass slides were washed by running excess amount deionized (DI) water for 5–10 min. Then the glass slides were rinsed with ethanol and methanol, respectively. The alcohol rinsed glass slides were dried under stream of nitrogen gas and then stored in an oven at 100 °C for 12 h prior to use.

5.5.3 Coating of glass slides with DMOAP

0.1% (v/v) DMOAP solution in DI water was poured into cleaned glass slides placed in a coplin jar and kept as such for 5 min at room temperature. Then the glass slides were rinsed with DI water to remove excess DMOAP from the glass surface. Then the DMOAP coated glass slides were dried under flow of nitrogen gas and kept in an oven at 100°C for 3 h for crosslinking of DMOAP with glass surface.

5.5.4 Fabrication of 5CB filled gold grids

The DMOAP coated glass slides were cut into square shapes with a diamond tipped knife. Then, a gold grid was placed on the square glass slide. After that, 0.3 mL of 5CB was spread onto the grid followed by removal of excess 5CB with help of a capillary syringe.

5.5.5 Preparation of DLPC vesicles

First solid DLPC was placed into a round bottom flask and dissolved in chloroform (0.5 mL). The chloroform was slowly evaporated from the flask by applying vacuum for 3 h. The resulted lipid film formed inside the flask was kept under a stream of nitrogen for 30 min. Then the thin film of lipid was hydrated with DI water for at least 30 min and vortexed for 1 min. Then, the resulted cloudy solution (indicative of large multilamellar vesicles) was sonicated using a probe ultrasonicator (1×15 min at 25 W) until a clear solution was obtained. The hydrodynamic diameter of DLPC vesicle was 54.1±2.3 nm.

5.5.6 Formation of DLPC laden LC Films

The DLPC laden 5CB interface was formed by contacting the gold grid impregnated with 5CB to the DLPC solution in the optical cell for a period of 2 h. The DLPC laden interface was washed twice with Tris buffer (pH 7.4) prior to use.

5.5.7 Optical imaging of LC films using polarized optical microscope (POM)

The optical appearance of the LC dispensed on the gold grid was observed by using a polarizing optical microscope (Zeiss Axioscope A1, Germany) in the transmission mode. All images were captured with an Axiocam digital camera fixed on the top of the microscope with an exposure time of 40 ms.

5.5.8 Tilt angle measurements

Using tilting compensator (type 2357 K, equipped with a calcite compensator plate, Leitz, Germany) first we measured the optical retardance of 5CB film. The reported optical retardance values are the average of optical retardance of 5CB confined within four squares of the gold grids. For a thin film of nematic LCs with homeotropic anchoring θ_1= 0° at the DMOAP-treated glass interface and a tilt of angle of θ_2 away from the surface normal at the aqueous–LC interface, the tilt of the LC across the film varies linearly with position (considering splay and bend elastic constants of the LCs to be equal) to minimize the elastic energy. The relationship between optical retardance (Δr) of the film of LCs and the tilt of the director at the aqueous–LC interface (θ_s), namely equation 1

$$\Delta r \approx \int_0^d \left(\frac{n_e n_o}{\sqrt{n_o^2 sin^2\left(\frac{z}{d}\theta_s\right) + n_e^2 cos^2\left(\frac{z}{d}\theta_s\right)}} - n_o \right) dz$$

Where η_e and η_o are the indices of refraction parallel (extraordinary refractive index) and perpendicular (ordinary refractive index) to the optical axis of the LCs, respectively, and θs is the tilt angle of LCs measured relative to the surface normal.[28] Using retardance values

and numerically solving eqn (1) tilt angle values were obtained. The indices of refraction of 5CB were n_e =1.711 and n_o =1.5296 (λ= 632 nm at 25 °C). In following the detailed of the procedure has been explained using an example.

After tilting the compensator plate from zero position to both positive and negative directions, two readings for the position of the compensator was observed 7° and 4°. To measure phase difference we need to add up this two values i.e. (2.9°+2.1°) =5°

Now we need to calculate corresponding log f value of 5. From table of log f values we got log f (5) = 19. Next, the value obtained was multiplied with log C value. log C is known as compensator constant. The value of log C is again dependent on wavelength of light used for this experiment. Here log C value will be 4.54 when λ= 632 nm. After multiplying this value with 19 we get (19 x 4.54) = 86.26.

Next to determine optical retardance (Δr), we need to divide the phase difference value from the thickness of the LC. For our experiment thickness of LC is 20000 nm.

Therefore, (Δr) will be (86.26/20000) = 0.004313. Next putting Δr, n_e and n_o values to equation 1 we get

$$.004313 = \frac{1.74 \times 1.52}{\sqrt{(1.52^2 sin^2\,\theta + 1.74^2 cos^2\theta)}} - 1.52$$

$$.004313 = \frac{2.6448}{\sqrt{(1.52^2 sin^2\,\theta + 1.74^2 cos^2\theta)}} - 1.52$$

$$\sqrt{(1.52^2 sin^2\,\theta + 1.74^2 cos^2\theta)} = \frac{2.6448}{1.52 + 0.004313}$$

$$\sqrt{(1.52^2 sin^2\,\theta + 1.74^2 cos^2\theta)} = 1.735$$

$$1.52^2 sin^2\,\theta + 1.74^2(1 - sin^2\,\theta) = 3.01$$

$$0.7172\ sin^2\,\theta = 3.01$$

$$sin\,\theta = 0.1566°$$

$$\theta = 9.009°$$

Therefore the tilt angle (θ) value obtained is 9.009°

5.5.9 Dynamic light scattering (DLS) Experiment

Using Malvern Zetasizer Nano ZS90 (Malvern Instruments, Southborough, Massachusetts) hydrodynamic diameter of DLPC were performed. The detector angle was kept: 90º, incident laser was fixed at wavelength: 632 with laser power 4 mW. All Samples were prepared in Tris buffer (pH 7.4). Temperature was maintained at 25 °C.

5.5.10 Circular dichorism (CD) measurements

Chirascan Spectrophotometer (Applied Photophysics, UK) was used for measuring CD for all the samples. Samples were taken in a 1 mm path length quartz cell. Scan range was 190–260 nm and 1 nm as step size.

5.5.11 Vibrational circular dichroism (VCD) measurements

The VCD spectra were measured in the 1800-800 cm^{-1} range using a Bruker FT-IR spectrometer equipped with the Bruker polarization modulation accessory PMA 50. In the PMA 50 module, the light beam is focused onto the sample passing through an optical low pass filter (blocking wavenumbers >1800 cm^{-1}), a KRS-5 wire grid polarizer, and a ZnSe Photoelastic Modulator (PEM) with an oscillation frequency of 42 kHz. The light is

focused by a ZnSe lens to a MCT detector. The detector signal comprises two components: a low-frequency modulation which corresponds to the IR absorption bands, i.e., the A signal, and a high-frequency modulated signal (42 kHz) corresponding to the dichroic absorptions, i.e., the ΔA signal. Additionally, the reference signal direct from the PEM (42 kHz) is mixed to the high-frequency modulated detector signal. These two high-frequency modulated signals are demodulated by an internal synchronous demodulator integrated in the electronic units of the TENSOR and VERTEX series FTIR spectrometers. The sample was held in demountable cell with BaF_2 windows and a 100 μm spacer. Spectra were measured in D_2O solvent at a concentration of 10 mg mL^{-1}. For each measurement, the intensity calibration factor was obtained using a multiple-wave retardation plate combined with the second wire grid polarizer, whereby the system tuning was exactly the same as for the sample measurement. The spectra were corrected by subtracting the absorption (or VCD) of the corresponding solvent and were plotted in Origin 8 software.

5.6 References

(1) Galdiero, S.; Vitiello. M.; Falanga, A.; Cantisani, M.; Incoronato, N.; Galdiero, M. *Curr. Drug Metab.* **2012**, *13*, 93-104.

(2) Falanga, A.; Cantisani, M.; Pedone, C.; Galderio, S. *Protein Pept. Lett.* **2009**, *16*, 751-759.

(3) Clardy, J.; Fischbach, M. A.; Currie, C. R. *Curr. Biol.* **2009**, *19*, 437-441.

(4) Frecer, V.; Ho, B.; Ding, J. L. *Antimicrob. Agents Chemother.* **2004**, *48*, 3349-4457.

(5) Uhilg, T.; Kyprianou, T.; Martinelli, F. G.; Oppici, C. A.; Heiligers, D.; Hills, X.; Calvo, R.; Verhaert, P. *EuPA Open Proteom.* **2014**, *4*, 58-69.

(6) Habermann, E. *Science*, **1972**, *177*, 314-332.

(7) Raghuraman, H.; Chattopadhyay, A. *Biosci. Rep.* **2007**, *27*, 189-223.

(8) Irudayam, S. J.; Berkowitz, M. L. *Biochim. Biophys. Acta* **2012**, *1818*, 2975-2981.

(9) Lee, M. T.; Chen, F. Y.; Huang, H. W. *Biochemistry* **2004**, *43*, 3590-3599.

(10) Sengupta, D.; Leontiadou, H.; Mark, A. E.; Marrink, S. J. *Biochim. Biophys. Acta* **2008**, *1778*, 2308-2317.

(11) Shai, Y. *Biochim. Biophys. Acta*, **1999**, *1462*, 55-70.

(12) Vale, N.; Aguiar, L.; Gomes, P. *Front. Pharmacol.* **2014**, *5*, 1-13.

(13) Klocek, G.; Schulthess, T.; Shai. Y.; Seelig, J. *Biochemistry* **2009**, *48*, 2586-2596.

(14) Georghiou, S.; Thompson, S. M.; Mukhopadhyay, A. K. *Biophys. J.* **1982**, *37*, 159-161.

(15) Rex, S.; Bian, J.; Silvius, J. R.; Lafleur, M. *Biochim. Biophys. Acta*, **2002**, *1558*, 211-221.

(16) Raghuraman. H; Chattopadhyay, A. *Biopolymers* **2006**, *83*, 111-121.

(17) Brown, L. R.; Brawn, W.; Kumar, A.; Wuthrich, K. *Biophys. J.* **1982**, *37*, 319-328.

(18) Brauner, J. W.; Mendelsohn. R.; Prendergast, F. G. *Biochemistry* **1987**, *26*, 8151-8158.

(19) Kleinschimdt, J. H.; Mahaney, J. E.; Thomas D. D.; Marsh, D. *Biophys. J.* **1997**, *72*, 767-778.

(20) Hall, K.; Lee, T. H.; Aguilar, M. I. J. *Mol. Recognit.* **2011**, *24*, 108-118.

(21) Lin, I. H.; Meli, M. V.; Abbott, N. L. *J. Colloid Interface Sci.* **2009**, *336*, 90-99.

(22) Sidiq, S.; Das. D.; Pal, S. K. *RSC Adv.* **2014**, *4*, 18889-18893.

(23) Agarwal, A.; Sidiq, S.; Setia, S.; Bukusoglu, E.; de Pablo, J. J.; Pal, S. K.; Abbott, N. L. *Small* **2013**, *9*, 2785-2792.

(24) Kinsinger, M. I.; Lynn, D. M.; Abbott, N. L. *Soft Matter* **2010**, *6*, 4095−4104.

(25) Gupta, J. K.; Meli, M. V.; Teren, S.; Abbott, N. L. *Phys. Rev. Lett.* **2008**, *100*, 48301-48305.

(26) Gupta, J. K.; Abbott, N. L. *Langmuir* **2009**, *25*, 2026−2033.

(27) Wang, P.; Yang, F.; Mondiot, Y.; Miller, D. S.; Chen; Z.; Abbott, N. L. *Chem. Comm.* **2015**, *51*, 16844-16847.

(28) Tan, L. N.; Orler, V. J.; Abbott, N. L. *Langmuir* **2012,** *28*, 6364-6376.

(29) Das, D.; Sidiq, S.; Pal, S. K. *ChemPhysChem* **2015,** *16*, 753–760.

(30) Popov, P.; Honaker, L. W.; Kooijman, E. E.; Mann, E. K.; Jákli, A. I. *Sens. Biosensing Res.* **2016,** *8*, 31-35.

(31) Chen, C. H.; Yang, K. L. *Anal. Biochem.* **2012**, *421*, 321-323.

(32) Hu, Q.-Z.; Jang, C. H. *ACS Appl. Mater. Interfaces* **2012**, *4*, 1791−1795.

(33) Tan, H.; Li, X.; Liao, S.; Yu; R.; Wu, Z. *Biosens. Bioelectron.* **2014**, *62*, 84–89.

(34) Das, D.; Sidiq, S.; Pal, S. K., *RSC Adv.* **2015**, *5*, 66476–66486.

(35) Bi, X.; Hartono, D.; Yang, K.-L. *Adv. Funct. Mater.* **2009,** *19*, 3760–376536.

(36) Wei, Y.; Yang, K. L. *J. Mater. Sci.* **2015**, *50*, 4741-4748.

(37) Sidiq, S.; Verma, I.; Pal, S. K. *Langmuir* **2015,** *31*, 4741–4751.

(38) Verma, I.; Sidiq, S.; Pal, S. K. *Liq. Cryst.* **2016,** *43*, 1126-1134.

(39) Brake, J. M.; Daschner, M. K.; Luk, Y.-Y.; Abbott, N. L. *Science* **2003,** *302*, 2094–2097

(40) Raynor, R. L.; Zheng, B.; Kuo, J. F. *J. Biol. Chem.***1991**, *266*, 2753-2758.

(41) Yang, S.; Carrasquer, G. *Acta. Pharmacol. Sin*. **1997**, *18*, 3-5.

(42) Epand, R. M. *Biochim. Biophys. Acta* 1**998**, *1376*, 353-368.

(43) Eliezer, D; Kutluay, E.; Bussell, Jr. R.; Browne, G. *J. Mol. Biol.* **2001,** *307*, 1061-1073.

(44) Rex, S. *Biophys. Chem.* **1996**, *58*, 75-85.

(45) Smith, L. J.; Clarke, D. C. *Biochim. Biophys. Acta* **1992**, *1121*, 111-118.

(46) Veen, M. V.; Georgiou, G. N.; Drake, A. F.; Cherry, R. J. *Biochem. J.* **1995,** *305*, 785-790.

(47) Keiderling, T. A. *Curr. Opin. Chem. Biol.* **2002,** *6*, 682-688.

(48) Ma, S.; Freedman, T. B.; Dukor, R. K.; Nafie, L. A. *Appl. Spectrosc.* **2010,** *64*, 615−626.

Chapter 6

Conclusions

As a whole the entire thesis describes various approaches to enable LC as promising tool to recognize several biomolecular interactions in a precise and quantitative way. Ordering transition of LC molecules in micrometer range is responsive towards external stimuli and able to amplify the interfacial events into optical read-out that are visible through naked eye.

First chapter concludes an overview of importance of biosensing in the growth of science from therapeutic and clinical point of view. We further discussed the emersion of LC, besides display application, as a noble medium in the field of bio-sensing. We further put the physical insights into the orieantation and interfacial anchoring of LC in molecular level. We have described the properties and functions of biomolecules and working principles of several instrumental techniques mentioned in different chapters.

Second chapter describes the application of aqueous-LC interface for imaging of crucial bacterial endotoxin (LPS)–protein binding events through interfacial ordering transition of LCs. In this chapter we have demonstrated that the optical appearance of interfacial LC changes from dark to bright after exposure of aqueous solutions of three different proteins such as hemoglobin (Hb), bovine serum albumin (BSA), and lysozyme (LZM) onto LPS-laden aqueous–LC interface. We have found that influence of three different proteins on self-assembled LPS had different consequence towards ordering transition of interfacial LC. Furthermore, epiflouescence study proves the interaction of these proteins with LPS at aqueous-LC interface and also explains the retention of these proteins at the interface. From the measurements of optical retardance value of LCs during LPS-protein binding events at the interface provides a quantitative insight into protein–LPS binding affinity. Interestingly, we found that the retardation values were in accord with the binding

constants values between LPS and different proteins; a higher binding constant resulted in a greater tilt angle of LC (LPS-Hb> LPS-BSA> LPS-LZM) Overall the entire result provide a noble analytical approach to report LPS-protein binding event in a quantitative way.

Third chapters concludes the fabrication of aqueous–LC interface to recognize the interaction between bacterial endotoxin and different bacterial cell membrane components such as, peptidoglycan (PG), lipoteichoic acid (LTA). Here we observed alteration in the optical appearance of LC from dark to bright on exposure of an aqueous solution of PG and LTA on LPS–laden aqueous–LC interfaces, which indicates strong interaction between PG and LTA with interfacially self-assembled LPS. We also have found the responsiveness of LC towards these interactions of PG and LTA with LPS are highly specific compared to other lipids. Aditionally, we also looked into the characterization of the LPS decorated aqueous-LC interface using Langmuir–Blodgett technique and PM-IRRAS measurement. Furthermore we have also quantified these binding events by measuring the optical retardance of the LC at aqueous–LC interfaces. We concluded that binding affinity of LTA towards LPS is higher compared to PG. Overall the entire result provide a promising approach to quantify the specific binding of PG and LTA on LPS at the aqueous-LC interface.

Fourth chapter concludes a design of aqueous-LC interface to study the interaction between milk protein lactoferrin and bacterial endotoxin. We observed that self assembly of LPS at aqueous/LCs interface orients interfacial nematic 4-cyano-4'- pentylbiphenyl (5CB) LC in a homeotropic fashion (exhibiting dark optical image). Whereas, on the exposure of Lf on LPS–laden aqueous-LC interface optical image of LC changed from dark to bright implying an ordering transition of interfacial LCs from homeotropic to tilted/planar state. The ordering transition reveals the strong interfacial binding between Lf and LPS. Using epifluorescence microscopy, we further confirmed the interfacial LPS-Lf binding event by imaging the presence of FITC tagged Lf at the LPS laden aqueous-LC interface. In our experiment, we also found that LPS-Lf binding phenomenon is highly specific over other membrane lipids as well as other milk proteins. In addition to that, we have set a quantitative correlation the anchoring transition of 5CB with this interfacial binding event

by measuring tilt angle of LCs. Finally, we have looked into the conformational behavior of Lf in solution as well as in presence of LPS using ciruclar dichroism (CD) spectroscopy and further confirmed with vibrational circular dichroism (VCD) spectroscopy. As a whole the results mentioned in this chapter establish a new approach to investigate the interaction between LPS and Lf based on ordering transitions of LC at aqueous-LC interface.

Fifth chapter describes the application of LC-based interface for quantitative imaging of melittin–phospholipid interaction through orientational alteration of interfacial 5CB. LCs undergoes from dark to bright appearance on exposure of melittin at 1,2-didodecanoyl-*sn*-glycero-3-phosphocholine (DLPC) laden aqueous-LC interfaces. This observation implies strong interaction of DLPC with melittin at those interfaces. Next we envisaged the crucial role of Ca^{2+} to accelerate dynamic response of the LC during this binding event. The influence of Ca^{2+} towards kinetics accelaration of this binding event is highly specific compared to other alkaline earth metal ions. Adittionally we put insights to the quantitative correlation of this interaction by measuring gray scale light intensity and optical retardance of the LCs. Finally, to put insights into conformational behavior of the melittin in solution as well as in presence of DLPC vesicles, We performed CD and VCD experiments and concluded that melittin adopts alpha helical arrangement in Tris buffer, while in presence of Ca^{2+} melittin espouses a less ordered α helical conformation which, possibly, could ease its interaction with phospholipid and leading to faster dynamic response through orientational switching of LC. But upon binding with DLPC we observed in phospholipid environment melittin adopted more ordered α helical conformation to attain maximum thermodynamic stability on its interaction with phospholipids. By and large, the whole experiments provide a promising approach in fabrication of a robust LC based analytical tool to explore and quantify the binding event of melittin with phospholipid membrane at aqueous-LC interfaces.

Taken as hole, in this thesis we have focused on developing the approaches to fabricate liquid crystal as suitable candidate to study interfacial biomolecular interactions and also have extended this method to recognize several biomolecular interactions which are yet to be explored.

List of publications

(1) Das, D.; Sidiq, S.; Pal, S. K. A simple quantitative method to study protein lipopolysaccharide interactions by using liquid crystals. *ChemPhysChem* **2015**, *16*, 753–760.

(2) Das, D.; Sidiq, S.; Pal, S. K. Design of bio-molecular interfaces using liquid crystals demonstrating endotoxin interactions with bacterial cell wall components. *RSC Adv*. **2015**, *5*, 66476–66486.

(3) Das, D.; Pal, S. K. Liquid Crystal Unveiled Interactions between Melittin and Phospholipids at Aqueous-Liquid Crystal Interface. *Chemistryselect* **2017**, *2*, 4779-4786

(4) Das, D.; Pal, S. K. Liquid crystal based interfacial study demonstrating the interaction of bacterial endotoxin with milk protein lactoferrin. *Manuscript to be communicated*.

(5) Sidiq, S.; Das, D.; Pal, S. K. A new pathway for the formation of radial nematic droplets within a lipid-laden aqueous-liquid crystal interface. *RSC Adv.* **2014**, *4*, 18889-18893.

Recognition

"A simple quantitative method to study protein lipopolysaccharide interactions by using liquid crystals was selected for inside cover image in *ChemphysChem*.

Conferences

(1) Poster presentation titled as "*A simple quantitative method to study protein lipopolysaccharide interactions by using liquid crystals*" at 20th national conference on liquid crystal (NCLC-20) held at Manipal University, Manipal (16-18 december, 2013).

(2) Poster presentation titled as "*Design of bio-molecular interfaces using liquid crystals demonstrating endotoxin interactions with bacterial cell wall components*" at 21st national conference on liquid crystal (NCLC-21) held at VSSD college, Kanpur (10-12 november, 2014).

(3) Poster presentation entitled "*A liquid crystal based study demonstrating the interaction of melittin apitoxin with phospholipid membrane at aqueous-liquid crystal interface*" at 22nd national conference on liquid crystal (NCLC) held at DIT University, Dehradun (21-23 december, 2015)

(4) Poster presentation entitled "*A* new *liquid crystal based interfacial study demonstrating the interaction of bacterial endotoxin with milk protein lactoferrin*" at 23rd national conference on liquid crystal (NCLC-23) held at ISM Dhanbad, Dhanbad (7-9 december, 2016).

(5) Poster presentation entitled "*Liquid crystal based interfacial study demonstrating the interaction of bacterial endotoxin with milk protein lactoferrin*" at 24th national conference on liquid crystal (NCLC-24) 24 held at IISER Mohali, Mohali. (11-13 october, 2017)

(6) Participated in national seminar on crystallography 43 held at IISER Mohali, Mohali. (13-17 october, 2014)